

Geodetic Applications of the Global Navigation Satellite System (GLONASS) and of GLONASS/GPS Combinations

Inauguraldissertation
der Philosophisch-naturwissenschaftlichen Fakultät
der Universität Bern

vorgelegt von

Heinz Habrich

von Deutschland

Leiter der Arbeit: Prof. Dr. G. Beutler
Astronomisches Institut Universität Bern
Prof. Dr. M. Rothacher
Technische Universität München

Geodetic Applications of the Global Navigation Satellite System (GLONASS) and of GLONASS/GPS Combinations

Inauguraldissertation
der Philosophisch-naturwissenschaftlichen Fakultät
der Universität Bern

vorgelegt von

Heinz Habrich

von Deutschland

Leiter der Arbeit: Prof. Dr. G. Beutler
Astronomisches Institut Universität Bern
Prof. Dr. M. Rothacher
Technische Universität München

Von der Philosophisch-naturwissenschaftlichen Fakultät angenommen.

Der Dekan:

Bern, den 4.11.1999



Prof. A. Pfiffner

Contents

Introduction.....	1
-------------------	---

I. Theory

1. The GLONASS System	2
1.1 Segments of GLONASS.....	2
1.1.1 Space Segment.....	2
1.1.2 Control Segment.....	4
1.1.3 User Segment.....	4
1.2 The Satellite Signal.....	5
1.3 The GLONASS Reference Frame.....	7
1.3.1 Definition of the GLONASS Reference Frame PZ-90.....	7
1.3.2 Transformation Parameters Between PZ-90 and WGS-94.....	8
1.4 GLONASS System Time.....	9
1.5 GLONASS Satellite Orbits.....	11
1.5.1 Satellite Orbit Motion.....	11
1.5.2 The Navigation Message.....	14
1.5.3 Computation of Satellite Positions.....	16
2. Modeling the GLONASS Observables	21
2.1 Pseudorange.....	21
2.2 Carrier Phase.....	23
2.3 Differences.....	24
2.3.1 Pseudorange Differences.....	24
2.3.2 Single Difference Phase Observable.....	25
2.3.3 Double Difference Phase Observable.....	25

2.3.4 Triple Difference Phase Observable.....	29
2.4 Linear Combination.....	30
2.4.1 Wide-lane Linear Combination L5.....	31
2.4.2 Ionosphere-free Linear Combination L3	33
2.4.3 Geometry-free Linear Combination L4.....	34
2.4.4 Melbourne-Wübbena Linear Combination L6	35
3. Pre-Processing GLONASS Phase Observations.....	37
3.1 Phase Jumps.....	37
3.2 Cycle Slips.....	38
3.2.1 Cycle Slips in the Triple Difference Phase Observable.....	39
3.2.2 Single Difference Phase Observable Differenced in Time.....	41
3.2.2.1 Modified Triple Difference Phase Residual	42
3.2.2.2 Cycle Slip Detection Algorithm	43
4. Ambiguity Resolution.....	45
4.1 Ambiguity Parameter.....	45
4.2 Ambiguity Resolution Algorithm.....	49
4.3 Ambiguity Resolution for Linear Combinations.....	53
5. Combined GLONASS/GPS Data Analysis.....	56
5.1 System Time Differences	56
5.2 Combined GLONASS/GPS Orbits.....	59
5.3 Combined Pseudorange Analysis	60
5.4 Combined Ambiguity Resolution.....	61
II. Applications and Results	
6. Results for Various Baselines.....	67
6.1 Code Single Point Positioning.....	68
6.2 Baseline of 5 m Length.....	76

6.2.1 Cycle Slip Detection.....	76
6.2.2 Ambiguity Resolution.....	80
6.3 Baseline of 6.6 km Length.....	87
6.4 Baselines of 16, 41 and 58 km Length.....	90
7. The International GLONASS Experiment (IGEX-98)	101
7.1 Routine Processing Scheme.....	103
7.2 Estimates of the System Time Difference.....	107
7.3 Transformation Parameters between PZ-90 and ITRF 96.....	116
7.4 Ambiguity Resolution.....	119
7.5 Coordinates of IGEX Stations.....	121
8. Conclusion	123
III. Appendices	
A. GLONASS Satellite Launch History	125
B. GLONASS Satellite Specifications	129
References	133

Introduction

The Global Navigation Satellite System or Global'naya Navigatsionnaya Sputnikovaya Sistema (GLONASS) is a satellite-based radionavigation system which enables the user to obtain three dimensional position and velocity vectors and timing information anywhere on or near the Earth's surface. It is operated by the Ministry of Defence (Russian Space Forces) of the Russian Federation. There are several other global positioning systems like TRANSIT, DORIS or PRARE, but the concept of GLONASS may be best compared with the NAVSTAR Global Positioning System (GPS) developed by the U.S. Department of Defence. GLONASS was developed for military navigation purposes and timing needs. But by decree of March 7, 1995, the government of the Russian Federation confirmed to put the system at the disposal of military and civil users. GLONASS is used for navigation and geodetic applications by civil users.

In this work we deal with geodetic applications of GLONASS and also with the combined processing of GLONASS and GPS data. The combination of both, GLONASS and GPS observations, leads to an improved reliability of the resulting products due to the usage of two autonomous systems. Furthermore the additional satellites contribute to shorter observation sessions for, e.g., ambiguity resolution in real-time kinematic (RTK) applications. RTK applications are not addressed here.

The first Chapter reviews the components of the GLONASS, in particular the space, control, and user segments. The satellite signal structure transmitted on the L1 and L2 frequencies are described and compared to that of GPS. The most important difference is the use of satellite-specific frequencies by GLONASS satellites. The definition of the GLONASS reference frame PZ-90 and the system time as defined in the interface control document [ICD, 1995] are discussed. The satellite positions, velocities, and accelerations for every 30 minutes are included in the navigation message and may be used to calculate the satellite position for a current epoch using formulas given in [ICD, 1995].

The observation equations for GLONASS observables are introduced in Chapter 2. They are similarly to those of GPS except for the satellite-specific GLONASS frequencies. A "new" single difference bias term remains in the double difference phase observable. Its size depends on the wavelength difference of the two satellites and is not present in case of GPS. Chapter 3 deals with the pre-processing of GLONASS phase observations. Cycle slips have to be detected on the single difference level and assigned to the correct satellites because of the single difference bias term.

An ambiguity resolution approach for processing GLONASS double difference phase observations is described in Chapter 4. The single difference bias term destroys the integer nature of the ambiguities for observations referring to satellite pairs with large differences in the carrier wavelengths, whereas the ambiguities for satellite pairs with small wavelength differences may be resolved easily. Our ambiguity resolution algorithm successively resolves

the ambiguities for all satellite pairs starting with satellite pairs with small wavelength differences. This approach is appropriate for long observation sessions and long baselines. In order to combine GLONASS and GPS a unique time scale for the observations and a unique reference frame for the satellite and receiver positions are required. Chapter 5 shows explicitly how the two requirements can be met. The new ambiguity resolution algorithm may also be used for GPS and combined GLONASS/GPS observations.

Results for short baselines are discussed in Chapter 6. In this case detected cycle slips and real-valued estimates for the ambiguities are close to integer numbers. Observations stemming from the International GLONASS Experiment (IGEX-98) were processed following our routine processing scheme which is explicitly shown in Chapter 7. Our analysis results include improved orbits for GLONASS satellites, system time differences between the GLONASS and the GPS, and transformation parameters between the PZ-90 and the ITRF terrestrial reference frames.

I. Theory

1. The GLONASS System

The first GLONASS satellite was launched on October 12, 1982. Additional satellites were launched during the following years and the GLONASS was officially declared operational on September 24, 1993 by the President of the Russian Federation. In January 1996 24 satellites were operational for the first time. A complete list of GLONASS satellite launches is given in Appendix A. Each launch of a rocket carries three satellites into orbit. There are three major components of the GLONASS system: Space segment, control segment and user segment. Today (May 1999) 15 satellites are healthy. New launches are badly needed.

1.1 Segments of GLONASS

1.1.1 Space segment

When fully deployed the space segment consists of 24 satellites in three orbit planes. The planes have a nominal inclination of 64.8 degrees and are separated by 120 degrees in longitude. 8 satellites are evenly distributed in each plane. The satellites in plane $i+1$ are displaced by 15 degrees in the argument of latitude compared to the satellites in plane i , $i=1,2,3$ (see Figure 1.01). The radius of the circular orbits is 25.510 kilometers. The orbital period is $8/17$ of a sidereal day or approximately 11 hour and 16 minutes. GLONASS satellites complete “exactly” 17 orbital revolutions in eight sidereal days. After eight sidereal days a particular satellite will thus reappear at the same position in the sky for an observer on

the Earth's surface. Because each orbital plane contains eight equally spaced satellites, an observer on the Earth will see one of these satellites at the same position in the sky at the same sidereal time each day. The constellation of 24 satellites guarantees that at least five satellites are seen simultaneously from 99 percent of the Earth's surface. A comparison of GLONASS and GPS orbit characteristics is given in Table 1.01.

	GLONASS	GPS
Total number of satellites	24	24
Orbital planes	3, spaced by 120 °	6, spaced by 60 °
Orbital plane inclination	64.8°	55 °
Satellites per orbital plane	8, equally spaced	6, unequally spaced
Orbital height	19,100 km	20,200 km
Revolution period	11 hours 16 min	11 hours 58 minutes
Ground track repeatability	every eighth sidereal day	every sidereal day

Table 1.01: GLONASS Satellite Orbit Characteristics

GLONASS satellites have expected life times of three years. The new generation of GLONASS-M satellites is designed to have a 5-year life time and an improved reliability. All GLONASS satellites are equipped with laser reflectors for satellite laser ranging (SLR). The satellite constellation as of March 17, 1999, is shown in Figure 1.01. The position of the satellites within the constellation is indicated by the slot numbers. The frequency channel number is used to determine the nominal frequency of the satellites' signal and will be explained in more details in Section 1.2.

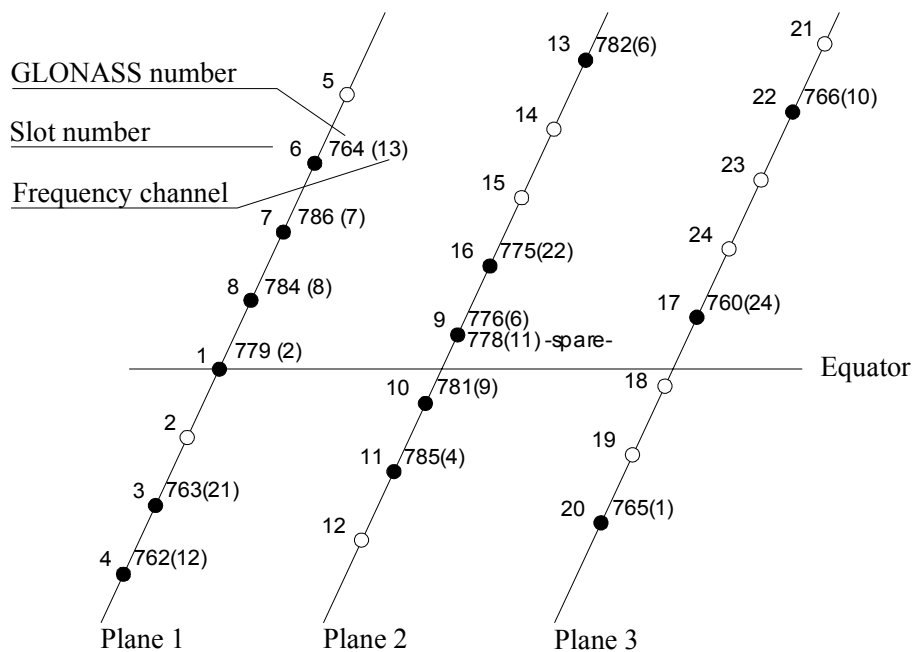


Figure 1.01: Constellation of GLONASS Satellites of March 17, 1999

1. The GLONASS System

Here we consequently use the slot numbers for the identification of the GLONASS satellites. In order to distinguish between GLONASS and GPS satellites we add the constant number of 100 to all GLONASS satellite numbers, which results in the numbers 100 to 124 for the GLONASS satellites 1 to 24.

1.1.2 Control Segment

The GLONASS satellite constellation is operated by the so-called ground-based Control Complex (GCC). It consists of the System Control Center (SCC) in the Moscow region and several Command Tracking Stations (CTS) located over a wide area of Russia [CSIC, 1997]. The CTSs track all GLONASS satellites in view and pass the ranging data and satellite messages to the SCC. Ranges to the satellites are measured by radar with a maximum error of between two and three meters [Fairheller, 1994]. This information is processed by the SCC to determine clock corrections, navigation messages and status information for each satellite. The updated information is transmitted to the CTSs and uploaded to the satellites. The ranges observed by the CTSs are periodically calibrated using a laser device at the Quantum Optical Tracking Stations (QOTS). The QOTS are part of the GCC. The GLONASS system time is generated on the basis of the Central Synchronizer and is explained in Section 1.4.

Status information of the GLONASS satellite constellation is also provided by the Coordinational Scientific Information Center (CSIC) of the Russian Ministry of Defence in Moscow.

1.1.3 User Segment

The user segment consists of an unlimited number of GLONASS receivers. There are different receiver types commercially available. In Section 1.2 the signal components transmitted by GLONASS satellites will be explained. They are similar as those of GPS satellites. One may classify GLONASS receivers according to the signal components processed in the same way as it is done in the case of GPS receivers. We make the distinction of:

- L1 Single Frequency Receivers,
- L1 and L2 Dual-Frequency Receivers,
- C/A-Code Receivers,
- P-Code Receivers.

In contrast to GPS antennas the GLONASS antennas require an increased band width in order to measure different frequencies. In the case of a combined GLONASS/GPS receiver the antenna even has to be designed for GLONASS and GPS frequencies.

1.2 The Satellite Signal

GLONASS satellites broadcast their signals in two sub-bands of the L-band of the radio frequency spectrum, L1 (~ 1.6 GHz) and L2 (~ 1.2 GHz). The carriers are modulated by two binary codes, the C/A-code and the P-code, and by the data message. The signals transmitted in the L1-band are modulated by both types of binary code, whereas the L2 signal only contains the P-code. The C/A-code is generated with a frequency of 0.511 MHz and is available for civil users, for the so-called Standard Precision Navigation. The P-code is modulated with a frequency of 5.11 MHz and is called High Precision Navigation Code. The P-code is not recommended for civil use without authorization of the Russian Space Forces [ICD, 1995]. The P-code may be changed by the Russian Space Forces without prior announcement. Selective Availability (SA) and Anti Spoofing (AS) degrading the GPS real-time performance do not exist in the case of GLONASS.

Each GLONASS satellite transmits its L1- and L2 signals on slightly different frequencies. A GLONASS receiver can separate the signal of a particular satellite from the total incoming signal of all visible satellites by assigning different frequencies to its tracking channels [Kleusberg, 1990]. This technique is called Frequency Division Multiple Access (FDMA). Because there is no need to distinguish satellites by signal modulation, all GLONASS satellites use the same code for modulation. FDMA is different to the technique used for the signals transmitted by GPS satellites. Each GPS satellite modulates its carrier with a different

	GLONASS	GPS
Carrier frequency	L1: 1602 ... 1615.5 MHz, L2: 1246 ... 1256.5 MHz, for channel number 0,1,...,24	L1: 1575.42 MHz, L2: 1227.60 MHz
Code	C/A-code on L1, P-code on L1 and L2, same code for all satellites	C/A-code on L1, P-code on L1 and L2, different codes for each satellite
Satellite separation technique	FDMA	CDMA
Code frequency	C/A-code: 0.511 MHz, P-code: 5.11 MHz	C/A-code: 1.023 MHz, P-code: 10.23 MHz
System time correction to UTC	UTC(SU)	UTC(USNO)
Satellite clock correction	clock offset, frequency offset	clock offset, frequency offset, frequency rate
Orbit parameters	every 30 minutes, satellite position, satellite velocity, satellite acceleration	every 60 minutes, modified Keplerian elements

Table 1.02: Satellite Signals for GLONASS and GPS

1. The GLONASS System

code. A GPS receiver identifies a particular signal by „looking at“ the code modulation and by rejecting all signals with a different code. This technique is called Code Division Multiple Access (CDMA). Therefore there is no need for different frequencies in GPS and all GPS satellites use the same frequency for L1 and L2. The signal structures of GLONASS and GPS are listed in Table 1.02.

The nominal carrier frequency for each GLONASS satellite may be computed as follows:

$$\begin{aligned}f_{(1)}^m &= f_{(1)}^0 + m \cdot \Delta f_{(1)} \\f_{(2)}^m &= f_{(2)}^0 + m \cdot \Delta f_{(2)}\end{aligned}\tag{1.01}$$

where $m = 0, 1, \dots, 24$ frequency channel number,

$$\begin{aligned}f_{(1)}^0 &= 1602 \text{ MHz}, & \Delta f_{(1)} &= 0.5625 \text{ MHz}, \\f_{(2)}^0 &= 1246 \text{ MHz}, & \Delta f_{(2)} &= 0.4375 \text{ MHz}\end{aligned}$$

The channel $m = 0$ is used only for test purposes. The frequency channel number is contained in the almanac message. The channel numbers assigned to the satellites as defined on March 17, 1999 are given in Figure 1.01. There is a constant ratio between the carrier frequencies of L1 and L2:

$$\frac{f_{(2)}^m}{f_{(1)}^m} = \frac{7}{9}\tag{1.02}$$

The FDMA technique requires different frequencies for all GLONASS satellites in view. Because two antipodal satellites may not be seen at the same time from one particular site on the Earth's surface, the satellites may transmit their signals at the same frequency. This is done to prevent interference between signals used for GLONASS, radio astronomy, and mobile satellite services. For the same reason it is planned to shift the frequency band of GLONASS in three steps:

Step 1: Until 1998

- Frequency channels 0,1,...,12,22,23 and 24 will be used for normal operation.
- Frequency channels 13,14 and 21 may be used under exceptional circumstances.

Step 2: 1998 - 2005

- Frequency channels 0,1,...,12 will be used.
- Frequency channel 13 may be used under exceptional circumstances.

Step 3: Beyond 2005

- Frequency channels -7,...,+6 will be used.
- Frequency channel 5 and 6 will be used for special technical purposes for limited periods of time.

1.3 The GLONASS Reference Frame

1.3.1 Definition of the GLONASS Reference Frame PZ-90

According to [ICD, 1995] the position of the transmitting antenna phase center for the GLONASS satellites are given in the Broadcast Ephemerides refer to the PZ-90 („Parametry Zemli“ or parameter of the Earth) reference frame. These positions are different from the center of mass of the satellites. The specifications of GLONASS satellites as given in Appendix B show on offset of 1.62 m between the phase center of the satellite antenna and the center of mass.

In order to investigate that the Broadcast Ephemerides refer to the transmitting antenna phase center two sets of coordinates for the GLONASS satellite positions have been calculated for the day 41 of the year 1999. For the generation of the first coordinate set (A) we used the Broadcast Ephemerides and applied the radial offset of 1.62 m in order to correct the positions given in the Broadcast Ephemerides to the center of mass of the satellites. The second set of coordinates for GLONASS satellite positions (B) was calculated from the Broadcast Ephemerides also, however the offset of 1.62 m was not applied. In section 7.1 the calculation of improved GLONASS satellite orbits will be given. Those resulting orbits were used for the calculation of the third set of coordinates of the satellite positions (C) which certainly refer to the center of mass of the satellites. A Helmert transformation between the coordinates (C) and (A) and (B), respectively results in a scale factor of approximately $6 \cdot 10^{-8}$ between (A) and (C). This scale factor was not found between (B) and (C). This leads to the assumption, that also the Broadcast Ephemerides describe the positions of the satellite's center of mass. Following this assumption the radial offset of 1.62 m applied to the satellite positions in the calculation of (A) and the orbital radius of 25,510 km leads to a theoretical scale factor of $6.35 \cdot 10^{-8}$ between (A) and (C) which has been confirmed approximately.

The PZ-90 is Earth-Centered, Earth-fixed (ECEF) and defined as follows:

Origin: Center of mass of the Earth;

Z-axis: Parallel to the direction to the mean north pole

1. The GLONASS System

according to the mean epoch 1900 - 1905 as defined by the International Astronomical Union (IAU) and the International Association of Geodesy (IAG);

X-axis: Parallel to the direction of the Earth's equator for epoch 1900 - 1905, the plane defined by X- and Z-axis is parallel to the mean Greenwich meridian;

Y-axis: Completes the right-handed rectangular coordinate system.

The datum parameters for PZ-90 are listed in Table 1.03.

1.3.2 Transformation Parameters Between PZ-90 and WGS-84

In order to combine GLONASS and GPS using Broadcast Ephemerides, the transformation parameters between PZ-90 and WGS-84 have to be known. The definitions of PZ-90 and WGS-84 are slightly different. But even if the definitions were identical, the realization of the coordinate system by two different satellite systems would be different. [Rossbach et al., 1996] determined a set of transformation parameters using stations with known relative coordinates in both systems. [Misra et al., 1996] used a set of GLONASS satellite positions determined in PZ-90 and WGS-84, to establish transformation parameters. Both methods came to comparable results, with accuracies limited by the quality of the Broadcast Ephemerides. The estimated transformation parameters are listed in Table 1.04. Another approach by [Bazlow et al., 1999] and results from the IGEX-98 campaign will be discussed in Chapter 7. Once a set of transformation parameters is known, GPS and GLONASS Broadcast Ephemerides may be computed in the same reference frame (PZ-90 or WGS-84) and both navigation systems may be combined.

Rotation rate of the Earth	$\omega = \dot{\Omega}$	$7292115 \cdot 10^{-11}$	rad / sec
Universal gravitational parameter of the Earth	$\mu = G \cdot M$	$398600.44 \cdot 10^9$	$\text{m}^3 / \text{sec}^2$
Gravitational parameter of Earth atmosphere		$0.35 \cdot 10^9$	$\text{m}^3 / \text{sec}^2$
Speed of light	c	299792458	m / sec
Second zonal geopotential coefficient of spherical harmonic expansion	C_{20}	$-1082.63 \cdot 10^{-6}$	
Semi-major axis of ellipsoid	a	6378136	m
Flattening	f	1/298.257	
Gravitational acceleration at equator of the Earth		978032.8	mgal
Correction to gravitational acceleration at sea level, caused by the atmosphere		-0.9	mgal

Table 1.03: Constants and Parameters of the PZ-90 Reference Frame

$\begin{matrix} x \\ y \\ z \end{matrix}_{WGS-84} = \begin{bmatrix} 1 & -0.33'' & 0 \\ 0.33'' & 1 & 0 \\ 0 & 0 & 1 \end{bmatrix} \cdot \begin{matrix} u \\ v \\ w \end{matrix}_{PZ-90}$	Roßbach et al., 1996
$\begin{matrix} x \\ y \\ z \end{matrix}_{WGS-84} = \begin{bmatrix} 0 \\ 2.5m \\ 0 \end{bmatrix} + \begin{bmatrix} 1 & -0.39'' & 0 \\ 0.39'' & 1 & 0 \\ 0 & 0 & 1 \end{bmatrix} \cdot \begin{matrix} u \\ v \\ w \end{matrix}_{PZ-90}$	Misra et al., 1996

Table 1.04: Transformation Parameters from PZ-90 to WGS84

When improving the orbits of GPS and GLONASS satellites, the orbit reference frame is defined by the coordinates of the fixed stations. If an identical set of station coordinates is used for the determination of GPS and GLONASS satellite orbits, transformation parameters are no longer required when combining both systems.

1.4 GLONASS System Time

The GLONASS system time is based on the Central Synchronizer within the ground based control complex. It is realized by hydrogen masers with a daily stability of better than $5 \cdot 10^{-14}$. On board time scales of GLONASS satellites are based on Cesium clocks. The daily stability of the satellite frequencies is better than $5 \cdot 10^{-13}$.

The GLONASS system time and the time scales of the satellites are compared twice a day at the control complex and the corrections are uploaded to the satellites. The accuracy of this clock corrections should be better than 10 nsec for the time of computation. This allows a synchronization of the satellite time w.r.t. the GLONASS system time of about 20 nanoseconds (one sigma) [ICD, 1995].

GLONASS time is synchronized to the Russian National Etalon time scale (UTC(SU)). UTC(SU) is maintained by the Main Metrological Center of Russian Time and Frequency Service at Mendeleev near Moscow [CSIC, 1997]. There is a constant offset of 3 hours between UTC(SU) and GLONASS time. The additional correction τ_c between GLONASS time and UTC(SU) should be less than 1 msec. The accuracy for τ_c should be better than 1µsec [ICD, 1995]. The leap seconds occurring in UTC also show up in GLONASS time. Corrections are performed (if necessary) on June, 30 and December, 31. In order to combine GLONASS and GPS the different system time scales must be taken into consideration. The

1. The GLONASS System

relationship between the corresponding time scales is given in Table 1.05; more details will be given in Section 5.1.

The following formula is used to correct the satellite clock reading at the moment of signal emission to UTC(SU):

$$t_{UTC(SU)} = t + \tau_c + \tau_n(t_b) - \gamma_n(t_b) \cdot (t - t_b) \quad (1.03)$$

with

- t : Reading of the satellite clock at emission time of the signal
- τ_c : GLONASS time scale correction to UTC(SU), given for the calendar day number within the 4-year period beginning with the leap year
- t_b : Time of ephemerides, this is the time within the current day in UTC(SU) + 3 hour; the ephemerides information refers to t_b
- τ_n : Correction for the satellite clock of satellite n to GLONASS time at time t_b calculated as:

$$\tau_n(t_b) = t_c(t_b) - t_n(t_b) \quad (1.04)$$

- $t_c(t_b)$: GLONASS time at time t_b
- $t_n(t_b)$: Reading of the clock for satellite n at time t_b
- $\gamma_n(t_b)$: Frequency offset for satellite n at time t_b

Eqn. (1.03) may be used to calculate the satellite ephemerides at the moment of the navigation parameters measurements [ICD, 1995]. It is also an example for the usage of the broadcast satellite clock corrections τ_n and γ_n in ,e.g., the observation equations of Chapter 2. The correction τ_c is broadcast as part of the GLONASS navigation message. Alternative methods to determine this correction are illustrated in Chapter 5.

TAI	International Atomic Time	continuous		
UTC	Universal Time Coordinated	leap seconds	TAI - UTC = $\underline{31\text{ s}}$	
GPS	GPS system time	continuous	UTC - GPS = $\underline{-12\text{ s}}$ + C0 TAI - GPS = 19 s + C0	C0 < 100 ns
GLONASS	GLONASS system time	leap seconds	UTC - GLONASS = 0 s + C1 TAI - GLONASS = $\underline{31\text{ s}}$ + C1	C1 < 1 μs , since July 1, 1997
Numerical values for TAI-UTC, TAI-GPS and TAI-GLONASS refer to July 1997. Daily values of C0 and C1 are determined at the BIPM, Time Section in Paris and published in it's Circular T [BIPM, 1999].				

Table 1.05: Relationship between Time Scales

1.5 GLONASS Satellite Orbits

1.5.1 Satellite Orbit Motion

The orbital acceleration acting on a satellite is caused by the Earth's gravitational attraction and a number of perturbing accelerations. A simple mathematical model for the orbital motion is based on the following assumptions:

- The Earth has a spherically symmetric gravity field,
- the mass of the satellite is very small compared to the Earth's mass and is neglected,
- the gravitational attraction of other celestial bodies is neglected, and
- there are no non-gravitational forces (like sky-drag and solar radiation pressure).

These assumptions, Newton's law of gravitation, and the basic three Newtonian hypotheses lead to the equation of motion for an Earth satellite. The equations of motion are a system of second order differential equations:

$$\ddot{\mathbf{r}} = -GM \cdot \frac{\mathbf{r}}{r^3} \quad (1.05)$$

with

\mathbf{r} : geocentric position vector of the satellite in an inertial reference frame

1. The GLONASS System

- $\dot{\mathbf{r}}, \ddot{\mathbf{r}}$: first and second time derivate (velocity and acceleration of \mathbf{r})
 r : length of \mathbf{r}
 GM : product of gravitational constant and mass of the Earth, sometimes called geocentric gravitational constant

A solution of the differential equations may be calculated if (1) initial values for the position and the velocity at the epoch t_0

$$\begin{aligned}\mathbf{r}(t_0) &= \mathbf{r}_0(q_1, q_2, \dots, q_6) \\ \dot{\mathbf{r}}(t_0) &= \dot{\mathbf{r}}_0(q_1, q_2, \dots, q_6)\end{aligned}\tag{1.06}$$

or (2) boundary values for the positions at the epochs t_1 and t_2 .

$$\begin{aligned}\mathbf{r}(t_1) &= \mathbf{r}_1(q_1, q_2, \dots, q_6) \\ \mathbf{r}(t_2) &= \mathbf{r}_2(q_1, q_2, \dots, q_6)\end{aligned}\tag{1.07}$$

are known.

Numerical integration techniques or the well-known Keplerian (or other analytical formulas) may be used to determine the orbit $\mathbf{r}(t)$ as a function of the time and of the six parameters q_1, q_2, \dots, q_6 . Possible choices of these parameters are:

$$\text{a) } (q_1, q_2, q_3) = \mathbf{r}_0^T \qquad (q_4, q_5, q_6) = \dot{\mathbf{r}}_0^T \tag{1.08}$$

$$\text{b) } (q_1, q_2, q_3) = \mathbf{r}_1^T \qquad (q_4, q_5, q_6) = \mathbf{r}_2^T \tag{1.09}$$

$$\text{c) } (q_1, q_2, \dots, q_6) = (a, e, i, \Omega, \omega, u_0), \tag{1.10}$$

where \mathbf{r}^T is the transpose of \mathbf{r} .

The six Keplerian elements $(a, e, i, \Omega, \omega, u_0)$ illustrated in Figure 1.02 are:

- a : semi-major axis of the orbit
 e : eccentricity
 i : inclination of the orbit plane
 Ω : right ascension of ascending node
 ω : argument of perigee
 u_0 : argument of latitude, the sum of argument of perigee and the true anomaly at time t_0

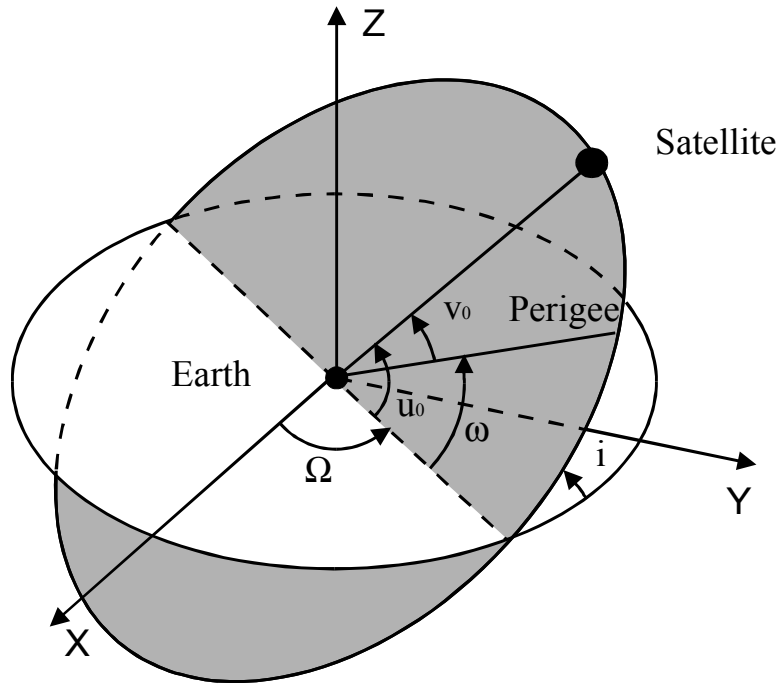


Figure 1.02: The Keplerian Elements

If we assume an inertial frame in Figure 1.02, the x-axis is in direction of the vernal equinox, the z-axis coincides with the celestial ephemerides pole and the y-axis completes a right-handed coordinate system. The intersection line of the equatorial and ecliptic plane changes due to precession and nutation. The definition of the inertial frame requires furthermore the definition of a reference epoch for the equator and equinox (e.g., J2000). In Chapter 7 we will show results of the International GLONASS Experiment (IGEX) including improved orbits for GLONASS satellites. For this orbit improvement the Kepler elements in an inertial system are estimated.

It has to be mentioned that GPS broadcast ephemerides are given in an Earth-fixed reference frame and include „pseudo“-Keplerian elements. Also, the broadcast positions and velocities of GLONASS satellites are given in an Earth-fixed reference frame (explained in Section 1.5.2). The transformation of $\ddot{\mathbf{r}}$ from the inertial to an Earth-fixed reference system is required in order to compute GLONASS and GPS satellite positions in the Earth-fixed reference system from the corresponding broadcast ephemerides. Formulas for the case of GLONASS will be given in Section 1.5.3.

The assumptions made in eqn. (1.05) are not met for a real satellite and we have to take into consideration a number of perturbing accelerations affecting the orbital motion of the satellite:

$$\ddot{\mathbf{r}} = -GM \cdot \frac{\mathbf{r}}{r^3} + \mathbf{a}(t, \mathbf{r}, \dot{\mathbf{r}}, p_1, p_2, \dots, p_n) \quad (1.12)$$

with

a: perturbing acceleration, characterized by $\mathbf{t}, \mathbf{r}, \dot{\mathbf{r}}$ and the parameters p_1, p_2, \dots, p_n

The most significant perturbing forces are:

- Non-central part of the Earth gravitational potential,
- gravitational effects of Sun and Moon,
- solid earth tidal effects, and
- solar radiation pressure.

Other forces with smaller effects on the satellite motion are due to ocean tides, the Y-bias of the solar radiation pressure, albedo and relativistic effects. The modeling of the perturbing forces and the induced orbital errors for GPS satellites are given, e.g., in [Rothacher, 1992].

1.5.2 The Navigation Message

The navigation message of a GLONASS satellite is generated at the System Control Center and then uploaded to the satellite by the Command Tracking Stations. The navigation message includes the position and velocity of a particular satellite in the PZ-90 reference frame as well as almanac information for all GLONASS satellites.

The satellite broadcasts the information as digital data at a 50 bps bit rate. It is coded by the Hamming code and transformed to a relative code [ICD, 1995]. A superframe structure is generated from the digital data and continuously repeated. Each superframe has a duration of 2.5 min and consists of five frames. Each frame includes the ephemerides of the transmitting satellite and has a duration of 30 seconds. The GLONASS almanac is partitioned over all five frames. Each of the frames 1 to 4 contains the almanac of five satellites and frame 5 the almanac for four satellites, completing the 24 satellite constellation. Each frame includes 15 strings with 85 bits of digital data. The broadcast ephemerides parameters are given in Table 1.06.

Word	Effective Range	Units	Explanation
t_k	0,...,23 0,...,59 0,30	hours, minutes, seconds	time of the beginning of the frame within the current day related to satellite time scale
t_b	15,...,1425	min	time of ephemerides
$\gamma_n(t_b)$	$\pm 2^{-30}$	-	frequency correction
$\tau_n(t_b)$	$\pm 2^{-9}$	seconds	satellite clock correction
$x_n(t_b), y_n(t_b), z_n(t_b)$	$\pm 2.7 \cdot 10^4$	km	satellite position
$\dot{x}_n(t_b), \dot{y}_n(t_b), \dot{z}_n(t_b)$	± 4.3	km/s	satellite velocity vector
$\ddot{x}_n(t_b), \ddot{y}_n(t_b), \ddot{z}_n(t_b)$	$\pm 6.2 \cdot 10^{-9}$	km/s ²	satellite acceleration components caused by Sun and Moon
E_n	0,...,31	days	age of ephemerides
B_n	0,1	-	satellite health indicator

Table 1.06: GLONASS Broadcast Ephemerides (position, velocity, and acceleration in Earth-fixed system)

The time t_k refers to the satellite time scale. It is the time of the beginning of the frame within the current day. Possible values for the seconds are 0 and 30, due to the 30 second duration for each frame. The time of ephemerides t_b is given by the corresponding minutes within the current day according to UTC(SU) + 3 hours. The ephemerides information within each frame are referenced to t_b . The broadcast ephemerides may be computed for every 15 minutes at the System Control Center, which leads to multiples of 15 min for the range of t_b . Ephemerides at 15 and 45 minutes within every hour are broadcast under normal circumstances. The relative deviation of the predicted carrier frequency of satellite n from the nominal value is given by the parameter $\gamma_n(t_b)$:

$$\gamma_n(t_b) = \frac{f_n(t_b) - f_{Hn}}{f_{Hn}} \quad (1.13)$$

with

- $f_n(t_b)$: predicted carrier frequency value for satellite n , accounting for gravitational and relativistic effects at t_b ,
- f_{Hn} : nominal carrier frequency for satellite n .

The satellite clock correction of satellite n to GLONASS system time is given by $\tau_n(t_b)$. The satellite position and velocity vectors are given in the PZ-90 reference frame. The acceleration of the satellite caused by Sun and Moon is provided in the PZ-90 coordinate system, too.

The mean square errors for the predicted position and velocity vectors of a satellite as well as for the satellite clock synchronization are shown in Table 1.07 according to [ICD, 1995].

	Mean Square Error	
satellite position	along track	20 m
	cross track	10 m
	radial	5 m
satellite velocity vector	along	0.05 cm/s
	cross track	0.1 cm/s
	radial	0.3 cm/s
time scale synchronization		20 ns

Table 1.07: Mean Square Errors of Broadcast Ephemerides

Broadcast orbit information for GLONASS and GPS satellites are different, position and velocity are given for GLONASS and modified Keplerian elements for GPS. Therefore we have different format definitions for the corresponding satellite navigation message files (e.g., RINEX format).

1.5.3 Computation of Satellite Positions

The positions of GLONASS satellites in the PZ-90 coordinate system are transmitted within the broadcast ephemerides every 30 minutes. In order to calculate the position at any instant one may solve the equations of motion (1.12) using the given initial values at epoch t_0 for the position and the velocity. An integration interval of

$$\Delta t = t - t_0 \leq 15 \text{ min} \quad (1.14)$$

with

- t : current epoch
- t_0 : epoch of ephemerides

is sufficient in this case. The geocentric position vector \mathbf{r} in eqn. (1.12) is given in the inertial frame. Because the initial position and velocity are given in the Earth-fixed PZ-90 coordinate system a transformation between the inertial and earth-fixed coordinate systems have to be performed before the numerical integration.

Transformation between Inertial and earth-fixed Coordinate Systems

The transformation between inertial and earth-fixed coordinate systems for a specific instant of time is defined by a matrix as a function of three Eulerian angles. However, for practical use, some intermediate coordinate systems are introduced by approximating the motion of the Earth. Rotation matrices for precession, nutation, polar motion, and rotation around the

Earth's axis are introduced and we may write the transformation for the epoch t following the IERS Conventions [McCarthy, 1996] as:

$$\mathbf{r}_{INS} = \mathbf{PN}(t) \cdot \mathbf{R}_3(t) \cdot \mathbf{W}(t) \cdot \mathbf{r}_{EFS} \quad (1.15)$$

with

- \mathbf{r}_{INS} : position vector in the inertial system
- \mathbf{r}_{EFS} : position vector in the earth-fixed system
- $\mathbf{PN}(t)$: matrix for precession and nutation, describing the motion of the celestial ephemerides pole in the inertial reference system
- $\mathbf{R}_3(t)$: matrix for rotation of the Earth around the celestial ephemerides pole
- $\mathbf{W}(t)$: matrix for polar motion

A detailed description of these terms is given in [McCarthy, 1996]. For the time interval Δt in eqn. (1.14) precession, nutation and polar motion may be assumed perfectly known in the error budget of the broadcast ephemerides. Only the rotation matrix $\mathbf{R}_3(t)$ in eqn. (1.15) has to be taken into account with the rotation angle $\omega \cdot \Delta t$:

$$\mathbf{r}_{INS} \approx \mathbf{R}_3(t) \cdot \mathbf{r}_{EFS} \quad (1.16)$$

with

$$R_3(t) = \begin{vmatrix} \cos(\omega \cdot \Delta t) & -\sin(\omega \cdot \Delta t) & 0 \\ \sin(\omega \cdot \Delta t) & \cos(\omega \cdot \Delta t) & 0 \\ 0 & 0 & 1 \end{vmatrix}$$

- ω : Earth's rotation rate
- Δt : Time interval given in eqn. (1.14)

Assuming that the rotation angle $\omega \cdot \Delta t$ is infinitesimal the second derivative in time for eqn. (1.16) may be approximated as:

$$\begin{vmatrix} \ddot{x} \\ \ddot{y} \\ \ddot{z} \end{vmatrix}_{INS} \approx \begin{vmatrix} \ddot{x} \\ \ddot{y} \\ \ddot{z} \end{vmatrix}_{EFS} + \begin{vmatrix} -\omega^2 \cdot x - 2 \cdot \omega \cdot \dot{y} \\ -\omega^2 \cdot y + 2 \cdot \omega \cdot \dot{x} \\ 0 \end{vmatrix}_{EFS} \quad (1.17)$$

The transformation from the Earth-fixed system to the inertial system is now in linear form and may be carried out by adding a correction term as used in eqn. (1.18).

The resulting equation of motion for GLONASS satellites to be used for the numerical integration within a 15 min integration interval are given in [ICD,1995]:

$$\begin{aligned}
 \ddot{x} &= -\frac{\mu}{r^3} \cdot x + \frac{3}{2} \cdot C_{20} \cdot \frac{\mu \cdot a^2}{r^5} \cdot x \cdot \left| 1 - \frac{5 \cdot z^2}{r^2} \right| + \omega^2 \cdot x + 2 \cdot \omega \cdot \dot{y} + \ddot{X} \\
 \ddot{y} &= -\frac{\mu}{r^3} \cdot y + \frac{3}{2} \cdot C_{20} \cdot \frac{\mu \cdot a^2}{r^5} \cdot y \cdot \left| 1 - \frac{5 \cdot z^2}{r^2} \right| + \omega^2 \cdot y - 2 \cdot \omega \cdot \dot{x} + \ddot{Y} \\
 \ddot{z} &= -\frac{\mu}{r^3} \cdot z + \frac{3}{2} \cdot C_{20} \cdot \frac{\mu \cdot a^2}{r^5} \cdot z \cdot \left| 3 - \frac{5 \cdot z^2}{r^2} \right| + \ddot{Z}
 \end{aligned}
 \tag{1.18}$$

with

x, y, z	:	Components of \mathbf{r} in PZ-90
μ, a, C_{20}, ω	:	Parameters, as defined for PZ-90 and given in Table 1.03
$\ddot{X}, \ddot{Y}, \ddot{Z}$:	Accelerations caused by Sun and Moon available in the broadcast ephemerides

The right-hand terms of equation (1.18) include the central part of the Earth's gravitational potential and the oblateness of the Earth characterized by C_{20} . The Earth's rotation is taken into account using approximation (1.17). The numerical integration of equation (1.18) may be performed using, e.g., the Runge-Kutta method of order four.

Figures 1.03 and 1.04 show differences of positions for the GLONASS satellite slot number 3 after numerically integrating equations (1.18). The broadcast ephemerides of July 21 and 22, 1997 were used. The initial positions at 15 and 45 minutes were used for a forward and backward integration over 15 minutes. The resulting positions at 0 and 30 minutes were calculated from two different initial epochs and compared. The comparison leads to the absolute differences given in Figures (1.03) for the X-, Y- and Z-components. In order to demonstrate the effect of the size of the integration steps on the integration results, the position differences were calculated using four different integration widths, namely 450, 100, 10 and 1 sec (corresponding to 2, 9, 90 and 900 integration steps for the 15 minutes interval). Whereas the integration width of 450 sec leads to large position differences of 10 to 40 m, the position differences clearly decrease to 1 to 2 m using a 10 sec or 1 sec integration step. 10 sec and 1 sec integration width give almost identical results (within a few dm). Taking into consideration the actual errors of the broadcast ephemerides an integration width of 10 sec may be used without significant loss of accuracy through the numerical integration method with the Runge-Kutta integration of order four. Much longer steps might be taken when using higher order integration procedures as, e.g., used in program ORBGEN of the Bernese GPS software [Beutler, 1996].

Figure (1.04) shows the position differences after an integration over 30 min instead of 15, using the 10 sec integration width. The positions at 15 and 45 minutes given in the broadcast ephemerides were compared with the values computed by a numerical integration over 30 minutes from the previous message. The absolute difference of the extrapolated positions to the original values for the corresponding epochs are shown for the X-, Y- and Z-component.

The differences are much higher than those of the 15 min integration interval and confirm that the approximate equation (1.18) should only be used for intervals no longer than 15 min.

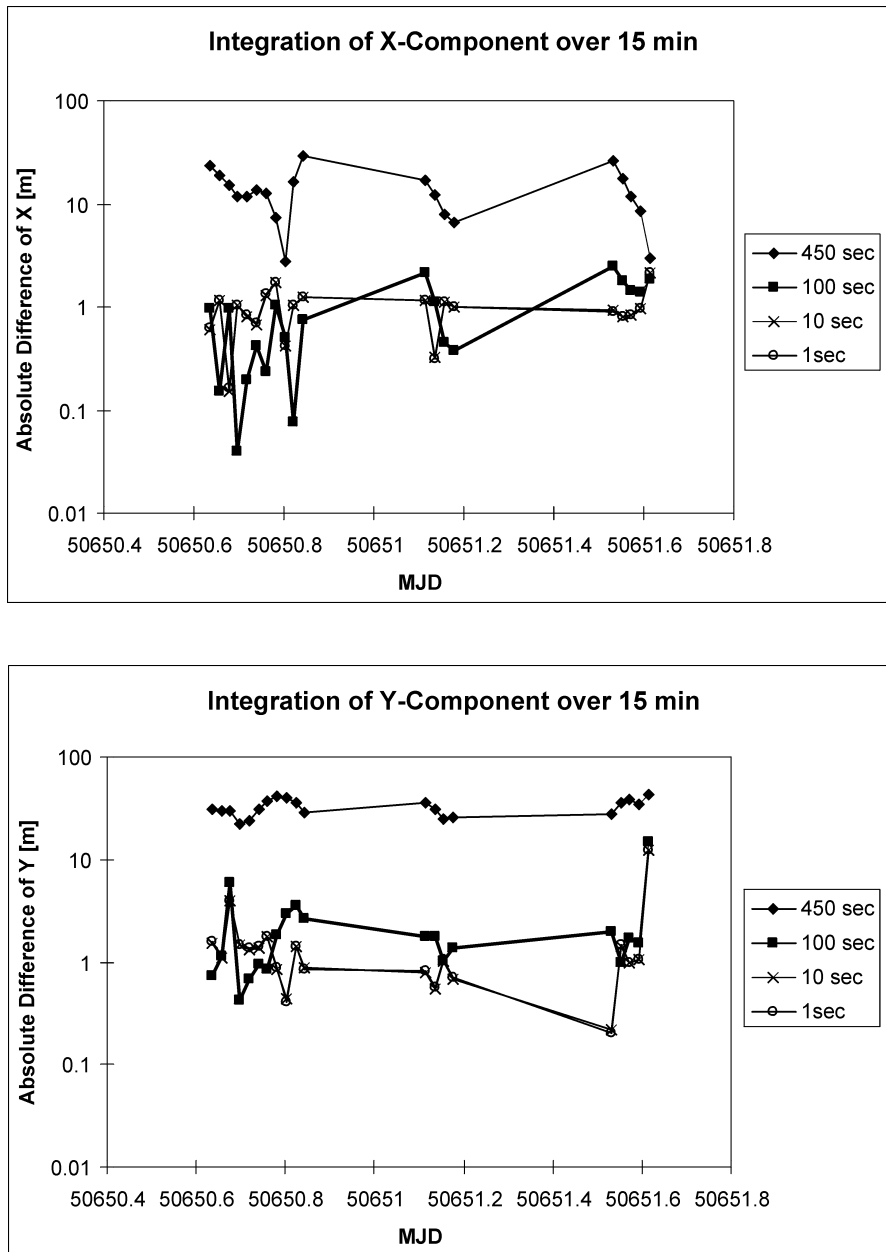


Figure 1.03: Numerical Integration for GLONASS Satellite Slot No. 3

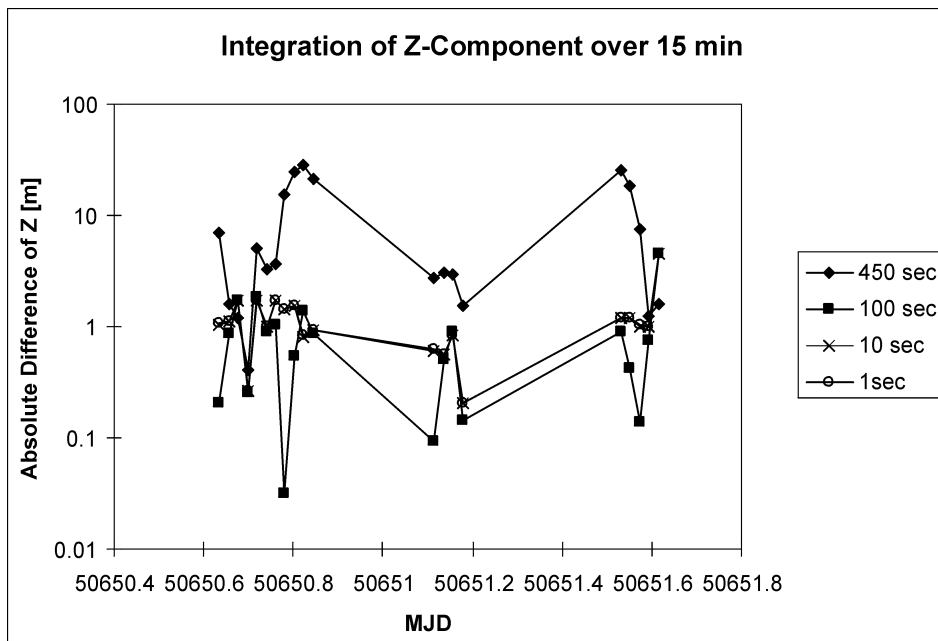


Figure 1.03: Numerical Integration for GLONASS Satellite Slot No. 3 (cont.)

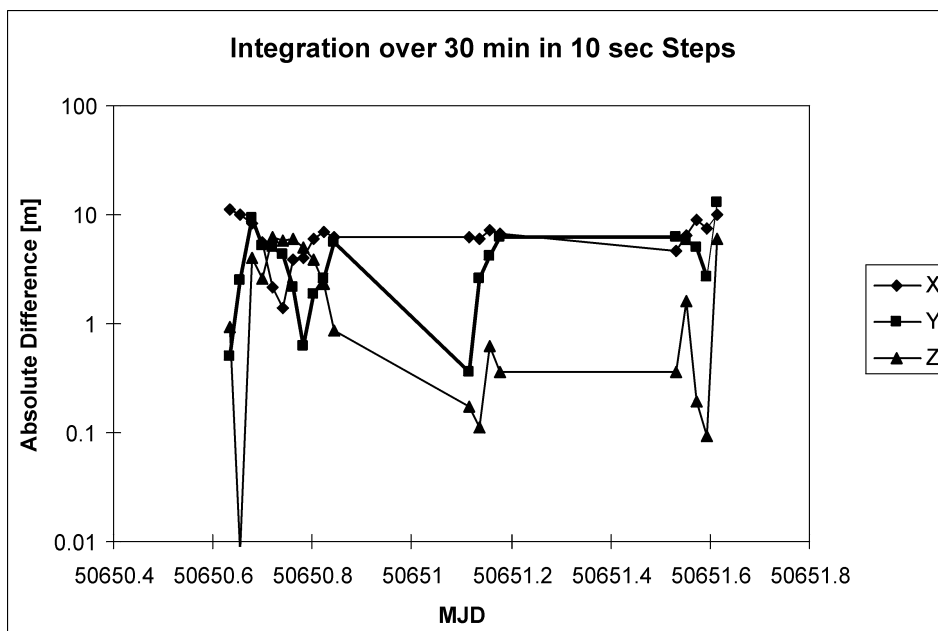


Figure 1.04: Numerical Integration for GLONASS Satellite Slot No. 3

2. Modeling the GLONASS Observables

According to the signal structure described in Section 1.2 the GLONASS measurement types are

- C/A-code on L1,
- P-code on L1 and L2,
- carrier phase on L1 and L2.

These measurement types are recorded by the receiver and represent the basic observables for the estimation of the relevant geodetic parameters. The observation equations for code and phase may be used to form differences and linear combinations in order to eliminate or reduce existing biases. For all equations the satellite-specific GLONASS frequencies must be taken into account. Observation equations for GPS are given, e.g., by [Rothacher, 1992, Mervart, 1995, Leick, 1995]. Only the most important aspects and differences between GLONASS and GPS are discussed here.

2.1 Pseudorange

The pseudorange is closely related to the distance between the satellite and the receiver at a specific epoch. The receiver generates a copy of the code generated by the satellite for signal modulation, and shifts it until maximum correlation with the received signal occurs. This allows the determination of the biased signal travel time between receiver and satellite (the distance is biased due to the satellite and receiver clock errors). The pseudorange observation equation may be introduced as

$$P_k^i = c \cdot (\bar{t}_k - \bar{t}^i) \quad (2.01)$$

with

- c : velocity of light
- t^i : time of emission of the signal from satellite i in GLONASS system time
- \bar{t}^i : reading of satellite clock at time t^i
- t_k : time of reception of the signal at receiver k in GLONASS system time
- \bar{t}_k : reading of receiver clock at time t_k

and where the errors Δt^i and Δt_k of the satellite and the receiver clock, respectively, are given by

2. Modeling the GLONASS Observables

$$\Delta t^i = \bar{t}^i - t^i \quad (2.02)$$

$$\Delta t_k = \bar{t}_k - t_k \quad (2.03)$$

Introducing the signal travel time τ_k^i between satellite i and receiver k

$$\tau_k^i = t_k - t^i \quad (2.04)$$

we may write:

$$P_k^i = c \cdot \tau_k^i + c \cdot \Delta t_k - c \cdot \Delta t^i \quad (2.05)$$

The term $c \cdot \tau_k^i$ contains the geometric distance ρ_k^i , the propagation delay, and relativistic effects. Both, the ionospheric and the tropospheric refraction, delay the code measurements and lead to

$$c \cdot \tau_k^i = \rho_k^i + \Delta\rho_{k,ion}^i + \Delta\rho_{k,trop}^i - \Delta\rho_{k,rel}^i \quad (2.06)$$

with

$\Delta\rho_{k,ion}^i$:	ionospheric refraction
$\Delta\rho_{k,trop}^i$:	tropospheric refraction
$\Delta\rho_{k,rel}^i$:	relativistic correction .

The geometric distance follows from the geocentric position vectors of receiver k and satellite i as

$$\rho_k^i = |r_k(t_k) - r^i(t_k - \tau_k^i)| \quad (2.07)$$

with

$r_k(t_k)$:	geocentric position vector of receiver k at signal reception time t_k
$r^i(t_k - \tau_k^i)$:	geocentric position vector of satellite i at signal emission time $t_k - \tau_k^i$.

Eqn. (2.07) shows that the reading of the receiver clock \bar{t}_k has to be corrected to t_k for the calculation of the geometric distance. The receiver clock error Δt_k thus has to be known. In our processing we use the double difference (between stations and receivers) mode in order to calculate the geometric distance between two stations. In this case the resulting error for the geometric distance caused by the receivers clocks is smaller than 1 mm if the receiver clock error is smaller than 1 μ sec , [see e.g. Beutler et al., 1996].

In the following we assume that

the receiver clock is known to better than 1 μsec (2.08)
(e.g., from code single point positioning).

Equations (2.01) to (2.07) are exactly the same as those used to represent GPS code measurements. The frequencies of the GLONASS satellites do not explicitly show up in these observations. Nevertheless, the specific frequencies of GLONASS and GPS satellites induce different ionospheric refraction delays that are neglected in this context. It must be noticed, however, that all clock information is given in GLONASS system time and that the satellite positions refer to PZ-90 in the case of broadcast ephemerides. The combination of GLONASS and GPS measurement requires a unique reference and time system. More details may be found in Section 5.2.

2.2 Carrier Phase

In general, satellite m generates the carrier phase on frequency f_n , with $m, n = 1, 2, \dots, 24$. Let us assume for the sake of simplicity that $m = n$ for the discussion of the observation equations and let satellite i generate the frequency i . With this assumption we may use index i for the satellite m as well as for the frequency n . According to [Rothacher, 1992] we may write the phase observation equation as:

$$\Psi_k^i = \lambda^i \cdot (\Phi_k^i(\bar{t}_k) - \Phi^i(\bar{t}^i) + N_k^i) \quad (2.09)$$

with

Ψ_k^i :	basic phase observable [m] for satellite i and receiver k
λ^i :	nominal wavelength of the signal from satellite i
$\Phi_k^i(\bar{t}_k)$:	reference phase generated by receiver k for satellite i at time \bar{t}_k
$\Phi^i(\bar{t}^i)$:	phase generated by satellite i and emitted at time \bar{t}^i
N_k^i :	unknown integer number of cycles (ambiguity).

Introducing the clock errors Δt^i and Δt_k as well as the signal travel time τ_k^i leads to:

$$\Psi_k^i = \lambda^i \cdot (\Phi_k^i(t_k + \Delta t_k) - \Phi^i(t_k - \tau_k^i + \Delta t^i) + N_k^i) \quad (2.10)$$

After a Taylor series development around t_k (truncated after the linear terms) we may write

$$\Psi_k^i = \lambda^i \cdot (\Delta t_k \cdot f^i + \tau_k^i \cdot f^i - \Delta t^i \cdot f^i + N_k^i) \quad (2.11)$$

with $f^i =$ nominal frequency of signal i

and eventually:

$$\Psi_k^i = c \cdot \tau_k^i + N_k^i \cdot \lambda^i + c \cdot \Delta t_k - c \cdot \Delta t^i \quad (2.12)$$

The term $c \cdot \tau_k^i$ may be calculated as

$$c \cdot \tau_k^i = \rho_k^i - \Delta \rho_{k,ion}^i + \Delta \rho_{k,trop}^i - \Delta \rho_{k,rel}^i \quad (2.13)$$

and shows an opposite sign for the ionospheric refraction compared to the code measurement in eqn. (2.06).

2.3 Differences

2.3.1 Pseudorange Differences

Differences of the original observations will eliminate or reduce existing biases. GLONASS pseudorange differences can be calculated using exactly the same formulas as for GPS. The *single difference observable* (between the receivers k and l) is defined by

$$\Delta P_{kl}^i = P_k^i - P_l^i \quad (2.14)$$

and results in

$$\Delta P_{kl}^i = c \cdot \Delta \tau_{kl}^i + c \cdot \Delta t_{kl} \quad (2.15)$$

with

$$\begin{aligned} \Delta \tau_{kl}^i &= \tau_k^i - \tau_l^i \\ \Delta t_{kl} &= \Delta t_k - \Delta t_l \end{aligned} .$$

The satellite clock error Δt^i is (almost) eliminated if the receiver clocks are synchronized to GLONASS system time to within some milliseconds so that the drift of the satellite clock can be neglected between the two epochs of signal emission.

Subsequently we assume that

$$\begin{aligned} &\text{the receiver clock is synchronized to GLONASS} \\ &\text{system time within one millisecond.} \end{aligned} \quad (2.16)$$

The *double difference observable* (between the receivers k and l and the satellites i and j) is defined by

$$\Delta\Delta P_{kl}^{ij} = P_{kl}^i - P_{kl}^j \quad (2.17)$$

and gives

$$\Delta\Delta P_{kl}^{ij} = c \cdot \Delta\Delta\tau_{kl}^{ij} \quad (2.18)$$

with

$$\Delta\Delta\tau_{kl}^{ij} = \Delta\tau_{kl}^i - \Delta\tau_{kl}^j \quad .$$

If assumption (2.08) is true the receiver clock errors allow the correct calculation of the geometric distance ρ_k^i (see section 2.1). In this case receiver clock errors are eliminated in the double difference observation equation.

2.3.2 Single Difference Phase Observable

If the signal from satellite i is „simultaneously“ observed by two receivers k and l , we may form the single difference phase observable

$$\Delta\Psi_{kl}^i = \Psi_k^i - \Psi_l^i \quad (2.19)$$

and we get the observation equation

$$\Delta\Psi_{kl}^i = c \cdot \Delta\tau_{kl}^i + N_{kl}^i \cdot \lambda^i + c \cdot \Delta t_{kl} \quad (2.20)$$

with

$$N_{kl}^i = N_k^i - N_l^i \quad .$$

The satellite clock error Δt^i is eliminated with the assumption (2.16).

2.3.3 Double Difference Phase Observable

Forming the difference of two single difference observable of satellite i and satellite j leads to the double difference phase observable

$$\Delta\Delta\Psi_{kl}^{ij} = \Delta\Psi_{kl}^i - \Delta\Psi_{kl}^j \quad (2.21)$$

and the observation equation

$$\Delta\Delta\Psi_{kl}^{ij} = c \cdot \Delta\Delta\tau_{kl}^{ij} + N_{kl}^i \cdot \lambda^i - N_{kl}^j \cdot \lambda^j \quad . \quad (2.22)$$

The receiver clock term $c \cdot \Delta t_{kl}$ is eliminated if condition (2.08) is met.

2. Modeling the GLONASS Observables

If we substitute

$$\lambda^i = \lambda^j + \Delta\lambda^{ij} \quad (2.23)$$

we may write equation (2.22) as:

$$\Delta\Delta\Psi_{kl}^{ij} = c \cdot \Delta\Delta\tau_{kl}^{ij} + N_{kl}^{ij} \cdot \lambda^i + N_{kl}^j \cdot \Delta\lambda^{ij} \quad (2.24)$$

using

$$N_{kl}^{ij} = N_{kl}^i - N_{kl}^j .$$

Because two antipodal GLONASS satellites may generate carriers with nominally the same frequency we have for such satellite pairs

$$\Delta\lambda^{ij} = 0 \quad (2.25)$$

for general GLONASS observations we have, however

$$\Delta\lambda^{ij} \neq 0 . \quad (2.26)$$

In this case a single difference bias term b_{kl}^{ij} remains in the double difference observable equation which is not present in GPS:

$$b_{kl}^{ij} = N_{kl}^j \cdot \Delta\lambda^{ij} \quad (2.27)$$

The Single Difference Bias Term

The single difference bias term (2.27) is the main problem in cycle slip detection and ambiguity resolution for GLONASS satellites. The bias depends on the frequency difference of the satellites i and j and on the single difference ambiguities N_{kl}^j . Obviously, when estimating double difference ambiguities, the bias term will destroy the integer nature of the ambiguities in eqn. (2.24). Therefore, the knowledge of the single difference ambiguities N_{kl}^j is required to resolve the double difference N_{kl}^{ij} ambiguities. It remains to be seen how accurately this term needs to be known.

The wavelength difference $\Delta\lambda^{ij}$ can be calculated as

$$\Delta\lambda^{ij} = \frac{c}{f_i} - \frac{c}{f_j} \quad (2.28)$$

with the frequencies f_i and f_j defined in eqn. (1.01).

With the approximation

$$\lambda^m \approx \lambda^0 + m \cdot \Delta\lambda \quad (2.29)$$

and with values for λ^0 and $\Delta\lambda$ defined in Table 2.01 we may write the single difference bias (2.27) in the form

$$b_{kl}^{ij} \approx N_{kl}^j \cdot (i - j) \cdot \Delta\lambda \quad (2.30)$$

Approximation (2.30) may be used for the analysis of formal errors. The data processing has to be performed using the correct wavelength differences. As $\Delta\lambda$ is much smaller than the unmodeled part of the ionosphere and the troposphere as well as the receiver noise, it is impossible to resolve N_{kl}^j in eqn. (2.24) to an integer number. The situation may change if information about the N_{kl}^j (e.g., all differences N_{kl}^{ij} known) becomes available. This will be discussed in Chapter 4.

The integer double difference ambiguities N_{kl}^{ij} may be found, if the bias term is small enough, e.g., smaller than 0.1 cycles. This is true for small wavelength differences between the two satellites or if the single difference ambiguities are known with an accuracy of a few cycles. The conversion of the bias term into units of cycles of λ^0 using

$$\frac{b_{kl}^{ij}}{\lambda^0} \approx N_{kl}^j \cdot (i - j) \cdot \frac{\Delta\lambda}{\lambda^0} \quad (2.31)$$

includes the ratio $\frac{\Delta\lambda}{\lambda^0}$, which must be calculated for L1 and L2 frequencies. Eqn. (1.02) gives

$$\frac{\lambda_2^m}{\lambda_1^m} = \frac{9}{7} \quad (2.32)$$

and the introduction of eqn. (2.32) into eqn. (2.23) results in

$$\frac{\Delta\lambda_1^{ij}}{\lambda_1^0} = \frac{\Delta\lambda_2^{ij}}{\lambda_2^0} \quad (2.33)$$

According to eqn. (2.33) the ratio $\frac{\Delta\lambda}{\lambda^0}$ is the same for L1 and L2 frequencies and is given in Table 2.01. Also, the bias term in units of cycles (2.31) is the same for L1 and L2 if we assume the same value for the single difference ambiguities N_{kl}^j in L1 and L2.

2. Modeling the GLONASS Observables

L1			L2		
λ_1^0	=	0.187136366 m	λ_2^0	=	0.240603899 m
$\Delta\lambda_1 = \lambda_1^1 - \lambda_1^0$	=	-65.7 μm	$\Delta\lambda_2 = \lambda_2^1 - \lambda_2^0$	=	-84.5 μm
$\frac{\Delta\lambda_1}{\lambda_1^0}$	=	-0.000351	$\frac{\Delta\lambda_2}{\lambda_2^0}$	=	-0.000351

Table 2.01: GLONASS Carrier Wavelength

Approximate wavelength differences for GLONASS satellites converted into units of cycles of λ^0 are given in Table 2.02. For the minimum wavelength difference between two satellites the single difference ambiguities N_{kl}^j have to be known with an accuracy of 285 cycles (which is possible, e.g., after computing a code single point positioning) in order to keep the bias term below 0.1 cycles. In this case the integer nature of the N_{kl}^j is well visible. Forming the double difference between satellites with maximum wavelength difference requires the knowledge of the N_{kl}^j with an accuracy of 12 cycles. The graphic representation in Figure 2.01 shows the considerable reduction of the maximum bias allowed for the single difference ambiguities N_{kl}^j , when the wavelength difference between the two satellites increases.

$(i-j) \cdot \frac{\Delta\lambda}{\lambda^0}$				maximum bias allowed in N_{kl}^j for $ b^j \leq 0.1$ cycles of λ^0			
i-j	L1 and L2	i-j	L1 and L2	i-j	L1 and L2	i-j	L1 and L2
1	-0.00035	13	-0.00456	1	285	13	22
2	-0.00070	14	-0.00491	2	142	14	20
3	-0.00105	15	-0.00526	3	95	15	19
4	-0.00140	16	-0.00562	4	71	16	18
5	-0.00175	17	-0.00597	5	57	17	17
6	-0.00211	18	-0.00632	6	47	18	16
7	-0.00246	19	-0.00667	7	41	19	15
8	-0.00281	20	-0.00702	8	36	20	14
9	-0.00316	21	-0.00737	9	32	21	13
10	-0.00351	22	-0.00772	10	28	22	13
11	-0.00386	23	-0.00807	11	26	23	12
12	-0.00421			12	24		

Table 2.02: GLONASS Wavelength Differences in Cycles of λ^0 and Maximum Bias allowed for the Single Differences Ambiguities N_{kl}^j

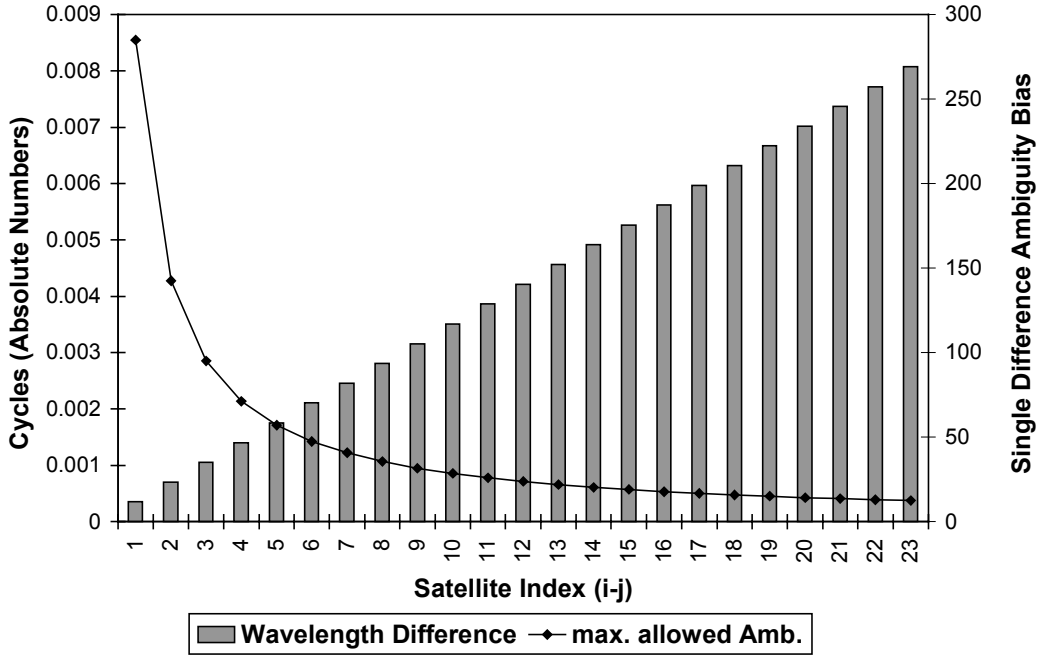


Figure 2.01: GLONASS Wavelength Differences in Cycles of λ^0 and maximum allowed size of Single Difference Ambiguities N_{kl}^j

2.3.4 Triple Difference Phase Observable

Double difference phase observables for two different epochs t_1 and t_2 may be used to form the triple difference phase observable:

$$\Delta\Delta\Delta\Psi_{kl}^{ij}(t_2, t_1) = \Delta\Delta\Psi_{kl}^{ij}(t_2) - \Delta\Delta\Psi_{kl}^{ij}(t_1) \quad (2.34)$$

If we assume that the ambiguity parameters N_{kl}^i and N_{kl}^j in eqn. (2.22) did not change during the time interval $(t_2 - t_1)$, the phase ambiguities are eliminated and we get the observation equation:

$$\Delta\Delta\Delta\Psi_{kl}^{ij}(t_2, t_1) = c \cdot \Delta\Delta\Delta\tau_{kl}^{ij}(t_2, t_1) \quad (2.35)$$

with

$$\Delta\Delta\Delta\tau_{kl}^{ij}(t_2, t_1) = \Delta\Delta\tau_{kl}^{ij}(t_2) - \Delta\Delta\tau_{kl}^{ij}(t_1)$$

2. Modeling the GLONASS Observables

The variation of the tropospheric refraction is usually small for short time intervals ($t_2 - t_1$) of, e.g., 30 sec, and the tropospheric refraction is adequately reduced in the triple difference observable. However, the ionospheric refraction may change rapidly. The triple difference observable is used to calculate a good approximation of the relative position vector between the receivers k and l and for cycle slip detection purposes.

2.4 Linear Combinations

The original code and phase observations may be used to form several linear combinations. New observation types, generated in this way, allow the elimination or reduction of different biases. Linear combinations may be formed for zero, single, and double difference measurements. Satellite-specific frequencies have to be taken into account in all measurement types.

A general form of a linear combination for phase observations is given by

$$L_{c,k}^i = \chi_{c,1} \cdot L_{1k}^i + \chi_{c,2} L_{2k}^i \quad (2.36)$$

where we introduce the restriction

$$\chi_{c,1} + \chi_{c,2} = 1 \quad (2.37)$$

with

$$\begin{aligned} L_{c,k}^i &: && \text{linear combination of phase observation [m]} \\ L_{1k}^i, L_{2k}^i &: && \text{phase observation [m] of the original carriers} \\ \chi_{c,1}, \chi_{c,2} &: && \text{coefficients of the linear combination.} \end{aligned}$$

The introduction of relation (2.12) into eqn. (2.36) and observing eqn. (2.37) gives:

$$L_{c,k}^i = c \cdot \tau_k^i + \chi_{c,1} \cdot N_{1k}^i \cdot \lambda_1^i + \chi_{c,2} \cdot N_{2k}^i \cdot \lambda_2^i + c \cdot \Delta t_k - c \cdot \Delta t^i \quad (2.38)$$

Single Difference of Phase Linear Combination

Similarly to the case of the original carriers L1 and L2 described in Section 2.3 the single difference of a phase linear combination observable

$$L_{c,kl}^i = L_{c,k}^i - L_{c,l}^i \quad (2.39)$$

gives rise to the observation equation

$$L_{c,kl}^i = c \cdot \Delta \tau_{kl}^i + \chi_{c,1} \cdot N_{1kl}^i \cdot \lambda_1^i + \chi_{c,2} \cdot N_{2kl}^i \cdot \lambda_2^i + c \cdot \Delta t_{kl} \quad (2.40)$$

Double Difference of Phase Linear Combination

For the double difference of a phase linear combination observable

$$L_{c,kl}^{ij} = L_{c,kl}^i - L_{c,kl}^j \quad (2.41)$$

we use eqn. (2.23) and write

$$L_{c,kl}^{ij} = c \cdot \Delta\Delta\tau_{kl}^{ij} + \underbrace{\chi_{c,1} \cdot N_{1kl}^{ij} \cdot \lambda_1^i}_{T_1} + \underbrace{\chi_{c,2} \cdot N_{2kl}^{ij} \cdot \lambda_2^i}_{T_2} + \underbrace{\chi_{c,1} \cdot N_{1kl}^j \cdot \Delta\lambda_1^{ij}}_{T_3} + \underbrace{\chi_{c,2} \cdot N_{2kl}^j \cdot \Delta\lambda_2^{ij}}_{T_4} \quad (2.42)$$

showing terms comparable to the double difference observation equation of the original carriers (2.24). Two terms T_1 and T_2 are determined by the double difference ambiguities N_{1kl}^{ij} , N_{2kl}^{ij} , and the wavelength of the original carriers λ_1^i, λ_2^i . The terms T_3 and T_4 are determined by the single difference ambiguities N_{1kl}^j, N_{2kl}^j , and the wavelength difference of the two satellites $\Delta\lambda_1^{ij}, \Delta\lambda_2^{ij}$. These terms represent the single difference bias term, corresponding to eqn. (2.27) for the original carriers, in a general form of the phase linear combination and we may write

$$b_{c,kl}^{ij} = \chi_{c,1} \cdot N_{1kl}^j \cdot \Delta\lambda_1^{ij} + \chi_{c,2} \cdot N_{2kl}^j \cdot \Delta\lambda_2^{ij} \quad (2.43)$$

Below we define the coefficients $\chi_{c,1}$ and $\chi_{c,2}$ for the more important linear combinations.

2.4.1 Wide-lane Linear Combination L5

The wide-lane linear combination is defined by the coefficients

$$\chi_{5,1} = \frac{f_1^i}{f_1^i - f_2^i} \quad \text{and} \quad \chi_{5,2} = \frac{-f_2^i}{f_1^i - f_2^i} \quad (2.44)$$

After the definition of the so-called *wide-lane* wavelength

$$\lambda_5^i = \frac{c}{f_1^i - f_2^i} \quad (2.45)$$

of approximately 84 cm and the new ambiguity types

$$N_{5kl}^i = N_{1kl}^i - N_{2kl}^i \quad (2.46)$$

$$N_{5kl}^{ij} = N_{1kl}^{ij} - N_{2kl}^{ij} \quad (2.47)$$

we use eqn. (2.42) to obtain for the double difference wide-lane (L5) observations

$$L_{5,kl}^{ij} = c \cdot \Delta\Delta\tau_{kl}^{ij} + N_{5kl}^{ij} \cdot \lambda_5^i + N_{1kl}^j \cdot \lambda_5^i \cdot \frac{\Delta\lambda_1^{ij}}{\lambda_1^i} - N_{2kl}^j \cdot \lambda_5^i \cdot \frac{\Delta\lambda_2^{ij}}{\lambda_2^i} \quad (2.48)$$

2. Modeling the GLONASS Observables

After the substitution

$$\lambda_5^i = \lambda_5^j + \Delta\lambda_5^{ij} \quad (2.49)$$

using the ratio (1.02) the double difference observation equation takes the form

$$L_{5,kl}^{ij} = c \cdot \Delta\Delta\tau_{kl}^{ij} + N_{5kl}^{ij} \cdot \lambda_5^i + N_{5kl}^j \cdot \Delta\lambda_5^{ij} . \quad (2.50)$$

In units of cycles of the wide-lane the single difference bias term (2.43) is given by

$$\frac{b_{5,kl}^{ij}}{\lambda_5^0} = \frac{\Delta\lambda_5^{ij}}{\lambda_5^0} \cdot N_{5kl}^j \quad (2.51)$$

with

$$\lambda_5^0 = \frac{c}{f_1^0 - f_2^0} = 0.84211365 \text{ m}$$

and depends on the wavelength difference of the two satellites and the single difference wide-lane ambiguity N_{5kl}^j . Relation (2.50) may be used to resolve the wide lane ambiguities N_{5kl}^{ij} , where the integer nature of these ambiguities is destroyed by the bias term (2.51).

If we write eqn. (2.45) in the form

$$\lambda_5^i = \lambda_1^i \cdot \frac{1}{1 - \frac{\lambda_1^i}{\lambda_2^i}} \quad (2.52)$$

the constant ratio (2.32) occurs in the expression and we obtain

$$\lambda_5^i = 4.5 \cdot \lambda_1^i \quad (2.53)$$

or, alternatively,

$$\lambda_5^i = 3.5 \cdot \lambda_2^i \quad (2.53)$$

which is true for the wavelengths of *all* satellites.

Using equation (2.53) results in

$$\frac{\Delta\lambda_5^{ij}}{\lambda_5^0} = \frac{\Delta\lambda_1^{ij}}{\lambda_1^0} . \quad (2.54)$$

The ratio (2.54) is important for the size of the bias term (2.51). Corresponding numerical values are the same for L1, L2 and L5 and are given in Table 2.02. It has to be mentioned, that Table 2.01 and Figure 1.01 are true for L1, L2 and L5 wavelengths, but the conversion of the maximum bias allowed for the single difference ambiguities in units of meter results in different numbers.

2.4.2 Ionosphere-free Linear Combination L3

As a good approximation the ionospheric propagation delay is proportional to the factor f^{-2} . Due to this fact the so-called *ionosphere-free* linear combination eliminates the ionospheric path delay (apart from higher order terms) and is defined by

$$\chi_{3,1} = \frac{f_1^{i^2}}{f_1^{i^2} - f_2^{i^2}} \quad \text{and} \quad \chi_{3,2} = \frac{-f_2^{i^2}}{f_1^{i^2} - f_2^{i^2}} \quad (2.55)$$

The ratio (1.02) leads to

$$\frac{f_1^2}{f_1^2 - f_2^2} = 2.53125 \quad (2.56)$$

and

$$\frac{f_2^2}{f_1^2 - f_2^2} = 1.53125 \quad (2.57)$$

for *all* GLONASS satellites.

We define the wavelength λ_3^i by

$$\lambda_3^i = \frac{c}{f_1^i + f_2^i} . \quad (2.58)$$

This wavelength λ_3^i is called *narrow-lane* and amounts to approximately 10 cm. After the substitution of N_2 by N_5 according to eqn. (2.47) and by using eqns. (2.42), (2.56), and (2.57) we may write the double difference L3 observation equation as

$$L_{3,kl}^{ij} = c \cdot \Delta\Delta\tau_{kl}^{ij} + c \cdot \frac{f_2^i}{f_1^{i^2} - f_2^{i^2}} \cdot N_{5kl}^{ij} + N_{1kl}^{ij} \cdot \lambda_3^i + N_{1kl}^j \cdot \Delta\lambda_3^{ij} + \frac{f_2^{i^2}}{f_1^{i^2} - f_2^{i^2}} \cdot N_{5kl}^j \cdot \Delta\lambda_2^{ij} . \quad (2.59)$$

The observation equation (2.59) may be used to resolve the double difference ambiguity N_{1kl}^{ij} , provided the double difference wide-lane ambiguity N_{5kl}^{ij} is known.

2. Modeling the GLONASS Observables

The single difference bias term (2.43) consists in case of the L3 linear combination of two parts requiring a priori information for the L1 and L5 single difference ambiguities N_{1kl}^j and N_{5kl}^j . The narrow lane bias term is given by

$$\frac{b_{3,kl}^j(1)}{\lambda_3^0} = \frac{\Delta\lambda_3^j}{\lambda_3^0} \cdot N_{1kl}^j \quad (2.60)$$

with

$$\lambda_3^0 = \frac{c}{f_1^0 + f_2^0} = 0.10526421 \text{ m.}$$

The definition of the narrow-lane wavelength in eqn. (2.58) and the ratio (1.02) give

$$\frac{\Delta\lambda_3^j}{\lambda_3^0} = \frac{\Delta\lambda_1^j}{\lambda_1^0} \quad (2.61)$$

According to relation (2.61) the numerical values of Table 2.02 and Figure 2.01 are true also for the bias $b_{3,kl}^j(1)$ if it is given in units of wavelength of the narrow-lane.

We write the second bias term in equation (2.59) in cycles of the narrow-lane and with the approximation (2.29) we obtain

$$\frac{b_{3,kl}^j(2)}{\lambda_3^0} \approx (i-j) \cdot \frac{\Delta\lambda_2}{\lambda_3^0} \cdot \underbrace{\frac{f_2^{i^2}}{f_1^{i^2} - f_2^{i^2}}}_{=-0.001229} \cdot N_{5kl}^j \quad (2.62)$$

This bias term depends on the wavelength difference between the two satellites and the single difference wide-lane ambiguity $N_{5,kl}^j$, but the numerical values of Table 2.02 cannot be used because of the factor -0.001229 in relation (2.62).

The L3 observable may be used in a parameter estimation to solve for the N_1 ambiguities if the known values of the N_5 ambiguities are introduced. In this case the second bias term is given by the N_5 ambiguities introduced which are not set up as unknown parameters in the normal equation system any longer. Therefore, the bias term cannot be changed or decreased by resolving more and more N_1 ambiguities. The effect of the bias term (2.62) on the estimation of the N_1 ambiguities is discussed in Chapter 4.

2.4.3 Geometry-free Linear Combination L4

The linear combination

$$L_4 = L_1 - L_2 \quad (2.63)$$

eliminates the geometry and the receiver and satellite clock. It contains only the ionospheric path delay and ambiguities and may, e.g., be used to determine ionospheric models.

2.4.4 Melbourne-Wübbena Linear Combination L6

The Melbourne-Wübbena linear combination is a combination of both, code and phase observations, and is given by

$$L_{6k}^i = \frac{1}{f_1^i - f_2^i} \cdot (f_1^i \cdot L_{1k}^i - f_2^i \cdot L_{2k}^i) - \frac{1}{f_1^i + f_2^i} \cdot (f_1^i \cdot P_1^i + f_2^i \cdot P_2^i). \quad (2.64)$$

The effects of the ionosphere, the geometry, the clocks and the troposphere are eliminated. We obtain for the

Zero Difference Observable

$$L_{6k}^i = \lambda_5^i \cdot N_{5k}^i \quad (2.65)$$

and

Double Difference Observable

$$L_{6kl}^j = \lambda_5^i \cdot N_{5kl}^j + \Delta\lambda_5^j \cdot N_{5kl}^j. \quad (2.66)$$

The double difference L6 linear combination is be used to solve for the wide-lane ambiguities N_{5kl}^j if high quality P-code observations are available. It can also be used for cycle slip detection in zero difference observations, but only the difference $N_{1k}^i - N_{2k}^i$ is checked in this way. The L6 double difference observable shows the same bias term as for the L5 linear combination.

A summary of constant ratios for the linear combinations is given in Table 2.03.

2. Modeling the GLONASS Observables

$\frac{\Delta\lambda_1}{\lambda_1^0} = \frac{\Delta\lambda_2}{\lambda_2^0} = \frac{\Delta\lambda_3}{\lambda_3^0} = \frac{\Delta\lambda_5}{\lambda_5^0} = -0.000351$	
$\frac{f_2}{f_1} = \frac{7}{9}$	$\frac{\lambda_2}{\lambda_1} = \frac{9}{7}$
$\frac{f_1^2}{f_1^2 - f_2^2} = 2.53125$	$\frac{f_2^2}{f_1^2 - f_2^2} = 1.53125$
$\lambda_1^0 = 0.18736366 \text{ m}$	$\Delta\lambda_1 = -65.7 \text{ }\mu\text{m}$
$\lambda_2^0 = 0.240603899 \text{ m}$	$\Delta\lambda_2 = -84.5 \text{ }\mu\text{m}$
$\lambda_3^0 = 0.10526421 \text{ m}$	$\Delta\lambda_3 = -36.9 \text{ }\mu\text{m}$
$\lambda_5^0 = 0.84211365 \text{ m}$	$\Delta\lambda_5 = -295.6 \text{ }\mu\text{m}$
$\lambda_5 = 4.5 \cdot \lambda_1$	$\lambda_5 = 3.5 \cdot \lambda_2$

Table 2.03: Summary of Constant Ratios between the GLONASS Wavelengths

3. Pre-Processing GLONASS Phase Observations

In order to use phase observations in a parameter estimation algorithm, they have to be checked for several types of data problems. Outliers have to be detected and marked. Phase jumps have to be reduced to a reasonable size due to numerical reasons. An observation with a cycle slip cannot simply be marked, because it affects all observations following the epoch where the slip occurred. It must be corrected or a new ambiguity parameter has to be set up. Cycle slip corrections have to be applied to the original observations L1 and L2. This must be accounted for when processing linear combinations.

3.1 Phase Jumps

This Section deals with a jump in the carrier phase observable for all satellites observed simultaneously. Two events have to be distinguished:

1) Clock Jump

A jump of the receiver clock will affect the observations of all satellites observed by a common offset (in units of meters). Such jumps in the phase observations are eliminated when forming double difference observables (as can be seen in eqn. (2.22)). Because a clock jump may amount to thousands of km (when multiplied with the speed of light c), it may lead to numerical problems in the least squares adjustment. Therefore, approximate corrections have to be applied to the phase observations. The same correction in meters has to be applied to all satellites.

2) Loss of Lock for all Satellites

A loss of lock of the receiver phase tracking loop causes a jump in the carrier phase observable of an integer number of cycles, called a „cycle slip“. The fractional part of the phase observable is not affected by cycle slips, but after the jump all observations are shifted by the same integer number of cycles. In this Section we assume a cycle slip in the observations of all satellites simultaneously observed. The general case of a cycle slip will be discussed in Section 3.2.

A clock jump as well as a loss of lock for all satellites lead to a jump in the phase observations for all satellites, but the true event cannot be reconstructed. Therefore, a method has to be found in order to account for both events and we have to distinguish between GPS and GLONASS.

Phase Jump in GPS Observations

The GPS phase observations to all satellites have to be corrected after a phase jump by a fixed number of cycles. Because all satellites show the same carrier frequency, the correction is the same in meters, too. This correction is an approximation only. It has the goal to avoid numerical problems in the least squares adjustment. The correct size of the phase jump cannot be determined precisely on the zero difference level due to the existing biases. A possible error of the approximation will cancel out on the double difference level.

Phase Jump in GLONASS Observations

The satellite specific frequencies of GLONASS satellites lead to different corrections in meters if a fixed number of wavelengths is applied to all satellites. Again, the correction applied to the zero difference observation is an approximation due to several biases. The error of this approximation is not eliminated on the double difference level for GLONASS satellites due to the single difference bias term (see eqn. (2.24)). Therefore, the ambiguities have to be initialised for all GLONASS satellites after a phase jump.

3.2 Cycle Slips

A cycle slip is caused by the loss of lock of the receiver phase tracking loop. In this section we deal with cycle slips occurring for a single satellite. In the case of a cycle slip the ambiguity parameters N_{kl}^i in eqn. (2.12) for two epochs t_1 before the slip and t_2 after the slip are different:

$$N_{kl}^i(t_2) \neq N_{kl}^i(t_1) \quad (3.01)$$

When performing a least squares adjustment of triple difference observations, a cycle slip affects only one triple difference observation and not all triple differences after the slip. One makes use of this fact when triple difference residuals are analysed for cycle slip detection.

The satellite-specific frequencies require that

$$\begin{aligned} &\text{cycle slips have to be recovered correctly on the single difference level} && (3.02) \\ &\text{for GLONASS observations.} \end{aligned}$$

In the following we account for the satellite-specific frequencies in the triple difference residuals in case of a cycle slip. In section 3.2.1 we discuss the usage of triple difference residuals for cycle slip detection. We will see that assumption (3.02) may not be fulfilled. In Section 3.2.2 we define a new type of single difference phase observation for the purpose of

cycle slip detection. This new observation type will be used in a first step to obtain “modified” triple difference observations in Section 3.2.2.1. Some advantages will be seen in this attempt compared to the triple difference observation of Section 2.3.4, but assumption (3.02) cannot be met either. In a second step we use the new type of single difference observation for a new cycle slip detection algorithm. This algorithm is described in Section 3.2.2.2 and was implemented in our software.

3.2.1 Cycle Slips in the Triple Difference Phase Observable

Some cycle slip detection algorithms make use of the fact that cycle slips show up as outliers in time series of triple difference residuals. Let us now assume that a cycle slip occurred between epochs t_1 and t_2 .

Triple difference observations are defined in eqn. (2.34) with the assumption that the ambiguity parameter N_{kl}^i did not change during the time interval $[t_1, t_2]$. Now we assume that eqn. (3.01) holds and use the double difference phase observations (2.22) for the epochs t_1 and t_2 to form the triple difference observation equation

$$\Delta\Delta\Delta\Psi_{kl}^{ij}(t_1, t_2) = c \cdot \Delta\Delta\Delta\tau_{kl}^{ij}(t_1, t_2) + b^i \cdot \lambda^i - b^j \cdot \lambda^j \quad (3.03)$$

with

$$\begin{aligned} b^i &= N_{kl}^i(t_2) - N_{kl}^i(t_1) \\ b^j &= N_{kl}^j(t_2) - N_{kl}^j(t_1) \end{aligned} .$$

The least squares adjustment of triple difference observations (3.03) generates residuals close to zero for epochs without cycle slips ($b^i = b^j = 0$). Epochs with cycle slips show up as outliers. We may now write equation (3.03) as

$$\Delta\Delta\Delta\Psi_{kl}^{ij}(t_1, t_2) = c \cdot \Delta\Delta\Delta\tau_{kl}^{ij}(t_1, t_2) + (b^i - b^j) \cdot \lambda^i + b^j \cdot \Delta\lambda^{ij} . \quad (3.04)$$

The triple difference residual $\Delta\Delta\Delta r_{kl}^{ij}(t_1, t_2)$ is defined as

$$\Delta\Delta\Delta r_{kl}^{ij}(t_1, t_2) = \Delta\Delta\Delta\hat{\Psi}_{kl}^{ij}(t_1, t_2) - \Delta\Delta\Delta\Psi_{kl}^{ij}(t_1, t_2) \quad (3.05)$$

with

$$\Delta\Delta\Delta\hat{\Psi}_{kl}^{ij}(t_1, t_2) \quad : \text{ estimate of the expected value of } \Delta\Delta\Delta\Psi_{kl}^{ij}(t_1, t_2)$$

and we obtain from eqn. (3.04)

$$\Delta\Delta\Delta r_{kl}^{ij}(t_1, t_2) = (b^i - b^j) \cdot \lambda^i + b^j \cdot \Delta\lambda^{ij} . \quad (3.06)$$

Eqn. (3.06) cannot be used to determine both, b^i and b^j , because the wavelength difference $\Delta\lambda^{ij}$ may be very small. Also, the difference $(b^i - b^j)$ cannot easily be solved for, because it

Example	b^i	b^j	$\Delta\Delta\Delta r_{kl}^{ij}(t_1, t_2)$
1	1	0	λ^i
2	0	-1	$\lambda^i - \Delta\lambda^{ij}$
3	1	1	$\Delta\lambda^{ij}$

Table 3.01: Examples for Cycle Slips in Triple Difference Residuals

is biased by the term $b^j \cdot \Delta\lambda^{ij}$, if $\Delta\lambda^{ij} \neq 0$. If $\Delta\lambda^{ij} = 0$, e.g., for GPS observations, one satellite may be selected as reference and the difference $(b^i - b^j)$ may be determined. The resulting difference may then be applied to satellite i or j , because both have the same wavelength.

Table 3.01 shows three examples of different cycle slip events. The observation noise and other errors are neglected in Table 3.01. The examples lead to the following conclusions:

No Assignment to Single Difference

If we assume that the noise level of the observations in examples 1 and 2 is low, we may easily detect the cycle slip of 1 cycle in the triple difference residuals for example 1 and 2. But the cycle slips cannot be assigned to the correct single difference observation, because the cycle slips in examples 1 and 2 only differ by $\Delta\lambda^{ij}$. This difference may be smaller than the observation noise.

If a cycle slip b^i for satellite i is applied to satellite j by mistake, all double difference observations between satellites i and j will be shifted after the cycle slip by the term $b^i \cdot \Delta\lambda^{ij}$. This happens when a slip of type 1 (Table 3.01) occurred but the correction was applied to the wrong satellite (example 2).

Undetected Cycle Slips

If both satellites, i **and** j , suffer from a cycle slip of the same size in one epoch, it may not be detected by analysing the triple difference residuals, as can be seen in example 3. The size of the residual does not significantly differ from zero. But the undetected slip leads to a systematic shift of $b^i \cdot \Delta\lambda^{ij}$ in the double difference observations.

A method has to be developed to assign detected cycle slips to the correct single difference observations. The problem of cycles slips of the same size referring to two satellites has to be solved to avoid systematic errors. As there is no a priori information available for b^i its size

may reach several hundred thousand cycles and may result in very large systematic errors $b^i \cdot \Delta\lambda^i$. As long as both, b^i and b^j , are unknown, eqn. (3.06) cannot be used for cycle slip detection purposes. If one of the cycle slips b^i or b^j would be known (e.g., if it is equal to zero), the second cycle slip could be detected and assigned to the correct single difference observation. However, also the selection of satellites which have no cycle slip at a common epoch is not trivial as we see from example 3 of Table 3.01. Let us define a new type of difference to address this problem.

3.2.2 Single Difference Phase Observable Differenced in Time

We form a new type of difference starting from the single difference phase observable (2.20)

$$\Delta\Delta\Psi_{kl}^i(t_1, t_2) = c \cdot \Delta\Delta\tau_{kl}^i(t_1, t_2) + c \cdot \Delta\Delta t_{kl}(t_1, t_2) \quad (3.07)$$

with

$$\begin{aligned} \Delta\Delta\Psi_{kl}^i(t_1, t_2) &= \Delta\Psi_{kl}^i(t_2) - \Delta\Psi_{kl}^i(t_1) \\ \Delta\Delta\tau_{kl}^i(t_1, t_2) &= \Delta\tau_{kl}^i(t_2) - \Delta\tau_{kl}^i(t_1) \\ \Delta\Delta t_{kl}^i(t_1, t_2) &= \Delta t_{kl}^i(t_2) - \Delta t_{kl}^i(t_1), \end{aligned}$$

called a single difference phase observable “differenced in time”. The residuals derived from the observation type (3.07) may be interpreted as sum of a possible cycle slip b^i and the change of the receiver clock in the time interval $[t_1, t_2]$, neglecting other error sources. We may thus write

$$\Delta\Delta r_{kl}^i(t_1, t_2) = b_i \cdot \lambda^i + c \cdot \Delta\Delta t_{kl}(t_1, t_2). \quad (3.08)$$

This residual can be expressed in cycles of satellite i and shows the integer nature of the cycle slip b^i , but it is biased by the receiver clock change. If the receiver clock change would be known to a few cm, eqn. (3.08) could be used directly to detect cycle slips. This will be discussed in Section 3.2.2.2. The receiver clock term derived from code measurements (single point positioning) shows an error of a few nanoseconds or some tens of cycles (a few 0.1 μ sec or some hundreds of cycles for GPS due to Selected Availability) and is certainly not good enough. In the following two sections we use the residuals (3.08) for two cycle slip detection approaches.

3.2.2.1 Modified Triple Difference Phase Residual

Using the residuals (3.08) for satellite i and j we may compute a new type of “triple difference”:

$$\frac{\Delta\Delta r_{kl}^i(t_1, t_2)}{\lambda^i} - \frac{\Delta\Delta r_{kl}^j(t_1, t_2)}{\lambda^j} = b_i - b_j - (i - j) \cdot \Delta f \cdot \Delta\Delta t_{kl}(t_1, t_2) \quad (3.09)$$

An attempt can be made to use eqn. (3.09) for the detection of cycle slip differences ($b^i - b^j$). However, the integer nature of the cycle slips will be biased by the receiver clock term $(i - j) \cdot \Delta f \cdot \Delta\Delta t_{kl}(t_1, t_2)$. The clock bias term is not depending on the unknown size of b^i . This is certainly an advantage compared to the bias term $b^i \cdot \Delta\lambda^{ij}$ in eqn. (3.06). Furthermore, the receiver clock term in eqn. (3.09) is obviously much smaller than the clock term in eqn. (3.08). It is reduced by a factor of approximately $(i - j) \cdot 3 \cdot 10^{-3}$ if both clock terms are converted into units of cycles. Assuming that the receiver clock change $\Delta\Delta t_{kl}(t_1, t_2)$ is known to about $0.1 \mu\text{sec}$ the clock bias term in eqn. (3.09) ranges between 0.06 and 1.3 cycles for L1 frequencies. Figure 3.01 shows the size of the term for all frequency differences $(i - j)$.

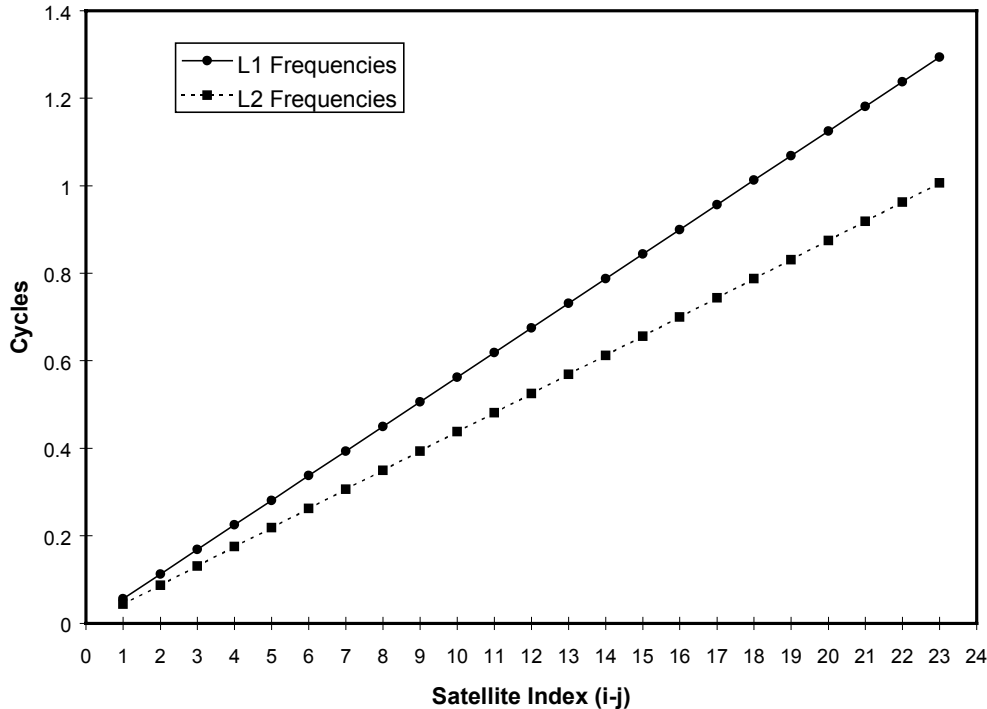


Figure 3.01: Receiver clock term $(i - j) \cdot \Delta f \cdot \Delta\Delta t_{kl}(t_1, t_2)$ assuming that $\Delta\Delta t_{kl}(t_1, t_2) = 0.1 \mu\text{sec}$

From eqn. (3.09) and Figure 3.01 we conclude:

- Equation (3.09) cannot be used for the determination of the differences $(b^i - b^j)$ because of the clock bias term.
- Equation (3.09) cannot be used for the assignment of cycle slips to the correct satellite or single difference.

3.2.2.2 Cycle Slip Detection Algorithm

We have seen in Section 3.2.1 that the triple difference residuals (3.06) cannot be used to detect all possible cycle slips and to correct them on the single difference level. Also, the modified triple difference residuals in eqn. (3.09) do not meet this requirements. However, the single difference residuals “differenced in time” (3.08) may be used to detect a cycle slip on the single difference level by computing

$$b^i = \frac{\Delta\Delta r_{kl}^i(t_1, t_2)}{\lambda^i} - f^i \cdot \Delta\Delta t_{kl}(t_1, t_2) \quad (3.10)$$

provided the receiver clock change is known exactly. In order to keep the receiver clock term $f^i \cdot \Delta\Delta t_{kl}(t_1, t_2)$ smaller than 0.1 cycles, $\Delta\Delta t_{kl}(t_1, t_2)$ has to be determined with a precision of $6 \cdot 10^{-11}$ sec (or a few cm in units of length).

In our approach we determine an estimate of the receiver clock change for every epoch. Therefore, we compute first the single difference residuals (3.08) “differenced in time” for all satellites of a common epoch. For those satellites which did not experience a cycle slip between epoch t_1 and epoch t_2 , the residuals $\Delta\Delta r_{kl}^i(t_1, t_2)$ directly give an estimate of the receiver clock term. With a majority voting procedure using the residuals $\Delta\Delta r_{kl}^i(t_1, t_2)$ from all satellites we detect and mark satellites obviously suffering from a cycle slip between t_1 and t_2 . The mean value of the residuals $\Delta\Delta r_{kl}^i(t_2 - t_1)$ of the “clean” satellites is used to estimate the receiver clock term:

$$\Delta\Delta \bar{t}_{kl}(t_1, t_2) = \frac{\sum_{i=1}^n \Delta\Delta r_{kl}^i(t_1, t_2)}{n} \quad (3.11)$$

with

- $\Delta\Delta \bar{t}_{kl}(t_1, t_2)$: estimated value for $\Delta\Delta t_{kl}(t_1, t_2)$
 n : number of satellites with obviously no cycle slip.

3. Pre-Processing GLONASS Phase Observations

New ambiguities for all satellites are introduced if the number n of “clean” satellites is lower than two. Using eqn. (3.10) for each satellite with the receiver clock estimate $\Delta\Delta\bar{t}_{kl}(t_1, t_2)$ the cycle slip

$$b^i = \frac{\Delta\Delta r_{kl}^i(t_1, t_2)}{\lambda^i} - f^i \cdot \Delta\Delta\bar{t}_{kl}(t_1, t_2) \quad (3.12)$$

may be detected and assigned to the correct satellite. This approach can also be used for GPS and combined GLONASS/GPS observations.

4. Ambiguity Resolution

Various approaches were proposed in the last few years to resolve the carrier phase ambiguities for GLONASS and combined GLONASS/GPS measurements. [Rossbach *et al.*, 1996] developed a method for combined GLONASS/GPS ambiguity resolution by introducing an auxiliary wavelength into the double difference observation equation. This new wavelength has to be an integer multiple of each of the two wavelengths used when forming double difference observations. This method may be used for GPS as well as for GLONASS and GLONASS/GPS combinations, because the single difference bias term is eliminated in all cases. The wavelength for a GLONASS/GLONASS double difference is about 65 μm and for a GLONASS/GPS double difference about 0.8 μm (for L1). It is thus impossible to assign the ambiguities to integers in the case of GLONASS-GLONASS or GLONASS-GPS combinations. Uncertainties of thousands resp. hundreds of cycles would remain in those cases. [Landau, 1999] assumed that the GLONASS single difference ambiguities may be determined with sufficient accuracy from the difference between code and phase single difference observations. These single difference ambiguities would cause a single difference bias term of the order of 1.6 mm for the largest wavelength difference between two GLONASS satellites and the double difference ambiguities could be resolved according to the methods used for GPS observations. [Walsh *et al.*, 1996] developed a method to resolve GLONASS and GPS ambiguities using a search strategy. Initial calibration values for the receiver channel delays are computed by performing a “GPS-only” solution. Once these calibration values are known, the ambiguity search strategy can be used for combined GLONASS/GPS observations.

Here we develop an ambiguity resolution approach well suited for long observation sessions and for long as well as short baselines. We process double difference phase observations in an iterative approach to solve one double difference ambiguity in each iteration step. The strategy cannot be used for fast ambiguity resolution (like “on the fly”, “rapid static”, or “search strategy”) of short observation sessions.

4.1 Ambiguity Parameters

The processing strategy described here is realized in, e.g., the Bernese GPS Software. In our strategy we have to account for the single difference bias term in the double difference observations. There are other approaches using single difference observations in the processing. In this case an additional receiver clock term has to be estimated to account for satellite specific frequencies.

Ambiguity resolution using double difference phase observations in the case of GPS implies that one single difference ambiguity is selected as reference ambiguity and that only double difference ambiguities N_{kl}^{ij} , as defined in eqn. (2.24), are fixed to integer numbers. For the reference single difference ambiguity N_{kl}^j an approximate value may be used. The approximate reference ambiguity has no effect on the double difference level. This can be seen in eqn. (2.24) if $\Delta\lambda^{ij} = 0$. No attempt has to be made or can be made to improve the reference single difference ambiguity during the parameter estimation process.

In Chapter 2 we have seen that a single difference bias term shows up in the observation equation (2.24) for GLONASS double difference phase observations because of the satellite-specific wavelengths. An error in the a-priori value of the single difference ambiguity N_{kl}^j is not completely eliminated on the double difference level. It contributes to the bias term (2.27) and destroys the integer nature of the double difference ambiguity N_{kl}^{ij} . As a *first consequence* we are not allowed to fix the reference single difference ambiguity to an a priori value. It has to be set up as an unknown parameter in the normal equation system and the system becomes singular. As a *second consequence* of the bias term the wavelength difference $\Delta\lambda^{ij}$ of the satellite i and j has to be taken into consideration. For small $\Delta\lambda^{ij}$ and an error in the single difference ambiguities smaller than approximately 300 cycles the bias term is very small and only slightly affects the integer nature of the ambiguities N_{kl}^{ij} (see Table 2.02). Satellite pairs (i,j) with a small $\Delta\lambda^{ij}$ therefore, have to be selected when resolving the first few double difference ambiguities N_{kl}^{ij} . If one ambiguity N_{kl}^{ij} is resolved, it is eliminated from the normal equation system and a new solution is estimated. If $\Delta\lambda^{ij}$ was not equal to zero for the resolved ambiguity, the bias term contributes to an improved estimation of the single difference ambiguity N_{kl}^j and this may allow it to resolve double difference ambiguities N_{kl}^{ij} with a larger $\Delta\lambda^{ij}$.

It is possible to improve the single difference ambiguity in the parameter estimation process using double difference observations only in the case of satellite-specific wavelengths, but not for „GPS only“ observations. The bias term makes the ambiguity resolution more complicated in comparison to GPS but it allows the improvement of the single difference ambiguities as a new feature. The following paragraphs deal with the ambiguity resolution approach in more detail.

Normal Equation System

If n satellites have been observed, we have to set up n single difference ambiguities N_{kl}^j (assuming for simplicity that each satellite has only one ambiguity). Using double difference phase observations only, the resulting normal equation system will be singular.

Three methods may be used in the case of GPS to remove the singularity:

1) *One* single difference ambiguity may be eliminated from the normal equation system or not set up from the very beginning and the normal equation system becomes regular. For the selected reference ambiguity an a priori value is used in all computations. The remaining $n-1$ ambiguity parameters may then be estimated and, possibly, fixed to integers.

2) The second approach removes the singularity by putting an a priori constraint (e.g., 300 cycles) on all single difference ambiguity parameters by introducing an artificial observation of the type $N_{kl}^j = 0$ with a small weight. In the first solution the RMS error of the estimated single difference ambiguities is determined by the value of the a priori constraint. At most $n-1$ single difference ambiguities can then be fixed to integers (on the double difference level) and *one* single difference ambiguity remains unresolved in the normal equation system. The remaining ambiguity will be estimated as a real value. No attempt can be made for GPS observations to resolve the remaining single difference ambiguity to an integer number.

3) In the third method the phase observations are processed simultaneously with code observations with a weight ratio between code and phase observations of, e.g., 0.0001 . The code observations regularize the normal equation system and the combined code/phase normal equation matrix may be inverted. In the first solution the RMS error of the estimated single difference ambiguities is determined by the noise of the code observations and the weight ratio between code and phase observations. The single difference ambiguities can be solved for as in method 2).

In the case of GLONASS observations the first method cannot be used. Due to the single difference bias term we are not allowed to eliminate a single difference ambiguity from the normal equation system. But the second and the third approach are candidate methods for ambiguity resolution even in the case of GLONASS. As soon as the first ambiguity N_{kl}^{ij} with $\Delta\lambda^{ij} \neq 0$ is successfully resolved to an integer value, the NEQ system becomes regular.

Initialization of the Single Difference Ambiguities

Let us now describe the ambiguity resolution for the original L1 and L2 carriers and for the L5 linear combination (see Section 2.4.1). The effect of the additional bias term (2.64) on the L3 linear combination will be discussed separately.

Good initial values for the single difference ambiguities N_{kl}^j are required to resolve a first GLONASS ambiguity N_{kl}^{ij} with $\Delta\lambda \neq 0$. Table 2.02 shows maximum errors we may accept in

4. Ambiguity Resolution

the a priori values of N_{kl}^j in order to ensure that the bias b_{kl}^j is smaller than 0.1 cycles, a prerequisite to allow the resolution of double difference ambiguities N_{kl}^j .

The following biases affect the initialization of the N_{kl}^j ambiguity terms:

1) Receiver Position Error and Orbit Error

The a priori values for N_{kl}^j are computed from the receiver-satellite distances using the a priori positions of the receivers and the a priori satellite orbits. The resulting errors in N_{kl}^j are different for the individual satellites. Three interesting aspects are:

- N_{kl}^i, N_{kl}^j are mainly affected by the *difference* between the position errors of the receivers k and l , i.e, the error in the *relative* position of the receivers.
- The receiver position error decreases below 1 m (≈ 5 cycles for L1) after carrying out a phase triple difference solution for short baselines.
- The effect of the satellite position error on N_{kl}^j increases with increasing baseline length.

2) Receiver Clock Error

A receiver clock error affects the determination of an a priori value for N_{kl}^j . The single difference ambiguities of all satellites are biased by the same amount (in units of length). Expressed in cycles, the bias is different for individual satellites. If we use code observations to determine and eliminate the receiver clock synchronization error, the size of the remaining synchronization error is of the order of 10 to 50 cycles (100 to 200 cycles for GPS).

3) Ionospheric and Tropospheric Correction Error

This bias depends on the quality of the models used. For short baselines we may neglect this bias.

The receiver clock error is the most important bias affecting the initialization of the single difference ambiguities N_{kl}^j . In summary, two important aspects should be mentioned concerning the quality of the initialization:

- Double difference ambiguities of satellite pairs with small wavelength differences are less sensitive to errors of the initialization of the single difference ambiguities.
- Using an external frequency standard for GLONASS receivers may reduce the initialization error.

4.2 Ambiguity Resolution Algorithm

Our algorithm consists of 7 steps. The ambiguities are resolved iteratively, one ambiguity N_{kl}^{ij} in each iteration step.

Step 1) Parameter Setup

For n satellites n single difference ambiguities N_{kl}^j are set up as unknown parameters in the normal equation system, assuming that there are no breaks or problems in the data forcing us to set up additional ambiguities. The normal equation system will be singular if double difference observations are used. The normal equation system will also be singular, if single difference observations are processed, because an additional receiver clock correction has to be estimated for each epoch.

Step 2) Removal of Singularity

After introducing an a priori constraint (e.g., 300 cycles) for each N_{kl}^j or combining phase and code observations, the normal equation matrix becomes regular and may be inverted.

Step 3) Estimation of Single Difference Ambiguities

After the normal equation system is solved the ambiguities are estimated as real values. These estimates show large formal errors, depending on the a priori constraints or on the noise of the code observations and the relative weighting of code and phase observations.

Step 4) Computation of Double Difference Ambiguities

Using the estimated single difference ambiguities N_{kl}^j and their covariance matrix Q , all possible double difference ambiguities N_{kl}^{ij} are computed with the corresponding formal errors

$$m_{ij} = \sigma_0 \sqrt{Q_{ii} - 2 \cdot Q_{ij} + Q_{jj}}, \quad (4.01)$$

where σ_0^2 is the a posteriori variance factor.

The formal errors m_{ij} of the double difference ambiguities N_{kl}^{ij} are small compared to those of the single difference ambiguities. They are highly correlated with the wavelength difference of the two satellites involved in the double difference ambiguities. Small wavelength differences lead to small m_{ij} values. This can be shown as follows:

4. Ambiguity Resolution

According to the double difference observation equation (2.22) the first design matrix A for the estimation of two single difference ambiguities N_{kl}^i and N_{kl}^j with n double difference observations may be written as :

$$A = \begin{bmatrix} \lambda_1^i & -\lambda_1^j \\ \vdots & \vdots \\ \lambda_n^i & -\lambda_n^j \end{bmatrix} \quad (4.02)$$

The a posteriori covariance matrix Q of the *single difference* ambiguities is given by

$$Q = (A^T P A)^{-1} \quad (4.03)$$

with

$$A^T P A = \begin{bmatrix} n \cdot \lambda^i{}^2 & -n \cdot \lambda^i \cdot \lambda^j \\ -n \cdot \lambda^i \cdot \lambda^j & n \cdot \lambda^j{}^2 \end{bmatrix}.$$

Introducing the constraint $N_{kl}^i = N_{kl}^j = 0$ with the weight

$$w = \left| \frac{\sigma_{apr}}{\sigma_{amb}} \right|^2 \quad (4.04)$$

σ_{apr} = a priori sigma for phase observations

σ_{amb} = a priori constraint for each single difference ambiguity

leads to the normal equation matrix

$$(A^T P A)^+ = n \cdot \begin{bmatrix} (\lambda^i{}^2 + \frac{w}{n}) & (-\lambda^i \cdot \lambda^j) \\ (-\lambda^i \cdot \lambda^j) & (\lambda^j{}^2 + \frac{w}{n}) \end{bmatrix} \quad (4.05)$$

which would be singular, without the constraints introduced.

The corresponding covariance matrix Q^+ results in:

$$Q^+ = \frac{1}{w \cdot (\lambda^i{}^2 + \lambda^j{}^2 + \frac{w}{n})} \cdot \begin{bmatrix} (\lambda^i{}^2 + \frac{w}{n}) & (\lambda^i \cdot \lambda^j) \\ (\lambda^i \cdot \lambda^j) & (\lambda^i{}^2 + \frac{w}{n}) \end{bmatrix}. \quad (4.06)$$

Q^+ has to be used for the computation of the formal errors m_{ij} in eqn. (4.01). With the substitution (2.23) the formal error of the *double difference* ambiguities is given by:

$$m_{ij} = \sigma_0 \cdot \sqrt{\frac{\Delta\lambda^{ij^2} + 2 \cdot \frac{w}{n}}{w \cdot (\lambda^i + \lambda^j + \frac{w}{n})}} \quad (4.07)$$

We conclude from formula (4.07) that the formal error m_{ij} is approximately linear in the wavelength difference $\Delta\lambda^{ij}$

$$m_{ij} \underset{approx.}{\sim} \Delta\lambda^{ij}. \quad (4.08)$$

The single difference bias term b_{kl}^{ij} is linear in $\Delta\lambda^{ij}$, also. Thus the formal error of the double difference ambiguities m_{ij} is affected by the single difference bias term and increases with increasing wavelength differences $\Delta\lambda^{ij}$.

Step 5) Fixing of *one* Double Difference Ambiguity

After the computation of all possible double difference ambiguities and their formal errors, a first double difference ambiguity parameter is fixed to an integer number, according to specified resolution criteria (see, e.g., [Beutler et al., 1996]). The correct integer number may be found if the single difference bias term is small, e.g., if the wavelength difference of the two satellites is small. According to formula (4.08) we will find small formal errors m_{ij} for small wavelength differences $\Delta\lambda^{ij}$. We may thus order the double difference ambiguities with increasing formal errors and start with the best determined double difference ambiguity.

This strategy is used for both, GLONASS and GPS observations.

Step 6) Elimination of *one* Single Difference Ambiguity

After fixing the first double difference ambiguity, one of the two single difference ambiguities involved in the double difference ambiguity may be eliminated from the normal equation system, taking into account the known double difference ambiguity.

Now we may distinguish two cases:

- 1) $\Delta\lambda^{ij} = 0$ in all iterations performed so far:

The normal equation system is still singular. The formal errors of the single difference ambiguities of the next iteration have approximately the same size as in the last iteration.

4. Ambiguity Resolution

2) $\Delta\lambda^{ij} \neq 0$ in at least one of the iterations performed so far:

The normal equation system is now regular even without constraints. The formal errors of the single difference ambiguities will decrease significantly in the next iteration.

After the elimination of the resolved ambiguity from the normal equation system the normal equation system is solved and next iteration step starts. After carrying out steps 3) to 5), the next ambiguity may be resolved and step 6) is performed again. Following this scheme, $n-1$ double difference ambiguities N_{kl}^{ij} may be resolved and $n-1$ single difference ambiguities may be eliminated from the normal equation system. The formal errors of the single difference ambiguities are reduced after each ambiguity with $\Delta\lambda^{ij} \neq 0$ that has successfully been resolved. If only one single difference ambiguity N_{kl}^j remains unresolved, this may be fixed to an integer number on the single difference level or it remains as an unknown parameter in the normal equation system. The resolution of the remaining ambiguity on the single difference level cannot be performed for „GPS only“ observations.

Step 7) Final Parameter Estimation

In the final solution the unresolved single difference ambiguities N_{kl}^j are estimated as real values.

All steps of the new approach are summarized in Figure 4.01.

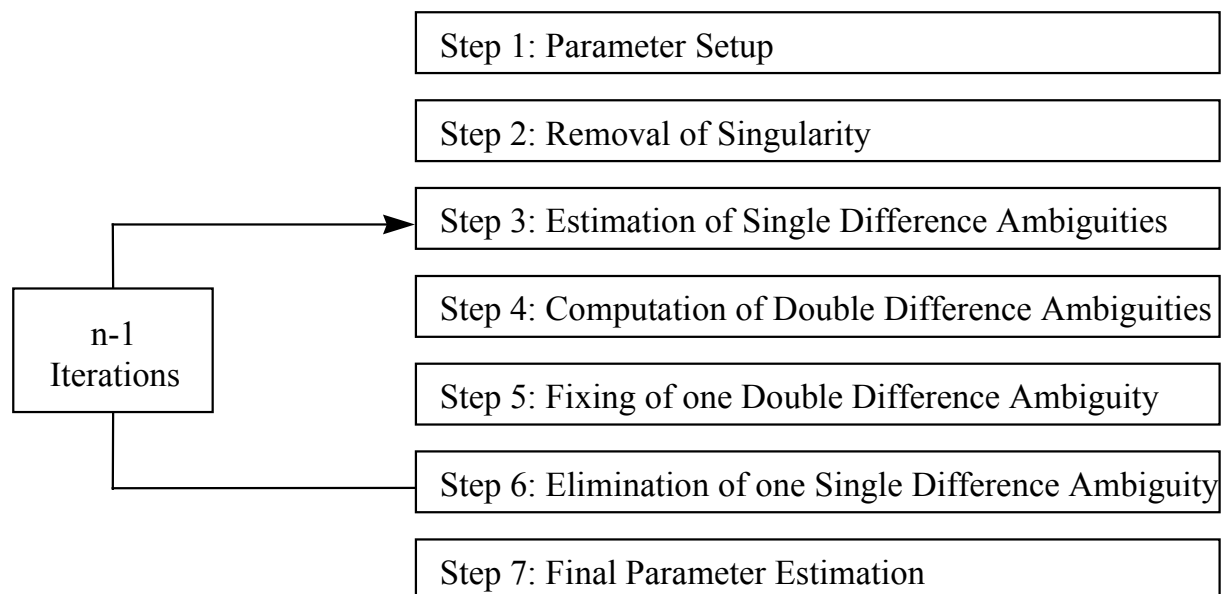


Figure 4.01: Scheme of Ambiguity Resolution Algorithm

4.3 Ambiguity Resolution for Linear Combinations

The ambiguity resolution algorithm outlined above is required due to the bias term in the double difference phase observation equation. As shown in Chapter 2, the size of the bias term is the same for L1, L2 and L5 observations, if the bias term is expressed in units of the corresponding wavelengths λ_1^0 , λ_2^0 and λ_5^0 . The ambiguity resolution algorithm as described in Section 4.2 obviously may be used for all the linear combinations L1, L2 and L5. However, if phase observations of the L3 linear combination are processed and wide-lane ambiguities N_{5kl}^j are introduced the additional bias term (2.62) has to be considered.

In order to study the effect of this additional bias term on the ambiguity resolution we write the double difference observation equation (2.59) for the ionosphere-free linear combinations in the form

$$L_{3,kl}^{ij} = c \cdot \Delta\Delta\tau_{kl}^{ij} + \lambda_3^i \cdot \frac{\lambda_5^i}{\lambda_2^i} \cdot N_{5kl}^{ij} + N_{1kl}^{ij} \cdot \lambda_3^i + \lambda_3^i \cdot \frac{\lambda_5^i}{\lambda_2^i} \cdot N_{5kl}^j \cdot \Delta\lambda_2^{ij} + N_{1kl}^j \cdot \Delta\lambda_3^{ij}, \quad (4.09)$$

where the wavelength definitions (2.45) and (2.58) were used.

The ratios (1.02), (2.33), (2.53) and (2.61) give

$$L_{3,kl}^{ij} = c \cdot \Delta\Delta\tau_{kl}^{ij} + (N_{1kl}^{ij} + 3.5 \cdot N_{5kl}^{ij}) \cdot \lambda_3^i + (N_{1kl}^j + 3.5 \cdot N_{5kl}^j) \cdot \Delta\lambda_3^{ij}. \quad (4.10)$$

The definition of the new parameter type \tilde{N}_{1kl}^i

$$\tilde{N}_{1kl}^j = N_{1kl}^j + 3.5 \cdot N_{5kl}^j \quad (4.11)$$

and the difference

$$\tilde{N}_{1kl}^{ij} = \tilde{N}_{1kl}^i - \tilde{N}_{1kl}^j \quad (4.12)$$

is used for substitution in eqn. (4.10) and results in

$$L_{3,kl}^{ij} = c \cdot \Delta\Delta\tau_{kl}^{ij} + \tilde{N}_{1kl}^{ij} \cdot \lambda_3^i + \tilde{N}_{1kl}^j \cdot \Delta\lambda_3^{ij}. \quad (4.13)$$

The double difference L3 observation equation (4.13) shows up in the same form as the L1, L2 and L5 quantities. It may be used for resolving the double difference ambiguities \tilde{N}_{1kl}^{ij} using the narrow-lane wavelength, where the integer nature of the ambiguities \tilde{N}_{1kl}^{ij} is biased by the term $\tilde{N}_{1kl}^j \cdot \Delta\lambda_3^{ij}$. If we introduce the wide-lane single difference ambiguities N_{5kl}^j as

4. Ambiguity Resolution

known parameters into a least squares adjustment of the single difference ambiguities \tilde{N}_{1kl}^j , the substitution (4.11) may be used to compute the L1 single difference ambiguities N_{1kl}^j and the double difference ambiguities N_{1kl}^{ij} .

An error of the wide-lane ambiguities N_{5kl}^j introduced will affect the resulting L1 ambiguities N_{1kl}^j and N_{1kl}^{ij} . In the following we distinguish between two cases for an error of the wide-lane ambiguities introduced:

1) Correct Wide-Lane Single Difference Ambiguities N_{5kl}^j introduced

If the wide-lane ambiguities N_{5kl}^j introduced are correct on the single difference level the term $3.5 \cdot N_{5kl}^j$ in eqn. (4.11) is equal to zero in the normal equation system and we obtain

$$\tilde{N}_{1kl}^j = N_{1kl}^j \quad (4.14)$$

and for the single difference bias term in eqn. (4.13) in units of wavelengths of λ_3^0

$$\tilde{N}_{1kl}^j \cdot \frac{\Delta\lambda_3^{ij}}{\lambda_3^0} = N_{1kl}^j \cdot \frac{\Delta\lambda_3^{ij}}{\lambda_3^0}. \quad (4.15)$$

With eqn. (2.61) the value of the single difference bias term (4.15) is the same in the L1, L2, L3 and L5 quantities in units of the corresponding wavelengths $\lambda_1^0, \lambda_2^0, \lambda_3^0$ and λ_5^0 and is given in Table 2.02 and Figure 2.01. The ambiguity resolution approach as described in Section 4.2 and the substitution (4.11) may be used to resolve the double difference ambiguities N_{1kl}^{ij} and possibly the single difference ambiguities N_{1kl}^j .

2) Correct Wide-Lane Double Difference Ambiguities N_{5kl}^{ij} introduced

Let us assume that the single difference wide-lane ambiguities N_{5kl}^j introduced into the normal equation system are wrong but that all single-difference ambiguities N_{5kl}^j are biased by the same error in units of wavelengths of the wide-lane. In this case the error of the single difference ambiguities N_{5kl}^j is eliminated on the double difference level and we obtain

$$\tilde{N}_{1kl}^{ij} = N_{1kl}^{ij}. \quad (4.16)$$

This is the case if we have processed the wide-lane observations and have used the ambiguity resolution approach of Section 4.2 to resolve the double difference wide-

lane ambiguities N_{5kl}^{ij} , but we could not resolve the single difference wide-lane ambiguities N_{5kl}^j . If we use the substitution (4.11) for the computation of the single difference ambiguities N_{1kl}^j using the estimated values of \tilde{N}_{1kl}^j , the N_{1kl}^j of all satellites will be biased by the same error of the single difference wide-lane ambiguities N_{5kl}^j multiplied by the factor 3.5.

We conclude that we may use the ambiguity resolution algorithm of Section 4.2 to resolve the L1 double difference ambiguities N_{1kl}^{ij} , if the L3 (ionosphere-free) observations are processed and the correct double difference wide-lane ambiguities N_{5kl}^{ij} are introduced into the normal equation system. If we make an attempt, however, to resolve the single difference ambiguities N_{1kl}^j , the wide-lane ambiguities N_{5kl}^j introduced have to be correct on the single difference level as well. Numerical examples are given in Chapter 6.

5. Combined GLONASS/GPS Data Analysis

The transmission of similar signals from both systems and the comparable satellite constellation ask for the combination of GLONASS and GPS data in the analysis. Major parts of the computation software for the calculation of GPS satellite positions and the processing of the observations may be used for GLONASS, too, without too many modifications. The same processing steps have to be performed and one may expect similar accuracies for GLONASS and GPS analysis. The combination of GLONASS and GPS nearly doubles the number of available satellites. This will increase the effectiveness of some applications, e.g., Realtime Kinematic (RTK) and troposphere estimates. The usage of two autonomous systems should also improve the reliability.

In order to combine GLONASS and GPS

- a *unique time scale* for all observations and satellite ephemerides and
- a *unique reference system* for all satellite and receiver positions

is required.

The observation equations for GLONASS described in Chapter 2 may also be used for combined GLONASS/GPS observations, provided the corresponding GPS frequencies are introduced. The differences between GPS and GLONASS frequencies and the wavelengths ratios (see Table 2.02 in the case of GLONASS) for GPS/GLONASS satellite pairs have to be considered, however. The wavelength difference of a GPS/GLONASS satellite pair is much larger than that of a pair of two GLONASS satellites and leads to an increased single difference bias term in the double difference phase observable. All required steps for the combination are shown in the following.

5.1 System Time Differences

Below we use the term *epoch* for the time tag to which a specific set of observations, clocks, or ephemerides refer. Three basic assumptions have to be observed during the processing:

Assumption 1: (5.01)

The epochs of observations and ephemerides must refer to a unique time scale (either UTC or GPS time).

Assumption 2: (5.02)

The clocks of all receivers have to be synchronized to a unique time scale to within some milliseconds (see eqn. (2.16)).

Assumption 3: (5.03)

GLONASS and GPS observations of a specific receiver have to be performed simultaneously (within some 10^{-12} sec) or with a known delay.

The third principle is required if we make an attempt to resolve the double difference ambiguity of a GLONASS/GPS satellite pair.

The epochs of GLONASS broadcast ephemerides are given in the GLONASS system time and those for GPS in GPS system time. There are different possibilities to account for the different time scales. One option consists of using GLONASS time for epochs of GLONASS observations and GPS time for GPS observation epochs. If broadcast ephemerides are used the first assumption is observed and the second assumption may be followed too. The third assumption is a problem due to two different receiver clocks for GLONASS and GPS introduced into the processing. This corresponds to the case where no double difference observations between GLONASS and GPS satellites are formed. If single difference observations are processed, two receiver clock parameters have to be estimated for each epoch.

Our approach is based on GPS time as reference time in all computations. If the observation epochs or ephemerides are given in GLONASS time, they will be transformed to GPS time. The processing of combined GLONASS/GPS observations has revealed the necessity of introducing a bias between GLONASS and GPS times (see Chapter 6) depending on the receiver type. This bias may be interpreted as the difference between the „GLONASS receiver clock“ and the „GPS receiver clock“ (see also Section 5.4). This term figures in the following transformation from GLONASS time to GPS time:

$$t_{GPS} = t_{GLONASS} + \tau_c + \tau_u + \tau_g + \tau_r \quad (5.04)$$

with

$$\tau_c = t_{UTC(SU)} - t_{GLONASS} \quad , \text{ see also (1.03)}$$

$$\tau_u = t_{UTC} - t_{UTC(SU)}$$

$$\tau_g = t_{GPS} - t_{UTC}$$

$$\tau_r = \text{receiver clock bias between GLONASS and GPS observations} \quad .$$

Numerical values for τ_u and τ_g are routinely published in the BIPM Circular T [BIPM, 1999]. The difference $t_{UTC} - t_{GLONASS}$ is given in this Circular as well and may be used to calculate τ_c with the formula

$$\tau_c = \tau_u - (t_{UTC} - t_{GLONASS}) \quad . \quad (5.05)$$

Some numerical values from the BIPM Circular T No. 128 for August 1, 1998 are given in Table 5.01. The uncertainty for the $t_{UTC} - t_{GLONASS}$ estimates is specified to be of the order of several hundreds of nsec and cannot be used for a correct transformation from $t_{GLONASS}$ to t_{GPS} . An additional parameter for the system time difference has to be estimated.

The largest value in eqn. (5.04) is associated with τ_g . It includes the known number of leap seconds between GPS time and UTC. In this approach we correct the epochs of the observations and the ephemerides for the leap seconds if they are given in GLONASS time. The remaining part of the system time difference will be estimated. In general, we distinguish between three observation types:

1) Observations to GPS satellites

The epochs of observations and ephemerides are given in GPS time. The first two assumptions are both met and require no further transformations of the epoch time scale. An estimation of the system time difference between GLONASS and GPS is obviously not possible.

2) Observations to GLONASS satellites

The receiver synchronizes to GLONASS time during the operation and this is the time scale for the raw observations and ephemerides. As stated, we use GPS time for all processing steps. Therefore, the epochs of observations *and* ephemerides have to be corrected for the same number of leap seconds. The first two assumptions are both met and the reference time is now approximately GPS time. No attempt can be made to estimate the system time difference.

3) Observations to GLONASS and GPS satellites

Let us assume that the receiver clock synchronizes to GPS time during the operation. In this case, the situation is the same as in 1) for GPS observations. The epochs of GLONASS observations also refer to GPS time, but the ephemerides are still given in GLONASS time and the first assumption does not hold. In our approach the epochs of the GLONASS ephemerides have to be corrected for the known number of leap seconds and the first assumption will be fulfilled approximately. The estimation of the system time difference GLONASS-GPS is mandatory.

The system time difference $t_{GPS} - t_{GLONASS}$ is the sum of τ_c , τ_u , τ_g and τ_r after taking into account the number of leap seconds. The system time difference may be determined in a code single point positioning procedure (section 5.3).

5.2 Combined GLONASS/GPS Orbits

In order to process GLONASS and GPS observations in the combined mode the positions of GLONASS and GPS satellites and of all receivers must refer to a unique reference system. In many cases the broadcast ephemerides are used as a priori orbit information. This implies different reference systems for GLONASS and GPS and requires the generation of a combined set of GLONASS/GPS orbits in a unique reference and time system. Figure 5.01 shows a flowchart for the orbit generation as realized in our processing scheme.

The resulting orbit file is referred to WGS-84 and it contains the satellite positions for predefined epochs in GPS time. GPS satellites transmit modified Kepler elements every hour in WGS-84 using GPS time as time scale. The Kepler elements are used to calculate the satellite positions for the epochs of the resulting orbit file. The positions are saved in the SP3 file format [Remondi, 1989].

GLONASS satellites transmit their positions and velocities every 15 and 45 minutes past the hour in PZ-90 and based on GLONASS time. The epochs of the ephemerides are approximately corrected to GPS time by applying the leap seconds between GPS time and UTC. The satellite positions are now interpolated to the epochs of the GPS positions. The interpolation is performed by using equations (1.18). Finally, the interpolated positions are transformed to WGS-84 by applying the transformation parameters given in Table 1.04. The result is saved in an SP3 file.

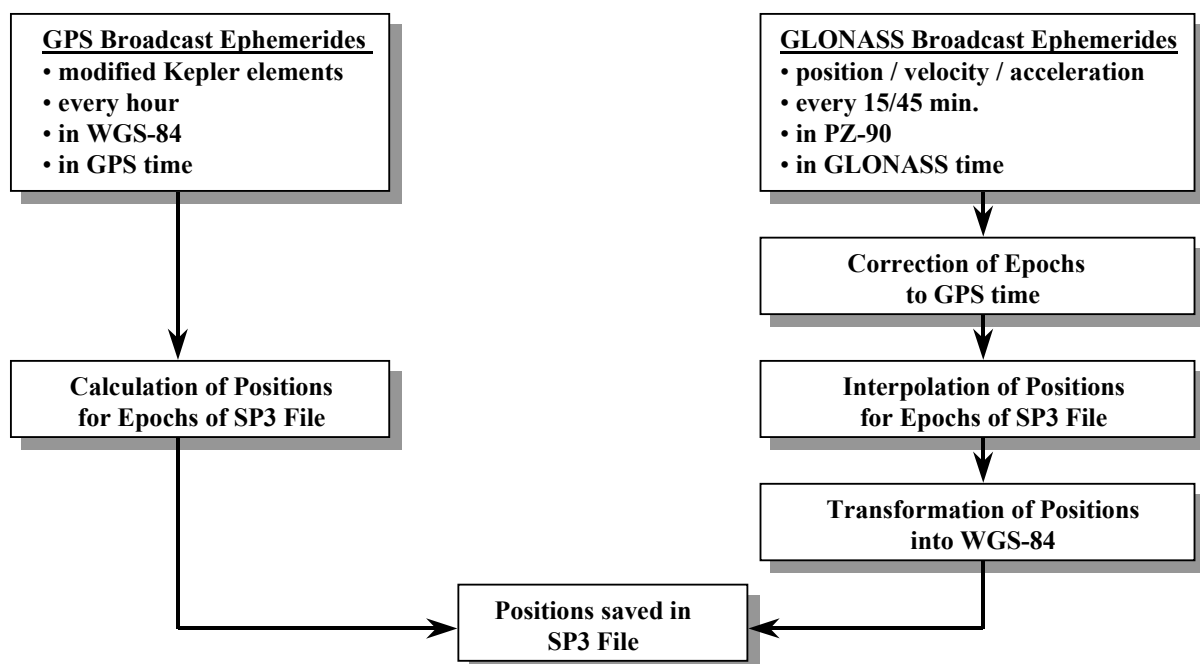


Figure 5.01: Combined GLONASS/GPS Orbit Generation

If the satellite orbits are improved during the data processing the resulting orbits are in the reference system of the fixed receiver coordinates, i.e., in the ITRF currently used (ITRF 97 at present).

5.3 Combined Pseudorange Analysis

As discussed in Section 5.1 the system time difference between GLONASS and GPS has to be estimated when processing combined observations. We introduce the new parameter into the pseudorange observation equation (2.05) as

$$P_k^i = c \cdot \tau_k^i + c \cdot \Delta t_k - c \cdot \Delta t^s + c \cdot \Delta t^s \quad (5.06)$$

with

$$\begin{aligned} \Delta t^s &= t_{GPS} - t_{GLONASS} - n = \text{system time difference} \\ n &= \text{leap seconds } (t_{GPS} - t_{UTC}). \end{aligned}$$

The use of GPS time in the processing leads to

$$\begin{aligned} \Delta t^s &= 0 \quad \text{for observations to GPS satellites} \\ \Delta t^s &\neq 0 \quad \text{for observations to GLONASS satellites} \end{aligned} \quad (5.07)$$

and the estimation of Δt^s requires *combined* observations.

Results from an Ashtech Z18 combined GLONASS/GPS receiver will be given in Chapter 6. The estimates for the system time difference and the receiver clock are used here for a comparison with the BIPM Circular T and Navigation Message quantities. The system time difference Δt^s for August 1, 1998, was estimated in the combined processing as 62 *nsec* (see Table 6.02). Using

$$\tau_c = \Delta t^s - \tau_u - \tau_g - \tau_r + n \quad (5.08)$$

with τ_u and τ_g from BIPM Circular T No. 128 and neglecting τ_r , we obtain $\tau_c = -105$ *nsec* (see Table 5.01).

For test purposes τ_c may also be computed by a separate processing of GLONASS and GPS observations. With this method Δt^s cannot directly be estimated but we obtain different results for the receiver clock estimates. The processing of the GPS observations allows the determination of the receiver clock correction Δt_k . The processing of the GLONASS observations estimates $\Delta t_k + \Delta t^s$, i.e., the receiver clock correction. The difference between the two estimates leads to a new value for Δt^s and according to eqn. (5.08), a new τ_c can be

Source	τ_c [nsec]	τ_u [nsec]	$\tau_g - 12 \text{ sec}$ [nsec]	τ_r [nsec]
BIPM Circular T No. 128	101 ¹⁾	182	-15	-
Navigation Message	365	-	-	-
Combined processing	-105 ²⁾	-	-	-
Separate processing of GLONASS and GPS	-79 ²⁾	-	-	-
¹⁾ calculated using eqn. (5.05) ²⁾ calculated using eqn. (5.08)				

Table 5.01: GLONASS/GPS System Time Difference for August 1, 1998 (DOY 213)

calculated (also given in Table 5.01). The calculation of τ_c using various approaches differ by less than 1 μsec .

5.4 Combined Ambiguity Resolution

The observation equations for GLONASS phase observables are given in Chapter 2. These equations may also be used for GPS phase observables with the specification $\Delta\lambda^{ij} = 0$. The combined processing of GLONASS and GPS also leads to phase differences between two satellites of both systems. The processing of a GLONASS/GPS phase difference implies:

- The system time difference $t_{GPS} - t_{GLONASS}$ must be accounted for.
- The wavelength difference $\Delta\lambda^{ij}$ for a GLONASS/GPS satellite pair is much larger than for a GLONASS/GLONASS satellite pair.

System Time Difference in the Phase Observables

The system time difference Δt^s is defined in eqns. (5.04) and (5.06) and consists of several terms. Some of the terms are the same for all GLONASS satellites and may be called „system-dependent“. These are in particular τ_c , τ_u and τ_g . In addition, the receiver-dependent term τ_r is included in Δt^s .

In order to introduce the system time difference into the phase observation equation we define:

$$\Delta t^s = \Delta t^v + \Delta t_w \quad (5.09)$$

with

$$\begin{aligned}\Delta t^v &= \tau_c + \tau_u + \tau_g - n \quad , \text{ system-dependent term} \\ \Delta t_w &= \tau_r \quad , \text{ receiver-dependent term}\end{aligned}$$

We introduce eqn. (5.09) into the zero difference phase observation equation:

$$\begin{aligned}\Psi_k^i &= c \cdot \tau_k^i + N_k^i \cdot \lambda^i + c \cdot \Delta t_k - c \cdot \Delta t^i + c \cdot \Delta t^v + c \cdot \Delta t_{wk} \\ \Psi_k^j &= c \cdot \tau_k^j + N_k^j \cdot \lambda_j + c \cdot \Delta t_k - c \cdot \Delta t^j\end{aligned}\tag{5.10}$$

with

$$\begin{aligned}i &= \text{GLONASS satellite} \\ j &= \text{GPS satellite}\end{aligned}$$

The phase single difference is then given by

$$\begin{aligned}\Psi_{kl}^i &= c \cdot \Delta \tau_{kl}^i + N_{kl}^i \cdot \lambda^i + c \cdot \Delta t_{kl} + c \cdot \Delta t_{wkl} \\ \Psi_{kl}^j &= c \cdot \Delta \tau_{kl}^j + N_{kl}^j \cdot \lambda^j + c \cdot \Delta t_{kl}\end{aligned}\tag{5.11}$$

with

$$\Delta t_{wkl} = \Delta t_{wk} - \Delta t_{wl} .$$

The system-dependent term Δt^v has been eliminated in eqn. (5.11).

For the double difference phase observable of a GLONASS/GPS satellite pair we then obtain:

$$\Psi_{kl}^{ij} = c \cdot \Delta \Delta \tau_{kl}^{ij} + N_{kl}^{ij} \cdot \lambda^i + N_{kl}^j \cdot \Delta \lambda^j + c \cdot \Delta t_{wkl}\tag{5.12}$$

The receiver-dependent term Δt_{wkl} of the system time difference is not eliminated on the double difference level. The term destroys the integer nature of the ambiguities in addition to the term $N_{kl}^j \cdot \Delta \lambda^j$. It has to be mentioned that only the relative difference between the receivers k and l shows up in eqn. (5.12) and only for a GLONASS/GPS satellite pair. As long as we do not make the attempt to resolve the ambiguity for the GLONASS/GPS satellite pair, the term $c \cdot \Delta t_{wkl}$ does not alter the processing results, provided the term does not change during the observation session.

When processing combined observations (see Chapter 6 and 7) some large values for the receiver-dependent term Δt_w were found, e.g., approximately 1 μ sec for 3S-Navigaiton receivers. In order to be able to resolve mixed GPS-GLONASS double difference ambiguities, this type of bias has to be eliminated completely on the double difference level, i.e., the size has to be identical for both receivers k and l .

Small values for Δt_{wkl} may be caused by frequency specific delays of the signal in the receiver, antenna and cables. These delays may even change with temperature [Walsh P., Daily P., 1996]. We were not able to detect such type of delays for GLONASS/GLONASS

satellite pairs. For GLONASS/GPS satellite pairs we found large fractional parts of some ambiguities which might be caused by the frequency-specific delays.

Due to the receiver-dependent term in eqn. (5.12) we can probably not resolve the ambiguities between GLONASS and GPS satellites. In the code single point positioning we determine Δt^s as sum of Δt^v and Δt_w . The difference of the estimates for two receivers directly leads to the term Δt_{wkl} , but the achieved accuracy is clearly not sufficient to correct the phase observations. The determination of Δt_{wkl} would become possible if all GLONASS and GPS ambiguities were resolved on the single difference level. In this case we could use eqn. (5.12) for the determination of Δt_{wkl} .

GLONASS/GPS Wavelength Differences

The wavelength differences for GLONASS/GPS satellite pairs are significantly larger than for GLONASS/GLONASS pairs. With the approximation (2.29) the wavelength differences can be calculated using

$$\Delta\lambda^{ij} \approx i \cdot \Delta\lambda + \Delta\lambda^s \quad (5.13)$$

with

$$\begin{aligned} i &= \text{GLONASS satellite} \\ j &= \text{GPS satellite} \\ \Delta\lambda^s &= \lambda^0 - \lambda^{GPS} \quad (\text{see Table 5.02}). \end{aligned}$$

Table 5.03 shows the wavelength differences expressed in cycles of λ^0 . The two wavelengths L1 and L2 have to be distinguished. The absolute values are shown in Figure 5.02 with dl(L1) and dl(L2) for L1 and L2, respectively.

The bias term b_{kl}^{ij} as defined in eqn. (2.30) is given by

$$b_{kl}^{ij} \approx N_{kl}^j \cdot (i \cdot \Delta\lambda + \Delta\lambda^s) \quad (5.14)$$

In order to keep the bias term smaller than 0.1 cycles of λ^0 the single difference ambiguities N_{kl}^j have to be known now to better than 6 cycles. It may be possible to reach such a precision

	L1	L2
Nominal Carrier Frequency	1575.42 MHz	1227.6 MHz
Wavelength	0.190293673 m	0.244210213 m
$\Delta\lambda^s$	-0.003157307 m	-0.003606315 m

Table 5.02: GPS Frequencies and Wavelengths

5. Combined GLONASS/GPS Data Analysis

after the successful resolution of all GLONASS/GLONASS ambiguities. These maximum allowed single difference ambiguity biases are given in Figure 5.02 with N_{\max} (L1) and N_{\max} (L2) for L1 and L2, respectively.

$\frac{i \cdot \Delta\lambda + \Delta\lambda^s}{\lambda^0}$			$\frac{i \cdot \Delta\lambda + \Delta\lambda^s}{\lambda^0}$		
i	L1	L2	i	L1	L2
1	-0.01722	-0.01533	13	-0.02143	-0.01955
2	-0.01757	-0.01569	14	-0.02178	-0.01990
3	-0.01792	-0.01604	15	-0.02213	-0.02025
4	-0.01827	-0.01639	16	-0.02248	-0.02060
5	-0.01862	-0.01674	17	-0.02283	-0.02095
6	-0.01897	-0.01709	18	-0.02318	-0.02130
7	-0.01932	-0.01744	19	-0.02354	-0.02165
8	-0.01967	-0.01779	20	-0.02389	-0.02200
9	-0.02003	-0.01814	21	-0.02424	-0.02235
10	-0.02038	-0.01849	22	-0.02459	-0.02271
11	-0.02073	-0.01884	23	-0.02494	-0.02306
12	-0.02108	-0.01920	24	-0.02529	-0.02341

Table 5.03: GLONASS/GPS Wavelength Differences in Cycles of λ^0 .

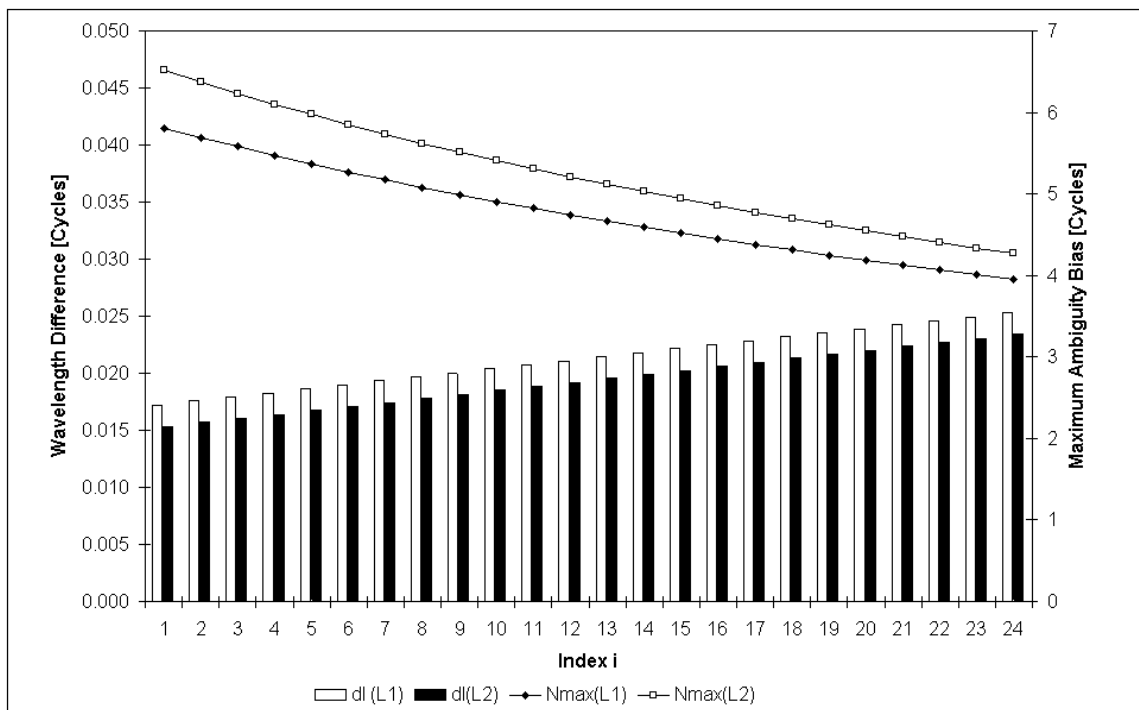


Figure 5.02: GLONASS/GPS Wavelength Differences and maximum allowed Single Difference Ambiguity Bias

GLONASS/GPS Ambiguity resolution

When solving for ambiguities of combined GLONASS/GPS observations, we distinguish three double difference ambiguity types:

Type 1: GPS-GPS difference or GLONASS-GLONASS with identical frequencies:

Two GLONASS satellites may transmit at identical carrier frequencies, if the two satellites are visible at different observation epochs but are included in one data file. The single difference bias term b^{ij} is zero for this ambiguity type. Ambiguity resolution is independent on the initialization of the single difference ambiguities. The successful resolution of ambiguities of this type does not improve the single difference ambiguities.

Type 2: GLONASS-GLONASS difference:

This type of ambiguity may be resolved if the bias term b^{ij} does not destroy the integer nature of the ambiguities. The ambiguity resolution algorithm in Section 4.2 will considerably reduce the size of the bias term after each successfully performed iteration step.

Type 3: GPS-GLONASS difference:

Due to the wavelength difference of this ambiguity type the bias term b^{ij} is much larger compared to type 2, as can be seen in eqn. (5.14). Furthermore, possible biases between the systems might prevent us from resolving these ambiguities, e.g., because of the term $c \cdot \Delta t_{wkl}$ in eqn. (5.12).

As outlined in Section 4.2, the a posteriori formal errors of the double difference ambiguities N_{kl}^{ij} are highly correlated with the wavelength difference of the two satellites. Consequently, the algorithm resolves the ambiguities according to the following scheme:

Let us assume n GPS satellites and m GLONASS satellites were observed and that, for simplicity, only one ambiguity was set up for each satellite. The ambiguity resolution is divided into three steps:

Step 1)

In the first step all ambiguities referring either to two GPS satellites or to two GLONASS satellites with identical frequencies (type 1) are

resolved. The expected formal errors are small compared to those of type 2 and type 3. For n GPS satellites $n-1$ ambiguities may be resolved (assuming no ambiguities of type 1 for two GLONASS satellites). The formal errors of the single difference ambiguities do not change.

Step 2)

In the second step we solve for ambiguities between two GLONASS satellites (type 2). Their formal errors are small compared to those of type 3. For m GLONASS satellites $m-1$ ambiguities may be resolved. The formal errors of the single difference ambiguities become smaller after each successfully resolved double difference ambiguity with $\Delta\lambda \neq 0$.

Step 3)

In the third step we solve for **one** ambiguity between a GPS satellite and a GLONASS satellite (type 3). This might be possible after successful resolution of ambiguities of type 2, if there are no significant receiver biases between the two systems.

Altogether $m+n-1$ ambiguities might be resolved on the double difference level and, if the formal errors of the single difference ambiguities decrease below 0.1 cycles, the remaining single difference ambiguity might be fixed to an integer number, too.

II. Applications and Results

6. Results for Various Baselines

In order to confirm and validate the theoretical aspects of processing GLONASS and combined GLONASS/GPS observations as discussed in the first part of this analysis, observations of various baselines have been processed. We want to prove that the software modified to process GLONASS and combined GLONASS/GPS data may be used to correct for the system differences between GLONASS and GPS and that phase observations may be successfully treated despite of the existing bias terms.

Two stations separated by approximately 5 m were occupied with combined GLONASS/GPS receivers. The observations of the L1 and L2 carriers were processed separately and show all GLONASS specific effects. Also, linear combinations of L1 and L2 were formed. This demonstrates the functionality of our developments concerning linear combinations and we may study the size of specific bias terms. Ionospheric refraction has no significant effect on double difference observations of this 5 m baseline.

Two more stations were set up forming a baseline with a length of approximately 6.6 km. These double difference phase observations are biased by ionospheric refraction, but ambiguity resolution using the original carriers L1 and L2 is still possible.

In order to study the reliability and efficiency of the ambiguity resolution algorithm, three other stations were selected and observed in such a way, that baselines of a length of approximately 20, 40 resp. 60 km could be formed.

Orbit related issues using a global network of receivers will be discussed in Chapter 7.

Observation Scheme

Ashtech Z18 combined GLONASS/GPS receivers were used for all measurements. The Z18 has ten channels for L1 and L2 GPS code and phase measurements, as well as eight channels for L1 and L2 GLONASS code and phase measurements. The receivers were operated using Ashtech's Geodetic Base Station Software (GBSS) and were connected to choke ring antennas with radomes. Table 6.01 shows the observation schedule for all stations. The stations KARN, KARS and KLOP are located near the city of Frankfurt am Main in Germany. WTZZ stands for a Z18 receiver which is permanently operated by the "Bundesamt fuer Kartographie und Geodäsie (BKG)" at the fundamental station Wettzell in the southern part of Germany. The stations BODE and BRUC are located near to Wettzell with the distances given in Table 6.01.

6. Results for Various Baselines

Date	Day of Year	Stations	Baseline Length	SessionLength	Sampling
Aug. 1, 1998	213	KARN, KARS	5 m	24 hours	30 sec
Aug. 2, 1998	214	KARN, KARS	5 m	24 hours	30 sec
Aug. 4, 1998	216	KLOP, KARS	6.6 km	24 hours	30 sec
Aug. 5, 1998	217	KLOP, KARS	6.6 km	24 hours	30 sec
June 15, 1999	166	WTZZ, BODE	16.5 km	5 hours	30 sec
		WTZZ, BRUC	41.4 km	5 hours	30 sec
		BODE, BRUC	57.7 km	5 hours	30 sec
June 16, 1999	167	WTZZ, BODE	16.5 km	8 hours	30 sec
		WTZZ, BRUC	41.4 km	8 hours	30 sec
		BODE, BRUC	57.7 km	8 hours	30 sec
June 17, 1999	168	WTZZ, BODE	16.5 km	8 hours	30 sec
		WTZZ, BRUC	41.4 km	8 hours	30 sec
		BODE, BRUC	57.7 km	8 hours	30 sec

Table 6.01: Observation Schedule for the Baselines

6.1 Code Single Point Positioning

The ionosphere-free linear combination of code observations for the three stations KARN, KARS and KLOP were processed in order to determine the station coordinates and receiver clock corrections for each epoch. In the case of combined GLONASS/GPS observations it is possible and mandatory to solve for the system time difference between GLONASS and GPS. Broadcast ephemerides for GPS and GLONASS have been used.

Table 6.02 shows the RMS error of the single point positioning, separately for the GLONASS and GPS code observations as well as for the combination of both. We clearly recognize the reduced RMS for GLONASS compared to GPS code observations thanks to the absence of Selected Availability (SA) in the GLONASS signals. This leads also to a reduced RMS value for the combined solution.

The estimates for the system time difference derived from the combined processing show day to day differences smaller than 25 *nsec* for both receivers. It has to be mentioned, that the same receiver was used to occupy KARN and KLOP. We also see that a systematic bias of about 11 *nsec* exists between the estimates of the two receivers and confirms the existence of the term τ_r in eqn. (5.04).

Session	Station	GLONASS RMS [m]	GPS RMS [m]	Combined RMS [m]	System Time Difference [nsec]
213	KARS	11.7	22.1	19.9	62.27 ± 0.38
	KARN	12.4	22.2	20.2	53.47 ± 0.84
214	KARS	12.5	23.7	21.4	54.03 ± 0.90
	KARN	13.3	24.1	21.7	43.33 ± 1.11
216	KARS	9.3	22.4	19.7	45.51 ± 0.83
	KLOP	9.2	22.5	19.7	31.47 ± 0.83
217	KARS	8.5	22.2	19.5	63.20 ± 0.82
	KLOP	8.5	22.2	19.4	54.05 ± 0.82

Table 6.02: Observation RMS Error of Code Single Point Positioning and System Time Difference

Separate Processing of GLONASS and GPS Code Observations

For session 213 the code observations for GLONASS and GPS were also processed separately. In this processing mode the receiver clock corrections were estimated for each epoch, but no system time difference. The estimated clock corrections for GLONASS and GPS differ, however, for the system time difference Δt^s , because the receiver clock during the observation was equal for both systems. Δt^s can thus be derived from separate GLONASS and GPS processing.

In Figure 6.1 we see the estimated receiver clock corrections for station KARS, session 213. The absolute corrections are given in the first picture. The estimates for GLONASS and GPS result in a common line for both quantities. The receiver clock has a drift of 47 msec/d during the 24-hour session. The second picture shows the receiver clock changes after removing a linear drift. The remaining changes are within an interval of 2.5 msec and again GLONASS and GPS values are on top of each other. In the third picture we can inspect the differences between the clock estimates for GLONASS and GPS. The differences vary between $-0.06 \mu\text{sec}$ and $0.2 \mu\text{sec}$ around a mean value of 57 nsec, the system time difference Δt^s . The system time difference of 57 nsec derived from separate GLONASS and GPS processing slightly differs from the value of 62 nsec, estimated in the combined GLONASS/GPS processing and given in Table 6.02. This is caused by different results for the station coordinates in both approaches.

6. Results for Various Baselines

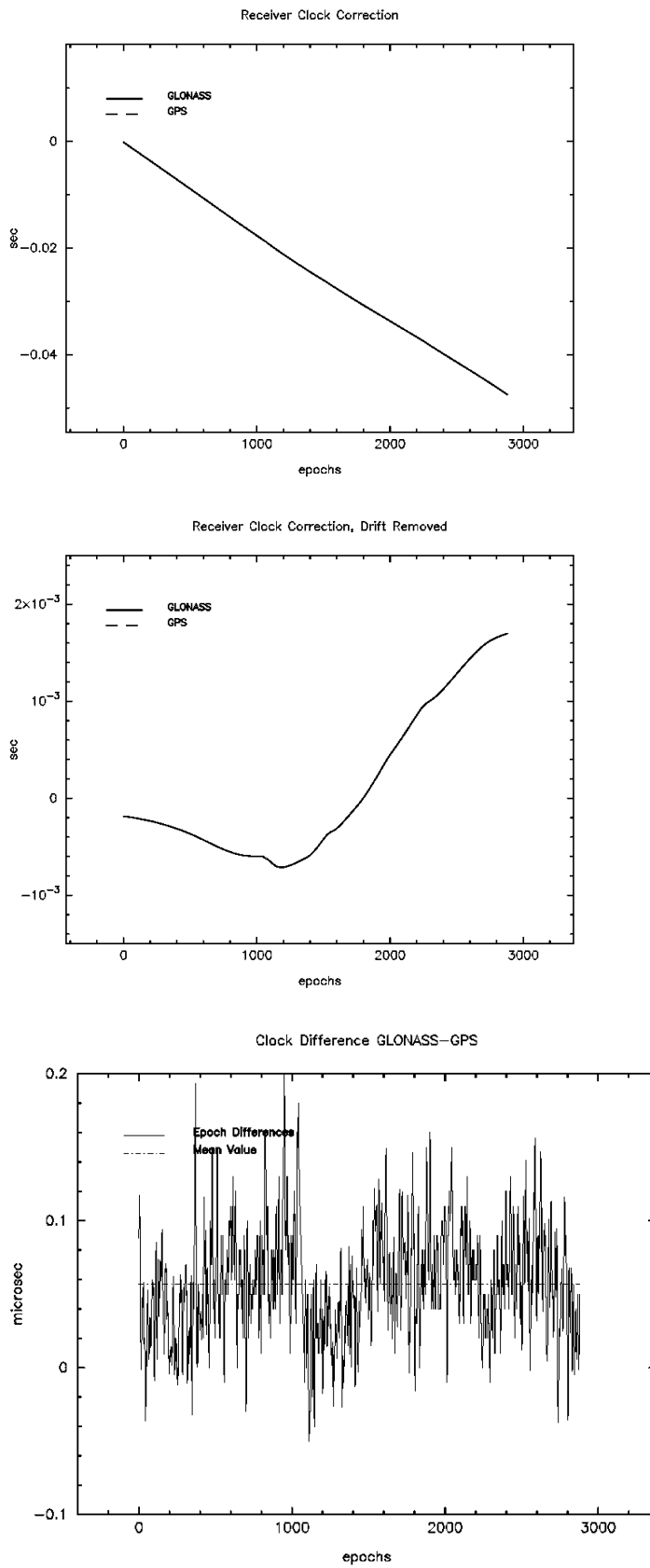


Figure 6.1: Separate Processing of GLONASS and GPS Code Observations for KARS, Session 213

Figure 6.2 shows the estimated receiver clock corrections from a separate processing of GLONASS and GPS for the station KARN, session 213. The absolute corrections given in the first picture show no significant linear drift for this receiver. The differences for the separate GLONASS and GPS estimates are plotted in the second picture and range from $-0.06 \mu\text{sec}$ to $0.2 \mu\text{sec}$. The mean value is 46 nsec for the system time difference. The difference w.r.t. the value of 53 nsec , given in Table 6.02, is caused by different station coordinate estimates.

The determination of the system time difference derived from a separate processing of GLONASS and GPS agrees with the figures given in Table 6.02 to within 10 nsec . Also, the difference between the clock system differences of two receivers was confirmed to be significant. It is of the order of 10 nsec in both approaches. The variations in the clock differences between GLONASS and GPS over the 24 hour session length in Figures 6.1 and 6.2 are comparable. Similar variations were found when processing combined GLONASS/GPS observations in hourly intervals and the estimation of the corresponding system time differences. These hourly estimates are given in Figure 6.3 for the station KARS. The mean value in Figure 6.3 is 62 nsec , the same number as in Table 6.2.

The variations of the clock differences in Figure 6.1 and 6.2 are caused mainly by Selected Availability (SA) of the GPS system. This emerges when using precise orbits and clock corrections for GPS satellites in the code single point positioning. Therefore, the processing of GPS code observations for the station KARS, session 213, was repeated, using precise GPS orbits from the Center for Orbit Determination in Europe (CODE). Precise clock corrections for GPS satellites for every 5 minutes, also from CODE, were used. This asked for a 5-minute sample interval for processing the code observations. The resulting estimates for the receiver clock corrections were used to compute the difference between the receiver clock corrections from separate GPS and GLONASS processing. The differences are given in Figure 6.4. If we compare Figure 6.4 to the clock differences in Figure 6.1, we clearly see that the short-time variations of the clock differences do no longer show up in Figure 6.4. This confirms, that the short-period variations in Figure 6.1 and Figure 6.2 are caused by SA. The remaining variations in Figure 6.4 result mainly from the orbit error of the GLONASS satellites, because no precise GLONASS orbits were available for session 213.

Biases in the receiver clock differences of separate GLONASS and GPS processing caused by orbit errors of both, GLONASS and GPS satellites, may be reduced significantly, if the difference of the corresponding values of two stations is computed. Figure 6.5 shows such differences between the two stations KARS and KARN. In this figure small variations between $-0.02 \mu\text{sec}$ and $0.04 \mu\text{sec}$ remain for the receiver clock difference. The reduced effect of orbit errors on the estimated receiver clock differences explains the smaller clock differences in Figure 6.5 w.r.t. Figure 6.4.

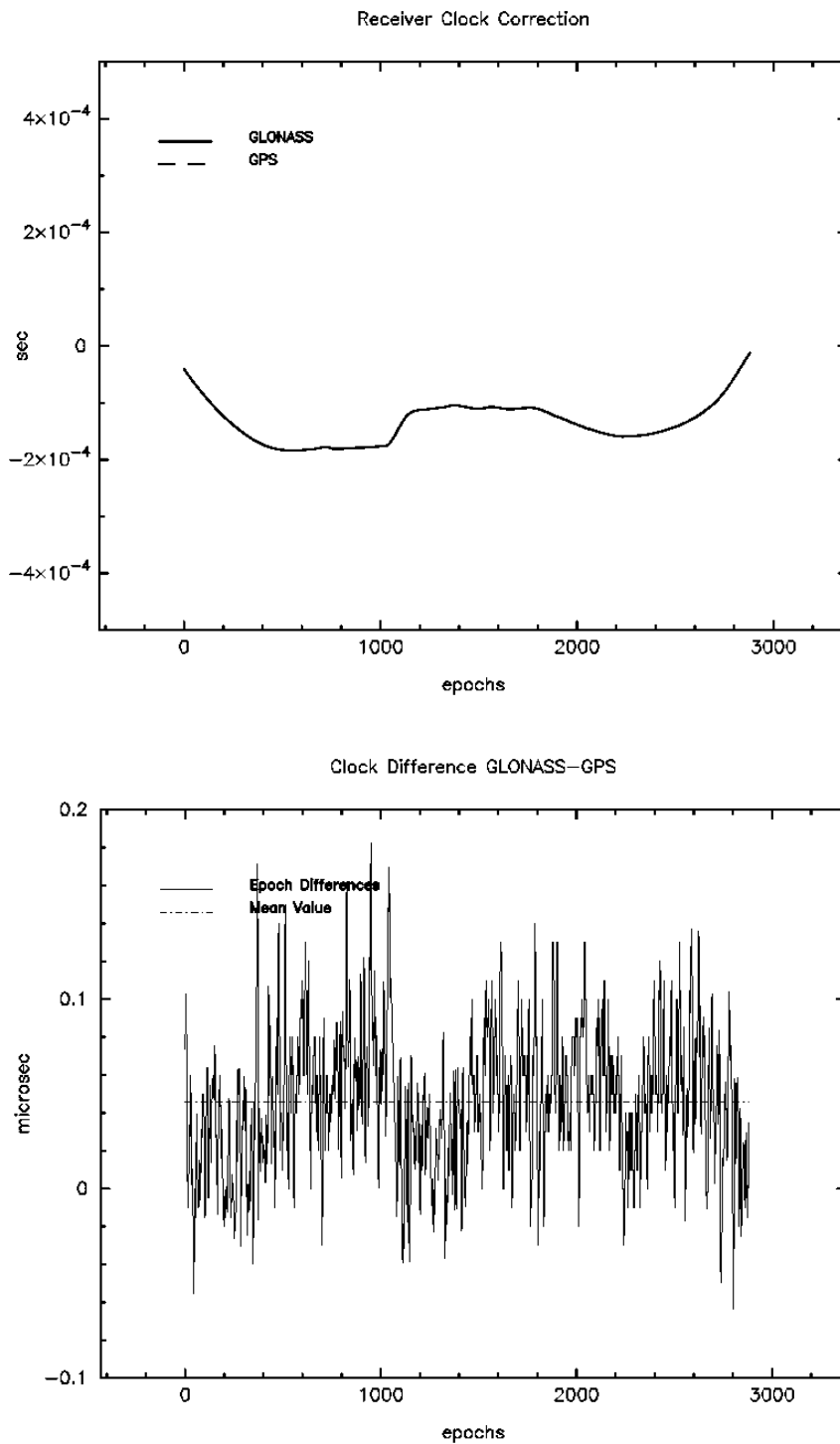


Figure 6.2: Separate Processing of GLONASS and GPS CODE Observations for KARN, Session 213

The mean value in Figure 6.5 of about 10 *nsec* may not be interpreted as system time difference Δt^s , but as the receiver-dependent term Δt_{wkl} (see eqns. (5.09) and (5.11)). The term Δt_{wkl} will show up in the double difference pseudorange observation equation, if we substitute Δt^s in eqn. (5.06) by eqn. (5.09). This difference in the system time difference Δt_{wkl} between the receivers at the stations KARS and KARN of the order of 10 *nsec* agrees with the numbers given in Table 6.2. A receiver-dependent term Δt_{wkl} of 10 *nsec* corresponds to approximately 3 m in units of length and, following eqn. (5.12), it will not be possible to resolve the double difference ambiguity N_{kl}^{ij} of a GLONASS/GPS satellite pair. This will be confirmed by the results of Section 6.2.2.

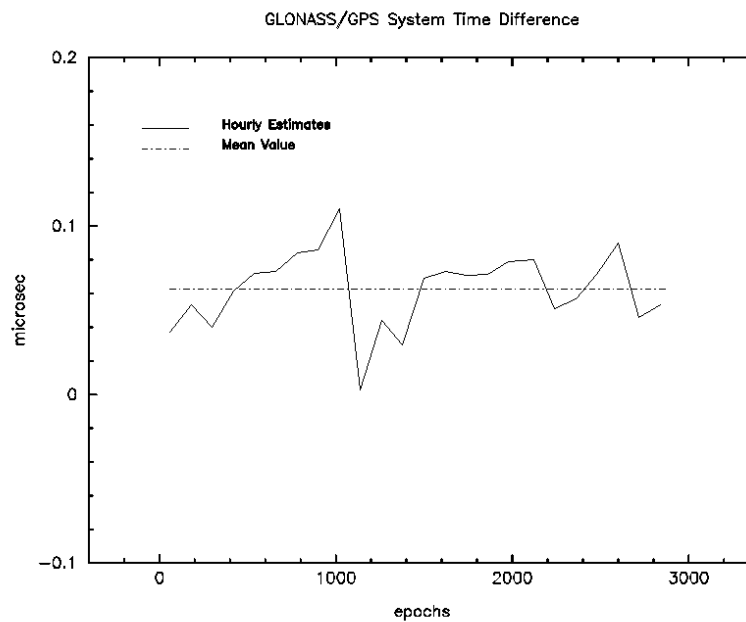


Figure 6.3: Combined Processing of GLONASS/GPS Code Observations for KARS in Hourly Intervals, Session 213

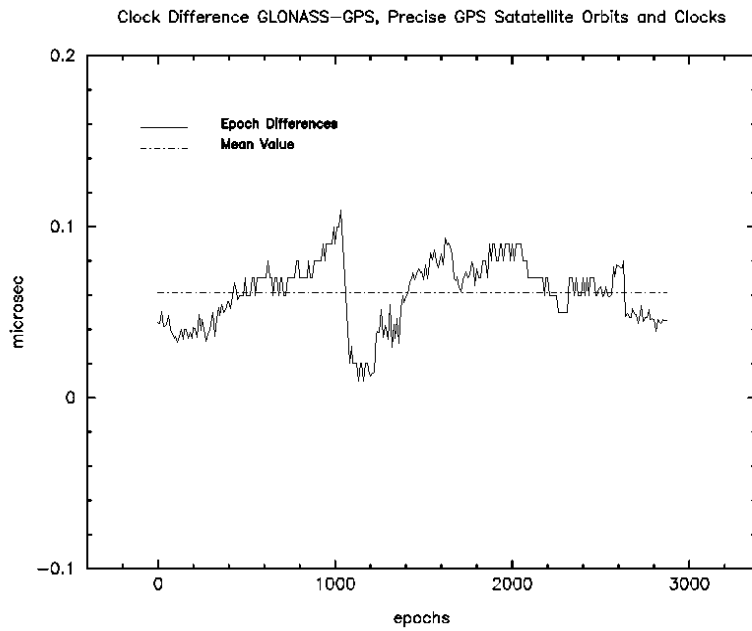


Figure 6.4: Separate Processing of GLONASS and GPS Code Observations for KARS, Session 213, Precise Orbits and Clocks for GPS Satellites

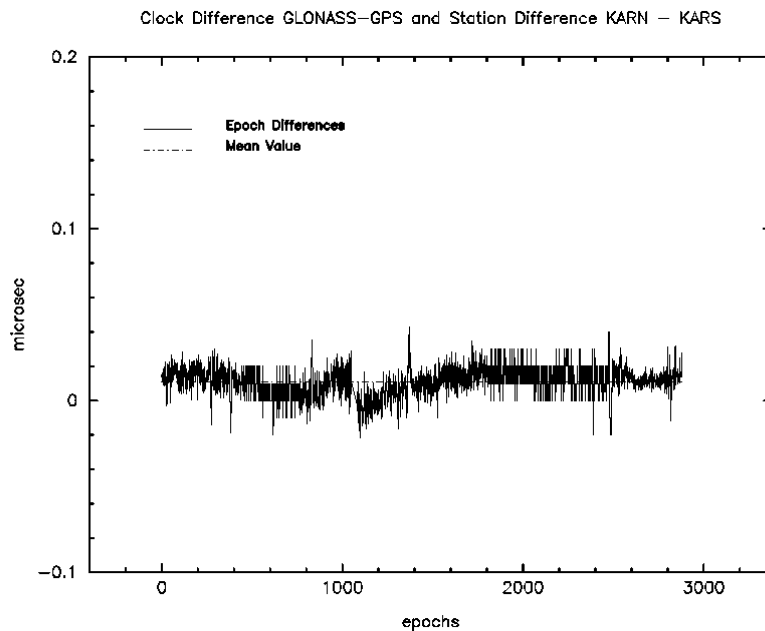


Figure 6.5: Difference between KARS and KARN, separate Processing of GLONASS and GPS Code Observations, Broadcast Orbits

Since the beginning of the IGEX experiment (see Chapter 7) on October 19, 1998, improved orbits for GLONASS satellites are available from, e.g., BKG. We used such orbits from BKG for June 15, 1999 to compute a code single point positioning for GLONASS observations of the combined GLONASS/GPS receiver in Wettzell (see Section 6.4 for the observation schedule) and solved for receiver coordinates and clock corrections. The use of the improved GLONASS orbits results in a formal error for a single code observation of 4.3 m, a significantly smaller value than the error of 9.4 m (see Table 6.9) resulting from using GLONASS broadcast ephemerides. The GPS code observations of this receiver were processed in a single point positioning using precise GPS orbits and clocks from CODE and we solved for receiver coordinates and clock corrections, again. The differences of such estimates of the receiver clock corrections by a separate GPS and GLONASS processing are given in Figure 6.6. This is an attempt to decrease the variations of these estimates given in Figure 6.4. The variations of the clock correction differences in Figure 6.6 range between 0.35 μ sec and 0.42 μ sec for the 24 hour session length and are significantly smaller than those in Figure 6.4. The effect of orbit errors of GLONASS satellites on the estimation of receiver clock corrections is reduced by using improved GLONASS orbits. It has to be mentioned, that broadcast clock corrections for GLONASS satellites were used in both approaches. The GLONASS satellite clocks cause the remaining variations in Figure 6.6.

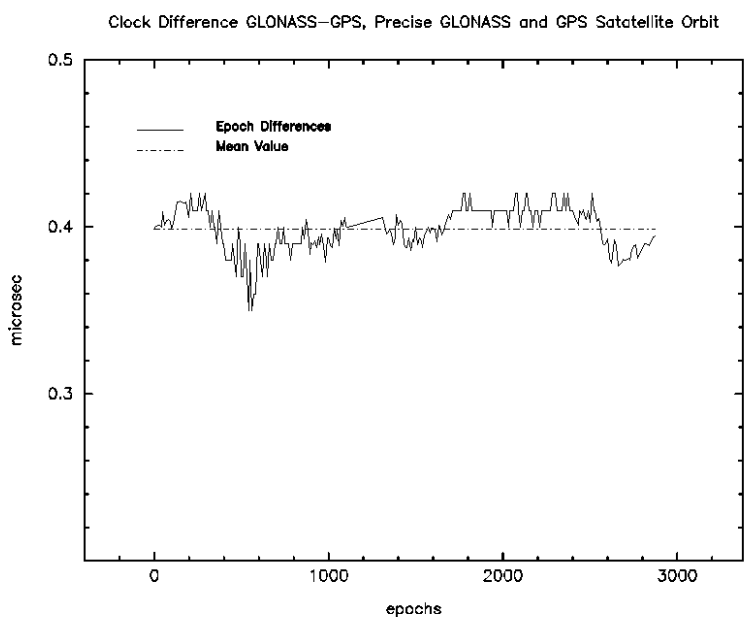


Figure 6.6: Separate Processing of GLONASS and GPS Code Observations for Station Wettzell, Session 166, 1999, Precise Orbits and Clocks for GPS Satellites, Precise Orbits for GLONASS satellites

6.2 Baseline of 5 m Length

The 5 m baseline has been processed in two modes, namely using the GLONASS L1 observations and using the combined GLONASS/GPS L1 observations. It will be shown that the new software detects and corrects the cycle slips in both modes. The ambiguity resolution approach as described in Chapter 4 is used for GLONASS and combined observations.

The preprocessing using the ionosphere-free linear combination L3 leads to cycle slip corrections that are identical to those resulting from a separate processing of L1 and L2 observations. This so-called „combined mode“ (using L3 and L5) is described in [Beutler et al., 1996].

6.2.1 Cycle Slip Detection

For the baseline KARS-KARN, session 213, a total number of 145 cycle slips on L1 and 131 cycle slips on L2 were detected for GLONASS satellites. The majority of the detected slips belongs to satellites 110 and 116. This satellite-specific problem was not studied in detail. Table 6.3 lists the cycle slips for GLONASS satellites except those for satellites 110 and 116.

GLONASS		Total Number of Slips: 145 (L1) 131 (L2)	
Epoch	Satellite	Cycle Slip	
		L1	L2
206	111	-4269272	-3320543
327	111	-3345314	-2601912
371	112	1	1
464	111	-3814699	-2966989
490	111	-739132	-574881
553	111	-1801639	-1401273
2631	109	-11405296	-8870786
GPS		Total Number of Slips: 0 (L1) 63 (L2)	

Table 6.3: Detected Cycles Slips for KARS-KARN, Session 213

Identical cycle slips were found for the separate processing of L1 and L2 observations, the separate processing of GLONASS and GPS satellites as well as for the „combined mode“. For the GPS satellites no cycle slip was found on L1, 63 on L2.

The single difference residuals “differenced in time” according to equation (3.07) were used for cycle slip detection as described in Section 3.2.2. They are shown in Figures 6.7 to 6.10.

Figure 6.7 shows the single difference residuals “differenced in time” (difference between two stations and two subsequent epochs) in meters. No receiver clock corrections were applied. Cycle slips show up as outliers and most of the outliers stem from satellites 110 and 116. The problem of these two satellites was not studied in detail and both satellites were removed in Figure 6.8. The large cycle slips for the satellites 111 and 109 are easily seen in Figure 6.8. The band of about 1 m height is caused by the accumulated receiver clock offset between the 30 sec epochs.

In Figure 6.9 and Figure 6.10 the residuals were corrected for the estimated receiver clock corrections. The corrections were calculated for each epoch using eqn. (3.11). Figure 6.9 uses a logarithmic scale for the residuals in units of cycles and thus allows to show big cycle slips as those in Table 6.3. The cycle slip of size 1 for satellite 112 and the observation noise is not visible in this figure. In Figure 6.10 a linear scale in units of cycles was used in order to visualize the cycle slip of size 1 for satellite 112. The cycle slip is easily detected after having corrected for the receiver clock behaviour.

Figure 6.11 shows the absolute numbers of the fractional parts of all detected cycle slips on L1, which reach a maximum value of 0.04 cycles. They indicate that we can use the cycle slip detection algorithm of Section 3.2.2.2 to correct cycle slips on the single difference level. After the correction of the single difference residuals “differenced in time” (3.08) for the estimated receiver clock correction (3.11) the correct integer numbers of any cycle slips in units of cycles of the specified satellite was found and applied to the single difference L1 observations. Due to the fact that the cycle slips were corrected on the single difference level, no frequency-specific bias term for GLONASS satellites shows up. The algorithm was successful for cleaning GLONASS and combined GLONASS/GPS observations.

6. Results for Various Baselines

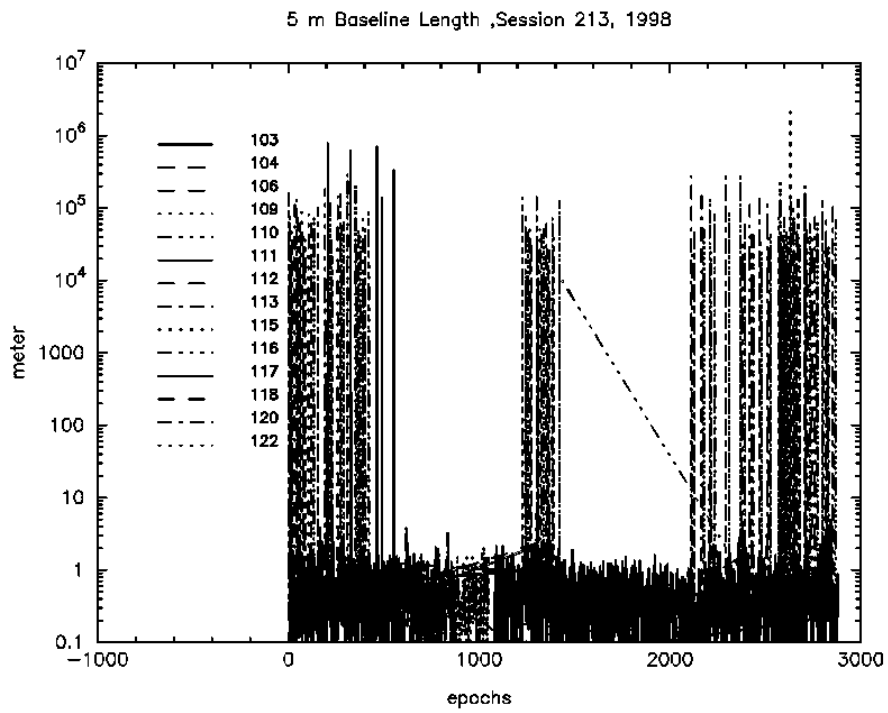


Figure 6.7: Single Difference Residuals “Differenced in Time”

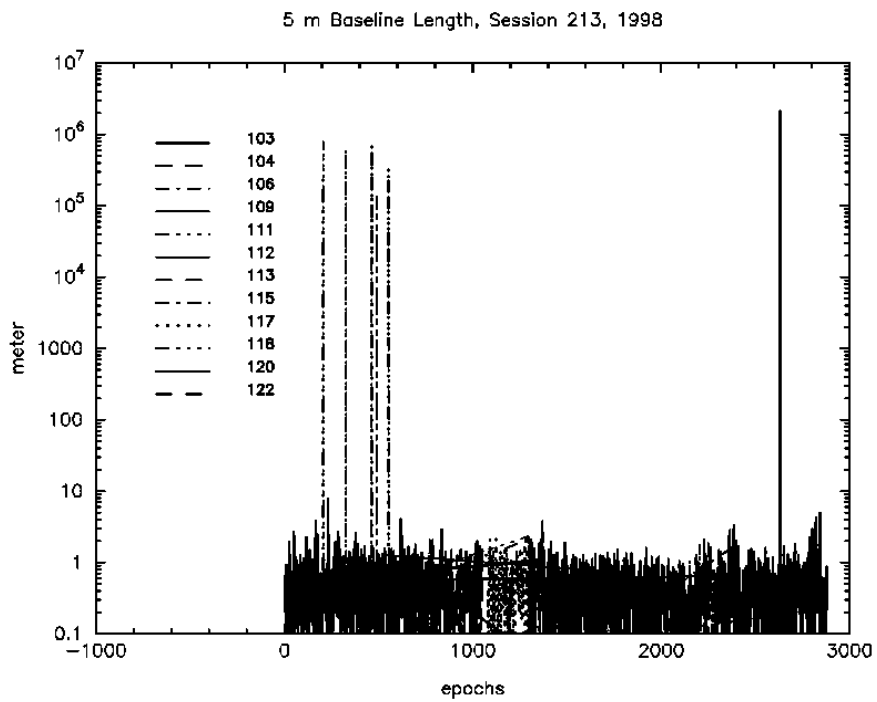


Figure 6.8: Single Difference Residuals “Differenced in Time”, Satellites 110 and 116 Removed

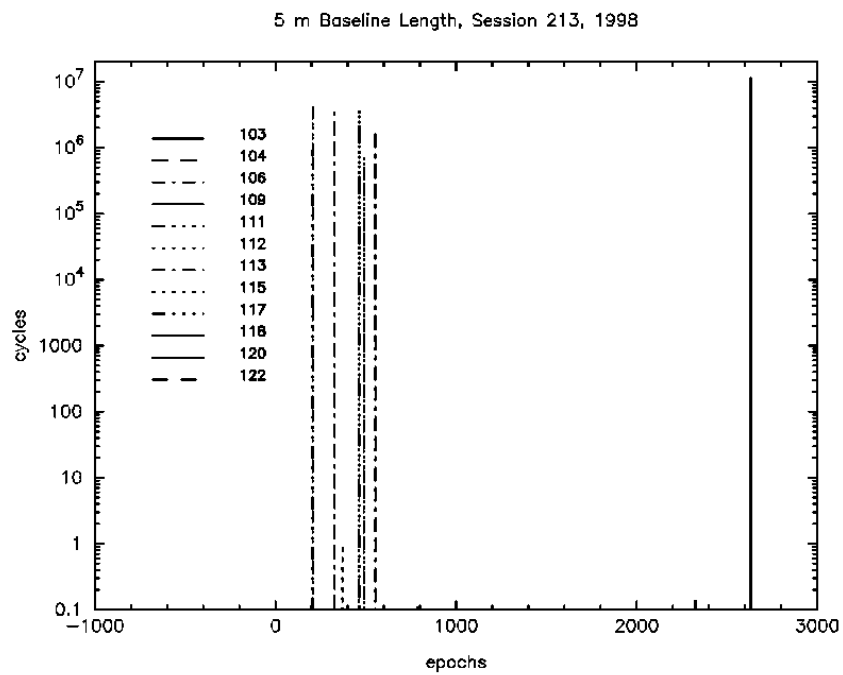


Figure 6.9: Single Difference Residuals “Differenced in Time” in Cycles, Receiver Clock Removed

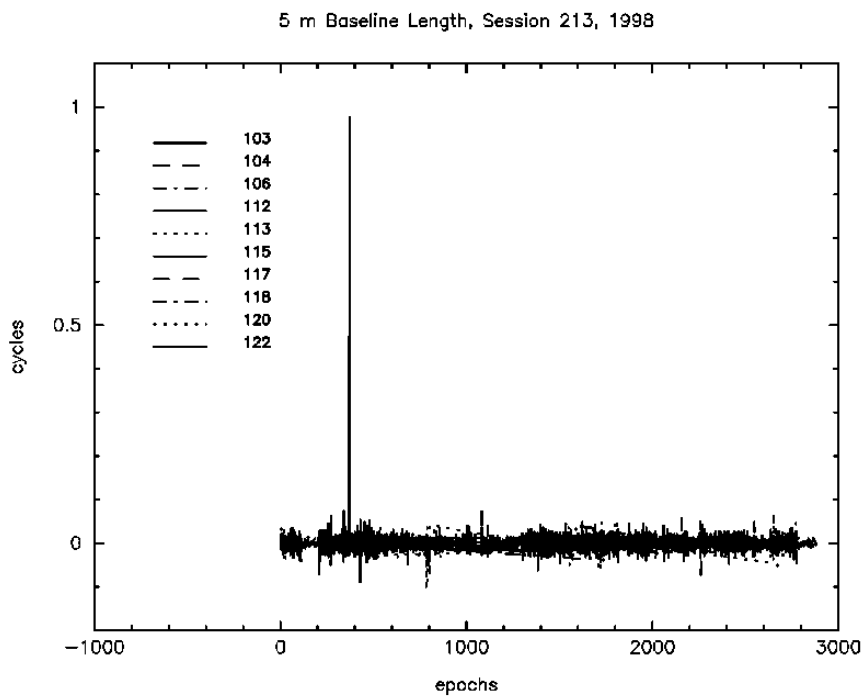


Figure 6.10: Single Difference Residuals “Differenced in Time” in Cycles, Receiver Clock Removed, Without Satellites 109 and 111

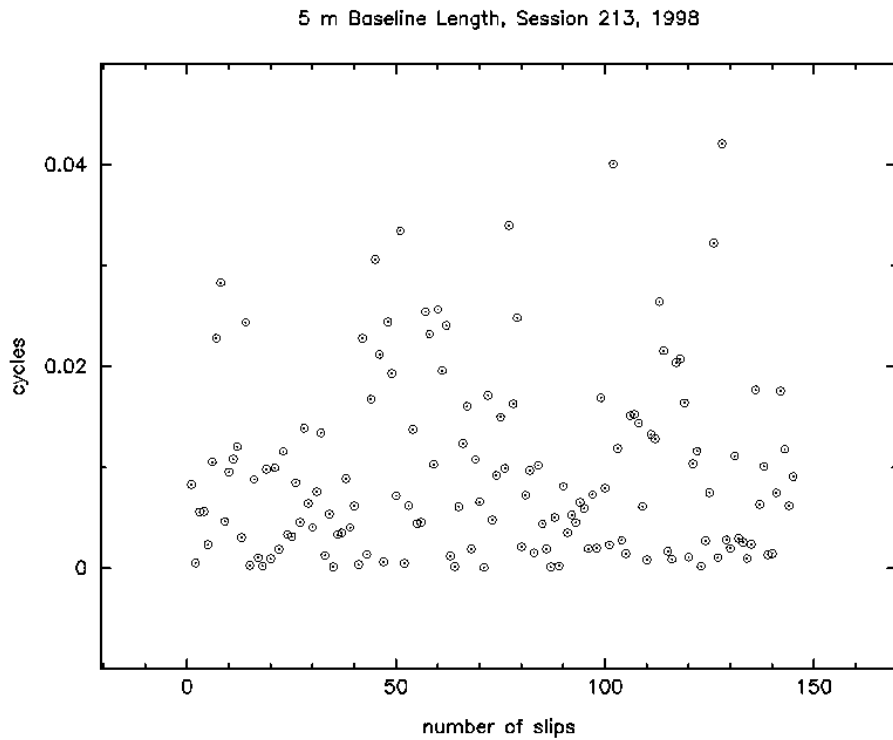


Figure 6.11: Fractional Parts of Detected Cycle Slips, GLONASS/GPS L1 Observations

6.2.2 Ambiguity Resolution

The ambiguity resolution algorithm described in Chapter 4 will be demonstrated using as an example the processing of the L1 observations for session 213 (Table 6.02). First, we use only GLONASS observations and resolve the ambiguities. A second processing step, independent from prior results, uses combined GLONASS/GPS observations and resolves the ambiguities for GLONASS as well as for GPS satellites.

Processing of GLONASS Observations

If we use only the GLONASS observations for session 213, there is a gap in the observations for all satellites. This divides the observations into two so-called „observation clusters“, following the naming conventions of the Bernese Software. In the following, the results of only one of these two clusters are shown in order to reduce the number of ambiguities for this demonstration.

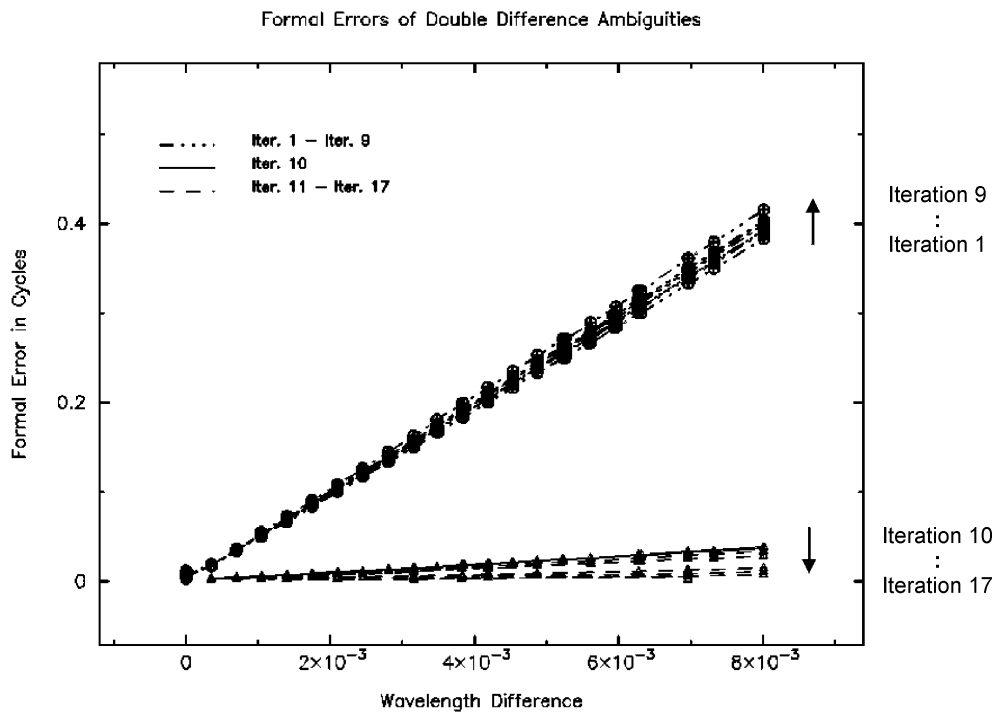


Figure 6.12: GLONASS L1 Observations, Session 213, 5 m Baseline Length

A total number of 18 single difference ambiguity parameters were estimated as real values in the first part of the parameter estimation program. The singularity of the normal equation system was removed by introducing an a priori constraint of 200 cycles on all single difference ambiguities. The formal errors of the single difference ambiguities before ambiguity resolution were approximately 48 cycles and are almost uniquely given by the a priori constraints. Following the scheme in Figure 4.1 all possible double difference ambiguities between two GLONASS satellites and their corresponding formal errors were calculated using the single difference estimates. These formal errors for the double difference ambiguities may be seen in Figure 6.12. The wavelength difference in Figure 6.12 is given by the ratio $\frac{\Delta\lambda^{ij}}{\lambda^j}$. The formal errors increase with increasing wavelength difference as expected according to equation (4.08). For the maximum wavelength difference between two GLONASS satellites the formal error is approximately 0.4 cycles in the first iteration step. This is a critical value when one intends to fix the ambiguities to an integer number. However, for small wavelength differences the formal errors are about 0.01 cycles and allow the fixing of a first ambiguity.

The ambiguity resolution approach orders all possible double difference ambiguities for each iteration step according to increasing wavelength differences and increasing formal errors. The double difference ambiguity of the satellite pair with the smallest wavelength difference and

6. Results for Various Baselines

smallest formal error is fixed to an integer number, provided the formal error does not exceed 0.07 cycles and there is exactly one integer value within the interval ± 0.21 cycles around the real valued estimates. Table 6.4 shows the resolved ambiguities for session 213. In the first iteration the difference between two single difference ambiguities for satellite 118 is resolved. In this case the wavelength difference of the “two” satellites is zero, although GLONASS frequencies were processed. After the elimination of one single difference ambiguity from the normal equation system the second iteration is performed.

The new estimates of the single difference ambiguities show formal errors of approximately the same size as in the previous iteration. The formal errors of the single difference ambiguities are given in Figure 6.13. The formal errors of the double difference ambiguities of the second iteration slightly increase compared to the first iteration. This is a well known effect caused by the elimination of an unknown parameter from the normal equation system. This effect appears for the iterations one to nine and is indicated by the upper arrow in Figure 6.12. In the second iteration the double difference ambiguity between the satellites 116 and 112 is resolved (see Table 6.4). The two satellites are antipodal and have the same carrier frequency.

Iteration No.	Satellite Pair	$\frac{\Delta\lambda^j}{\lambda^j}$	Fractional Part [cycles]	RMS of DD Ambiguity [cycles]
1	118 - 118	0.00000	0.005	0.005
2	116 - 112	0.00000	0.005	0.004
3	109 - 113	0.00000	0.028	0.003
4	111 - 115	0.00000	0.002	0.004
5	117 - 117	0.00000	0.004	0.004
6	110 - 110	0.00000	0.001	0.006
7	111 - 115	0.00000	0.012	0.006
8	120 - 120	0.00000	0.009	0.006
9	103 - 112	0.00035	0.000	0.018
10	104 - 106	0.00035	0.005	0.002
11	110 - 118	0.00035	0.004	0.003
12	112 - 117	0.00070	0.004	0.003
13	113 - 115	0.00070	0.003	0.002
14	118 - 106	0.00105	0.009	0.002
15	120 - 115	0.00105	0.013	0.002
16	106 - 115	0.00316	0.004	0.002
17	115 - 117	0.00694	0.026	0.002

Table 6.4: Resolved Double Difference Ambiguities, GLONASS L1 Observations, Session 213, 5 m Baseline Length

Following this scheme 8 ambiguities are successively resolved with a wavelength difference of zero for the corresponding satellite pairs. In the ninth iteration step a first ambiguity is resolved including two satellites with different wavelengths. However, the wavelength difference is still small compared to all possible values. Although the single difference bias term in eqn. (2.27) is not equal to zero in this case, it allows to solve the ambiguity to an integer number. The fractional part and formal error of the ambiguity to be resolved is significant smaller than 0.1 cycles as can be seen in Table 6.4. After the elimination of the corresponding single difference ambiguity from the normal equation system, the system becomes regular. The formal error of the single difference ambiguities in iteration number 10 is now significant smaller as can be seen in Figure 6.13. The formal errors of the double difference ambiguities are getting much smaller, too and this is shown in Figure 6.12. The formal errors in Figure 6.12 are mainly determined by the bias term (2.27), because the effect of other error sources is at the level of the observation noise for this 5 m baseline.

The bias term depends on the wavelength difference of the two satellites and on the error of the single difference ambiguities. In iteration number 10 the reduction in the error of single difference ambiguities leads to a smaller bias term. The formal errors of all double difference ambiguities is now smaller than 0.1 cycles, even for two GLONASS satellites with the maximum wavelength difference, and allows to resolve the ambiguities for all satellite pairs. The formal errors of the single difference ambiguities is successively improved during the iterations 11 to 17 (see Figure 6.13). The same improvement results for the formal errors of the double difference ambiguities, too, and is indicated with the lower arrow in Figure 6.12.

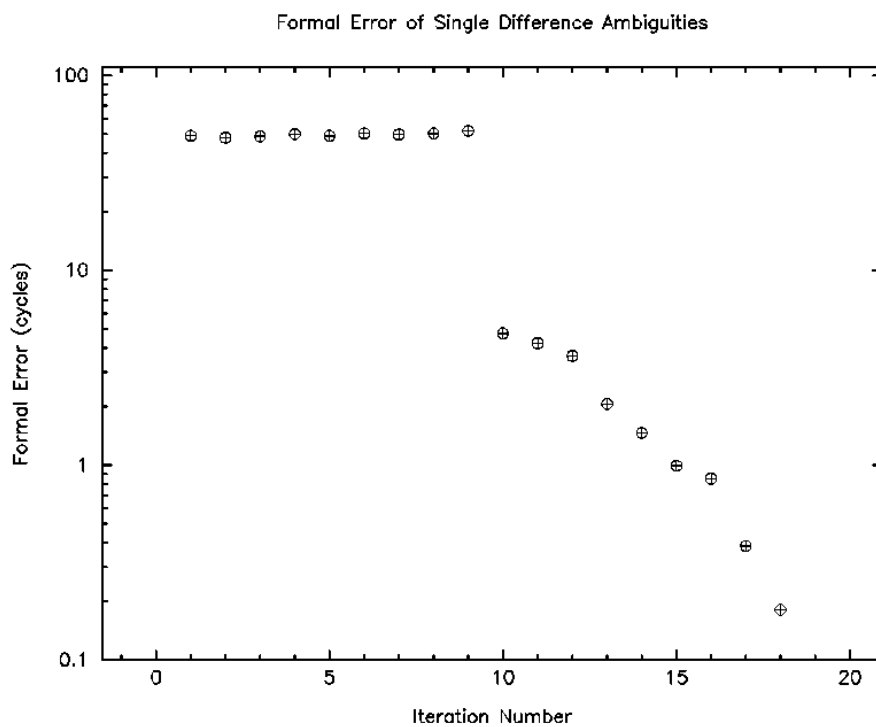


Figure 6.13: GLONASS L1 Observations, Session 213, 5 m Baseline Length

After performing iteration step 17 *one* single difference ambiguity remains unresolved in the normal equation system. The formal error of the real valued estimate for this last ambiguity is 0.18 cycles. An attempt might be made to resolve it to an integer number, but this was not done here.

Processing of Combined GLONASS/GPS Observations

The ambiguity resolution procedure for the L1 observations of session 213 was repeated using GLONASS and GPS observations. 77 single difference ambiguities were set up as unknown parameters. Their initial estimates from a first solution are used for the calculation of all possible double difference ambiguities. This includes also pairs of GLONASS and GPS satellites. The corresponding formal errors of the double difference ambiguities for this first iteration are given in Figure 6.14. The wavelength differences are given in meters and result in two “families”. The first family between 0.0 m and 0.0015 m contains all GLONASS-GLONASS satellite pairs, the second family between 0.00322 m and 0.00472 m all GLONASS-GPS pairs. As can be seen in Figure 6.14, it is not possible to resolve an ambiguity for a GLONASS-GPS pair after this first iteration. The formal errors are linear in the wavelength difference and confirm eqn. (4.08). In the first 68 iterations the formal errors are also affected by the a priori constraint that was introduced for the single difference ambiguities.

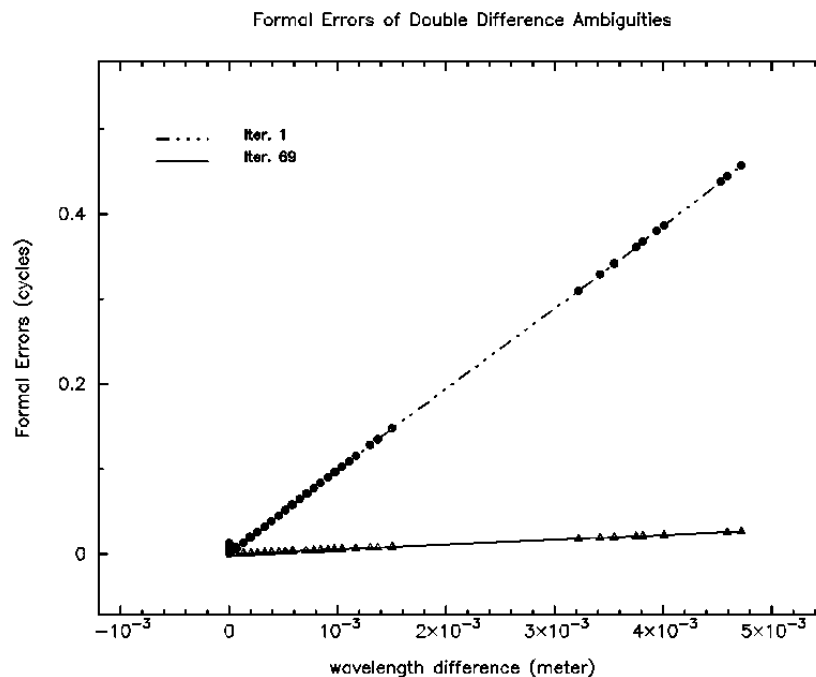


Figure 6.14: Combined GLONASS/GPS L1 Observations, Session 213, 5 m Baseline Length

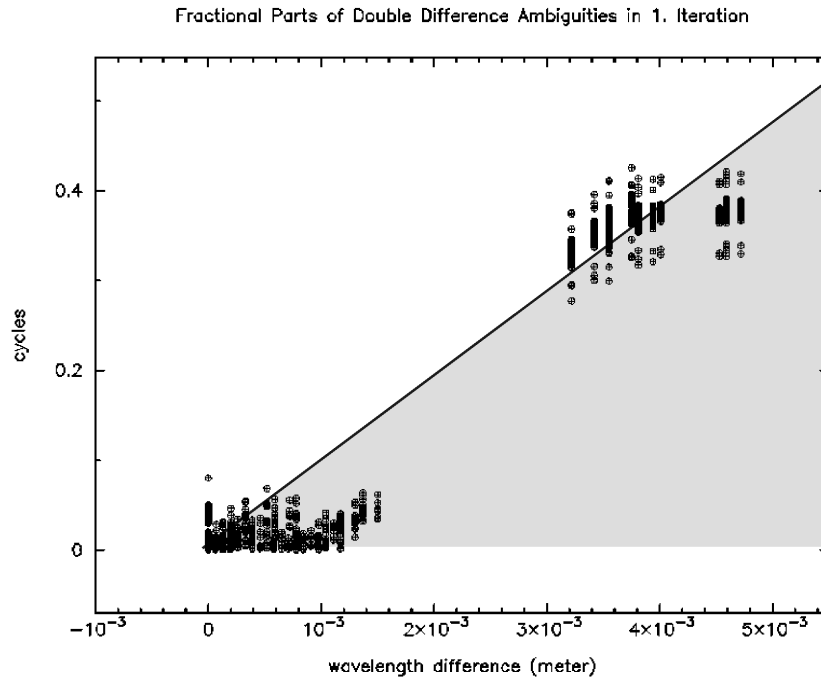


Figure 6.15: Combined GLONASS/GPS L1 Observations, Session 213, 5 m Baseline Length, 1st Iteration

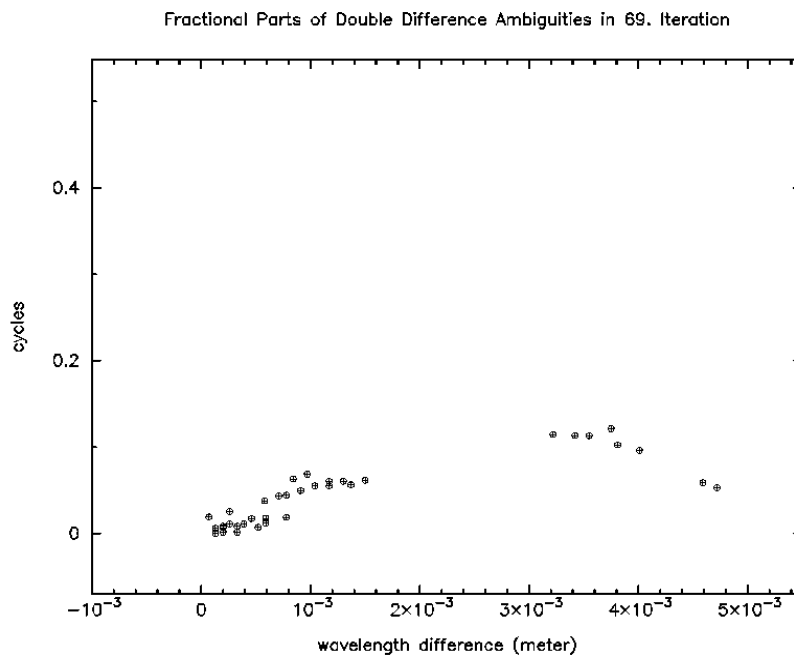


Figure 6.16: Combined GLONASS/GPS L1 Observations, Session 213, 5 m Baseline Length, 69th Iteration

Figure 6.15 shows the absolute values of the fractional parts of all possible double difference ambiguities for the first iteration step. Ambiguities for satellite pairs with large wavelength differences (and therefore with large RMS errors in Figure 6.14) have large fractional parts in Figure 6.15. Fractional parts of 0.4 cycle for GLONASS-GPS satellite pairs prevent such types of differences to be resolved in the first iteration step. The fractional parts of the double difference ambiguities are not affected by the a priori constraint that was introduced for the single difference ambiguities. However, they are affected by the error of the single difference ambiguities. In our processing we used the estimates of the receiver clocks from a code single point positioning in order to correct the receiver clock term $c \cdot \Delta t_{kl}$ in the single difference observation equations (2.20) and (5.11). Observations corrected in this way were used to compute initial values of the single difference ambiguities N_{kl}^j in the first iteration. An error of the receiver clock term $c \cdot \Delta t_{kl}$ of, e.g., 3.4 m results in an initialization error of the single difference ambiguities of 18 cycles for all GPS and GLONASS satellites in the case of L1 observations. For small errors of the receiver clock term (e.g., < 5 m) the transformation from length units into wavelength units of the corresponding satellite will result in almost the same integer number for all GPS and GLONASS satellites. An initialization error of the single difference ambiguities of $\Delta N_{kl}^j = 18$ cycles generates a single difference bias term of $b_{kl}^{ij} = \Delta N_{kl}^j \cdot \Delta \lambda^{ij}$ in the double difference observations and the bias term destroys the integer nature of the ambiguities. Values of this bias terms with the assumption $\Delta N_{kl}^j = 18$ for the corresponding wavelength differences are shown in Figure 6.15 as a solid line and define an error space of the double difference ambiguities caused by the assumed initialization errors (see grey triangle in Figure 6.15). As a matter of fact, the fractional parts of the double difference ambiguities reach values up to those given by the solid line and confirm the existence of the bias term. The fact that the fractional parts are distributed around the solid line and not over the entire grey triangle could be caused by a common initialization error of the single difference ambiguities for all GPS and GLONASS satellites. The example of the receiver clock error of 3.4 m might serve as an interpretation of the fractional parts in Figure 6.15.

In the iteration process the first ambiguity for two satellites with different carrier frequencies was resolved in step number 67. As already shown when processing only GLONASS observations, this leads to a regularization of the normal equation system and significantly improves the formal errors of the single difference and double difference ambiguities for all subsequent iterations. Figure 6.14 shows the formal errors of the double difference ambiguities in iteration number 69 (triangles). As expected the fractional parts are getting much smaller now (see Figure 6.16).

After performing 75 iterations two single difference ambiguities remain unresolved and these are given in Table 6.5. Although the formal errors of both ambiguities are quite small (0.13 cycles), the double difference ambiguity formed by the two single difference ambiguities cannot be resolved to an integer number. We have seen in the code single point positioning of the stations KARS and KARN (see Section 6.1) that the estimated system time difference between GLONASS and GPS results in two significantly different values when processing

Satellite No.	System	Fractional Part [cycles]	RMS [cycles]
117	GLONASS	0.24	0.13
27	GPS	0.04	0.13

Table 6.5: Unresolved Single Difference Ambiguities, Combined GLONASS/GPS L1 observations, Session 213

the code observations of the two receivers at KARS and KARN (see Table 6.2). This confirms the existence of the receiver-dependent term Δt_{wkl} (see eqn. (5.11)) of the system time difference, roughly 10 *nsec* for the two receivers at KARS and KARN. Due to this term Δt_{wkl} and according eqn. (5.12) we cannot resolve the double difference ambiguity of the remaining GLONASS/GPS satellite pair in Table 6.5. It is biased by the term $c \cdot \Delta t_{wkl}$. The GLONASS/GPS double difference ambiguity might be resolved, if the term Δt_{wkl} is not present or if it is known with an accuracy of a few millimeters.

6.3 Baseline of 6.6 km Length

The ionospheric refraction in eqn. (2.06) can no longer be neglected for a baseline with a length of 6.6 km. Therefore the ionosphere-free linear combination L3 is used as basic observable in the processing. The phase preprocessing as well as the ambiguity resolution have to be performed in the so-called „combined mode“ of the Bernese Software ,i.e., by using the L3 and L5 linear combinations as main observables.

Cycle Slip Detection

For session 216 and 217 (see Table 6.02) a total number of 125 and 116 cycle slips, respectively, were detected and corrected on L1 and L2. Again, the major part of the cycle slips occurred for the satellites 110 and 116.

Resolution of Wide Lane Ambiguities

The resolution of the double difference ambiguities for long baselines is performed in two steps:

- 1) We use the wide lane linear combination L5 (see eqn.(2.50)) for the resolution of the N_5 wide lane ambiguities. (Station coordinates are usually fixed to the values of an L3 ambiguity-free solution).

- 2) The known N_5 ambiguities are introduced into the processing of

6. Results for Various Baselines

the L3 observation equations (2.59) in order to resolve the remaining N_1 ambiguities. The N_2 ambiguities may then be calculated according to eqn. (2.47).

Table 6.6 gives a summary of the ambiguity parameters which were set up and resolved. Between 96 % and 100 % of the double difference ambiguity parameters could be resolved. Observe, that we could not resolve the double difference ambiguities between GLONASS and GPS satellite pairs due to the existing receiver-dependent term Δt_{wkl} (see Section 6.2.2). No attempt was made to resolve for the remaining single difference ambiguity. One double difference ambiguity between a GLONASS and GPS satellite was resolved, when processing the observations of the L5 linear combination of session 216, because the specified criteria for fixing the ambiguities (exactly one integer number within the interval ± 0.21 around the real estimates and formal error of the double difference ambiguity smaller than 0.07 cycles) happened to be met. This resolved double difference ambiguity might not be correct and this is “confirmed” by the fact, that the corresponding N_1 ambiguity could not be resolved.

Table 6.7 gives the resolved ambiguities for the satellites 111, 113 and 122 for session 216. The table lists the single difference values. However, only the double differences involved were fixed to integers. If we introduce the known N_5 ambiguities into the L3 observations, an additional bias term exists, as shown in eqns. (2.62) and (4.10). This term depends on the error in the single difference N_5 ambiguity and on the wavelength difference between the two satellites. In order to show the effect of this bias term on the ambiguity resolution the results of two computations are given in Table 6.7. In the first solution the standard initialization for ambiguity parameters was used. In the second solution the resolved N_5 ambiguities were all shifted by 20 cycles and the resulting values were introduced into the L3 processing to solve for the N_1 ambiguities. This change did not affect the double difference N_5 ambiguities.

We have seen in eqn. (4.10), that a bias in the single difference N_5 ambiguities of $\Delta N_5 = 20$ will change the results for the single difference N_1 ambiguities by $-3.5 \cdot \Delta N_5$ or -70 cycles in our case. Differences of this size were actually found in the processing, as can be seen in Table 6.7. As the single difference N_2 ambiguities are calculated according to eqn. (2.46) ,

Sess.	Observation Type	Number of Single Difference Ambiguities	Number of Unresolved Single Difference Ambiguities		Percentage of Resolved Double Difference Ambiguities	
			L5	L1	L5	L1
216	GLONASS	28	1	2	100 %	96 %
	GLONASS/GPS	74	1	2	100 %	100 %
217	GLONASS	29	1	2	100 %	96 %
	GLONASS/GPS	73	2	3	100 %	99 %

Table 6.6: Ambiguity Parameters for the 6.6 km Baseline

Satellite	Standard Initialization for Ambiguity Parameter			N5 Ambiguities shifted for 20 Cycles		
	L5	L1	L2	L5	L1	L2
111	437	1891	1454	457	1821	1364
	14119036	63535537	494165014	14119056	63535467	49416411
113	-120	-611	-491	-100	-681	-581
	8760371	39421587	30661216	8760391	39421517	30661126
	19110343	85996468	66886125	19110363	85996398	66886035
122	-887	-4065	-3178	-867	-4135	-3268
	10569971	47564793	36994822	10569991	47564723	36994732
	18264915	82191996	63927091	18264935	82191926	63926991

Table 6.7: Resolved Ambiguities, Session 216, 6.6 km Baseline

they will change by $-3.5 \cdot \Delta N_5 - \Delta N_5$ or -90 cycles in our case. The changes for N_5, N_1 and N_2 are the same for all single difference ambiguities within one ambiguity cluster and thus do not affect the double difference ambiguities. However, if we want to resolve the N_1 and N_2 ambiguities on the single difference level, the N_5 ambiguities have to be correctly resolved on the single difference level as well.

Four different coordinate solutions for the station KLOP were calculated using the data of session 216 and 217, while the station KARS was hold fixed. Table 6.8 shows the differences between coordinates resulting from the two sessions for float and fixed ambiguities. The session repeatability improves for both, GLONASS and combined GLONASS/GPS observations, after ambiguity resolution.

Observation Type	<u>Float Ambiguities</u> Coordinate Difference Session 216 - 217 [mm]	<u>Fixed Ambiguities</u> Coordinate Difference Session 216 - 217 [mm]
GLONASS	North: 1.0 East: -3.8 Up: 1.2	North: 1.4 East: -1.2 Up: 0.2
GLONASS/GPS	North: 0.4 East: -2.4 Up: 9.8	North: 0.4 East: -0.8 Up: 2.8

Table 6.8: Difference of Resulting Coordinates for KLOP, 6.6 km Baseline

6.4 Baselines of 16, 41 and 58 km Length

In order to study the reliability and efficiency of our ambiguity resolution algorithms, the stations WTZZ, BODE and BRUC were observed with Ashtech Z18 combined GLONASS/GPS receivers in June 1999 (see Table 6.1). Three baselines of 16.5, 41.4 and 57.7 km length were defined and processed. In all processing steps we used precise IGS orbits for GPS satellites and improved orbits for GLONASS satellites resulting from the IGEX campaign (see Chapter 7).

Code Single Point Positioning

The observation RMS errors after performing a code single point positioning for all stations are given in Table 6.9 for GLONASS, GPS and combined GLONASS/GPS observations. Also, the estimated system time difference Δt^s (see eqn. (5.06)) and the corresponding formal errors are included in this table. The significantly larger RMS error for the observations of the station WTZZ, session 168, is caused by orbit modeling problems for GLONASS satellite number 116 (this satellite was observed from the receiver in WTZZ only). The estimates of the system time difference Δt^s show differences between the three receivers involved and confirm the existence of the receiver-dependent term Δt_w in eqn. (5.09). All possible differences of the estimates of Δt^s between two receivers are given in Table 6.10. The differences of Δt^s change between the three sessions. These changes may be interpreted in two ways. The first interpretation uses the session to session repeatability of the differences of Δt^s as a more realistic value of the formal errors of Δt^s , compared to those values given in Table 6.9. The second interpretation concludes from the changes of the differences of Δt^s that the receiver-dependent term Δt_w in eqn. (5.09) may change between the sessions. We cannot decide which of the two interpretations is correct based on our results. However, if the second

Session	Station	GLONASS RMS [m]	GPS RMS [m]	Combined RMS [m]	System Time Difference [nsec]
166	WTZZ	9.4	23.7	21.0	-392.66 ± 0.95
	BODE	10.5	23.4	20.4	-442.95 ± 1.85
	BRUC	10.1	22.5	19.4	-412.08 ± 1.89
167	WTZZ	12.5	22.9	20.9	-405.50 ± 0.92
	BODE	8.8	23.2	19.9	-470.97 ± 1.60
	BRUC	8.0	23.7	19.3	-429.88 ± 1.37
168	WTZZ	17.2	25.2	24.2	-347.34 ± 1.10
	BODE	8.7	22.8	20.2	-438.13 ± 2.06
	BRUC	9.2	23.6	20.8	-392.88 ± 1.99

Table 6.9: Observation RMS Error of the Code Single Point Positioning and System Time Difference

Receiver Pair	Differences of Δt^s [nsec]		
	Session 166	Session 167	Session 168
WTZZ - BODE	50.29	65.47	90.79
WTZZ - BRUC	19.42	24.38	45.54
BODE - BRUC	-30.87	-41.09	-45.25

Table 6.10: Differences of the Estimates of the System Time Difference

interpretation is true and we assume changes of Δt^s during the session, we could not process double difference observations of a combined GLONASS/GPS satellite pair at all.

Ambiguity Resolution

The wide-lane linear combination of the observations of all baselines were processed to solve for the wide-lane N_5 ambiguities. The coordinates of an L3 float solution were held fixed in this processing step. We introduced an ionosphere model that was computed from an L4 solution and troposphere parameters for every 3 hours were set up for one of the two stations of each baseline. One double difference ambiguity was fixed to an integer value with each iteration step, if there was exactly one integer within the interval ± 0.21 cycles around the real estimate and if the formal error of the double difference ambiguity was smaller than 0.07 cycles. The resolved N_5 ambiguities were then introduced as known parameters into an L3 solution to solve for the N_1 ambiguities.

Baseline	Sess.	Number of Single Diff. Ambiguities	Unresolved Single Difference Ambiguities				Percentage of Resolved Double Difference Amb.	
			Expected		Realized		L5	L1
			L5	L1	L5	L1		
WTZZ-BODE 16.5 km	166	21	2	2	2	2	100 %	100 %
	167	28	4	4	6	7	75 %	71 %
	168	20	4	4	5	6	80 %	70 %
WTZZ-BRUC 41.4 km	166	19	2	2	2	2	100 %	100 %
	167	32	3	3	1	3	100 %	96 %
	168	23	4	4	5	5	95 %	95 %
BODE-BRUC 57.7 km	166	14	2	2	2	2	100 %	100 %
	167	25	4	4	4	8	100 %	81 %
	168	17	4	4	8	9	38 %	31 %

Table 6.11: Number of Single Difference Ambiguity Parameters and Resolved Double Difference Ambiguities

6. Results for Various Baselines

Table 6.11 shows the number of single difference ambiguities that were set up as unknown parameters in the normal equation system for each baseline. We solved for the double difference ambiguities and made no attempt to resolve the last remaining single difference ambiguity (see Section 4.2) to an integer number. Due to the receiver-dependent term Δt_w , that we have found in the code single point positioning, we may not expect to resolve the ambiguity of a GLONASS/GPS satellite pair. Therefore, we expect 2 single difference ambiguities to remain unresolved and in this case we claim to have 100 % of the double difference ambiguities resolved. This is the situation for all three baselines of session 166. The observations of sessions 167 and 168 have large observation gaps and we would expect more than 2 single difference ambiguities to be unresolved. The expected number of unresolved single difference ambiguities will be discussed below using selected baselines as examples.

Baseline BODE-BRUC, Session 166

Figure 6.17 shows the observations of each satellite that were processed for the baseline BODE-BRUC (57.7 km length) for session 166. The frequency numbers used by the GLONASS satellites are given in column “CHN”. The GLONASS satellites involved allow it to compute double difference ambiguities of two GLONASS satellites with small wavelength differences (e.g., satellites 108 and 110). This is performed in “Step 4” of the ambiguity resolution algorithm of Section 4.2. The single difference bias terms (2.27) are small for such satellite pairs and allow the resolution of a first double difference ambiguity for a satellite pair with different wavelengths (provided the ambiguity resolution criteria as mentioned above is fulfilled). Following the scheme in Figure 4.01 the next ambiguity may then be resolved. Due to the receiver-dependent term Δt_w two single difference ambiguities remain unresolved for this baseline. These unresolved single difference ambiguities are marked with “W” for the N_5 and with “A” for the N_1 ambiguities in Figure 6.17.

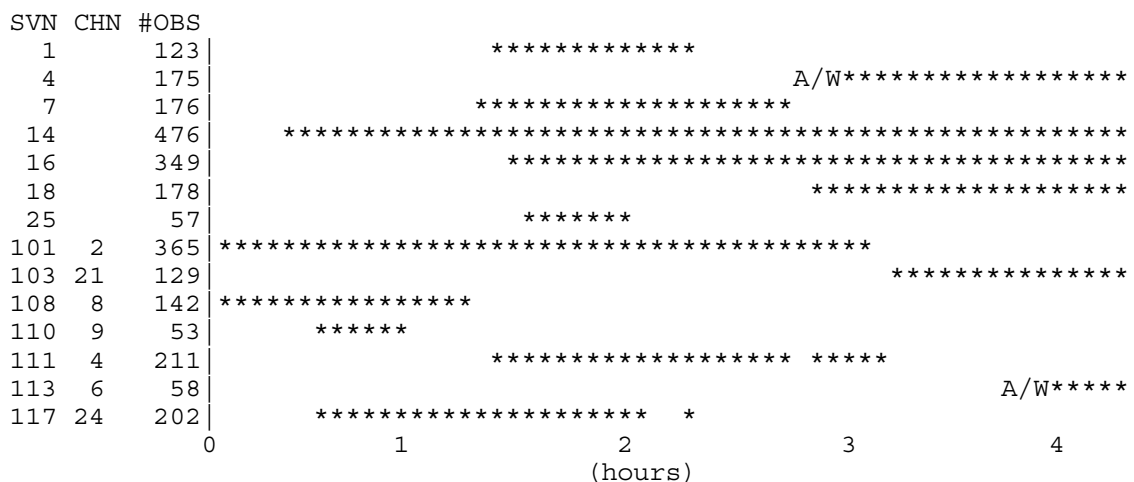


Figure 6.17: Observations of Baseline BODE-BRUC, Session 166

Figure 6.18 shows the formal errors of all possible double difference ambiguities of the 1. and 9. iteration steps when processing the wide-lane linear combination. In the 8. iteration step a first double difference ambiguity of a satellite pair with different wavelengths was resolved. Therefore, the formal errors of the double difference ambiguities were getting much smaller in the 9. Iteration step. Figure 6.18 is comparable to Figures 6.12 and 6.14. The formal errors in Figure 6.18 are given in cycles of the wide-lane linear combination.

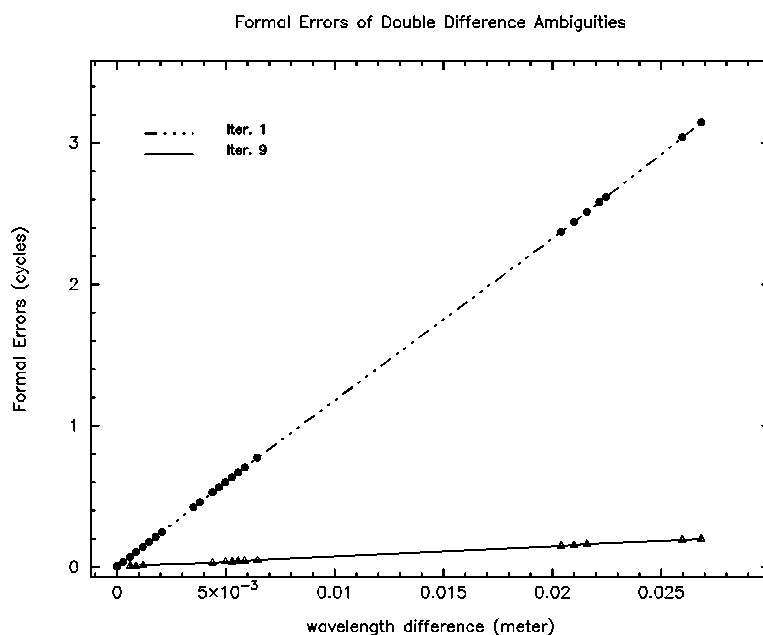


Figure 6.18: Baseline BODE-BRUC, Session 166, L5 Linear Combination

Figure 6.21 shows similar results when processing the L3 linear combinations. We introduced the known N_5 ambiguities and solved for the N_1 ambiguities. Due to the fact, that no N_5 double difference ambiguity between a GLONASS and a GPS satellite was resolved and therefore could not be introduced as known, we could not resolve any N_1 combined GLONASS/GPS double difference ambiguity. This is why only GPS/GPS and GLONASS/GLONASS double difference ambiguities are included in Figure 6.21.

The fractional parts of all possible double difference ambiguities of the 1. and 9. iteration steps are given in Figures 6.19 and 6.20 for the N_5 ambiguities and in Figures 6.22 and 6.23 for the N_1 ambiguities. The fractional parts in Figure 6.19 are larger than 0.5 cycles for wavelength differences larger than 0.025 m and may not all be drawn correctly (fractional parts larger than 0.5 are ambiguous). The same effect may be seen in Figure 6.22 for wavelength differences larger than 0.006 m.

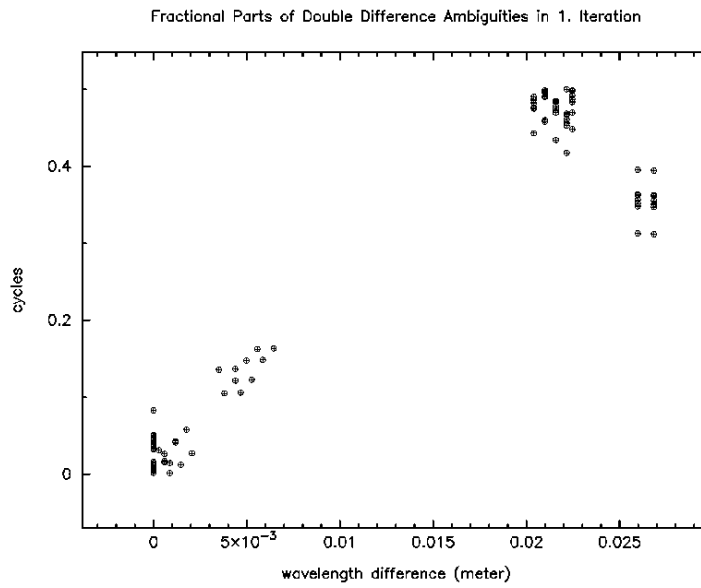


Figure 6.19: Baseline BODE-BRUC, Session 166, L5 Linear Combination

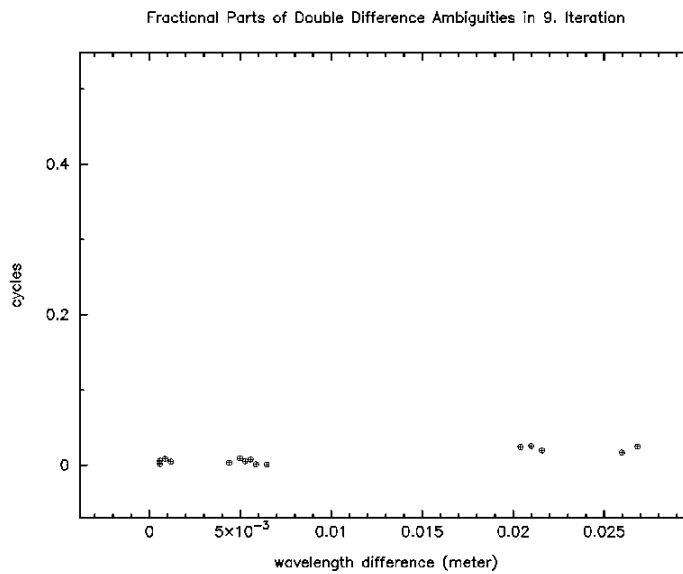


Figure 6.20: Baseline BODE-BRUC, Session 166, L5 Linear Combination

	N_5 Ambiguity			N_1 Ambiguity		
	Formal Error of Single Difference Ambiguity		Difference of Single Difference Ambiguity [Cycles]	Formal Error of Single Difference Ambiguity		Difference of Single Difference Ambiguity [Cycles]
	Initial Solution [Cycles]	Final Solution [Cycles]		Initial Solution [Cycles]	Final Solution [Cycles]	
Unresolved GPS Ambiguity	97.82	0.32	25.53	65.26	0.86	217.83
Unresolved GLONASS Ambiguity	100.33	0.33	21.56	66.45	0.88	178.19

Table 6.12: Changes of Initial Single Difference Ambiguities in the Ambiguity Resolution Iterations, Baseline BODE-BRUC, Session 166

The fractional parts in Figures 6.22 and 6.23 are much larger than those in Figures 6.19 and 6.20. As mentioned in Section 6.2.2, the fractional parts of the double difference ambiguities of the first iteration step are affected by the error of the initial single difference ambiguities. Table 6.12 shows the formal errors of the single difference ambiguities of the initial and the final solution. The numbers are given for the two satellites whose ambiguities remained unresolved. The single difference ambiguities were improved by the iterative ambiguity resolution procedure and Table 6.12 gives the differences between their initial and final values, as well. Due to the fact, that the formal error of the single difference ambiguities in the final solution is smaller than one cycle of the L5 resp. L1 wavelength, we may use the difference between the final and the initial values as an approximation for the error of the initial single difference ambiguities. This would lead to much larger errors of the initial N_1 single difference ambiguities (217.83 and 178.19 cycles) compared to the values for the N_5 single difference ambiguities (25.53 and 21.56). It would explain the larger fractional parts in Figure 6.22 compared to Figure 6.19. Although we found fractional parts of up to 0.5 cycles of the L1 wavelength in the ninth iteration step (see Figure 6.23), all double difference N_1 ambiguities between GLONASS satellites could be resolved (see Table 6.11). The fractional parts were getting smaller after each iteration step of the ambiguity resolution process.

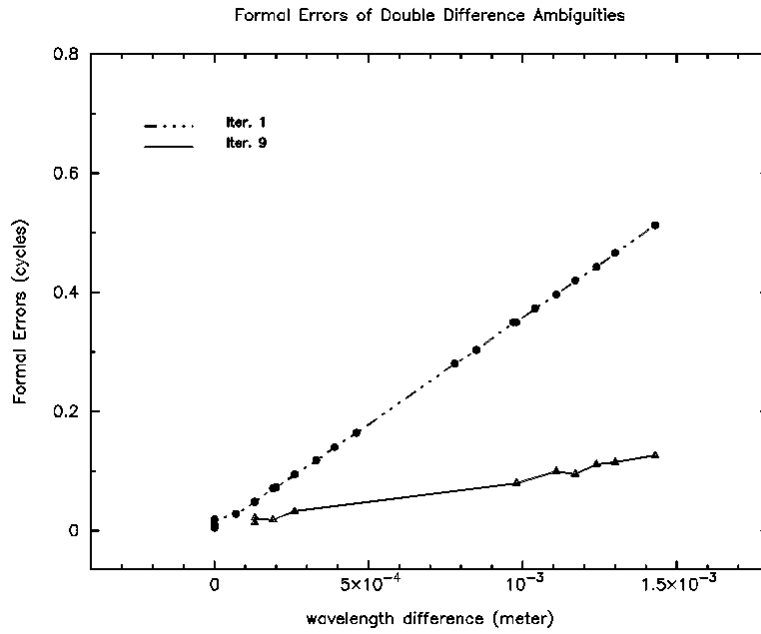


Figure 6.21: Baseline BODE-BRUC, Session 166, L3 Linear Combination

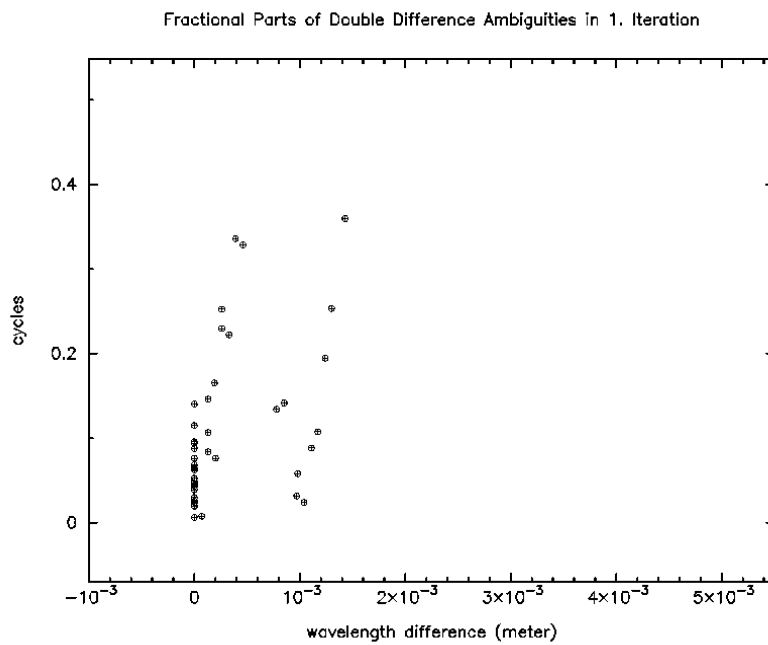


Figure 6.22: Baseline BODE-BRUC, Session 166, L3 Linear Combination

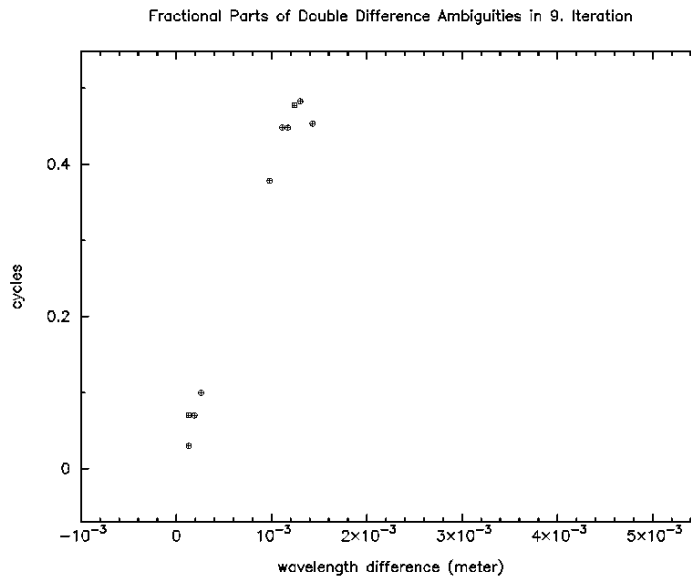


Figure 6.23: Baseline BODE-BRUC, Session 166, L3 Linear Combination

Baseline WTZZ-BODE, Session 167

The observations for the baseline WTZZ-BODE (16.5 km length) for session 167 are given in Figure 6.24. An observation gap for all satellites divides this session into two “observation clusters”. We may not expect to resolve any double difference ambiguity for two satellites belonging to different observation clusters. Therefore, we expect 4 single difference ambiguities to remain unresolved (see Table 6.11). In fact, we found 6 N_5 and 7 N_1 single difference ambiguities unresolved. This may be explained by the frequencies of the GLONASS satellites involved in the second observation cluster. The signals of three GLONASS satellites were observed in this observation cluster with frequency numbers 2, 10 and 24. The frequencies of these three satellites are very different and do not allow it to resolve a first double difference ambiguity between any two of these satellites because any combination has a large single difference bias term. No double difference ambiguity could be resolved in the second observation cluster. One double difference ambiguity of the first cluster remained unresolved due to a small number of observations.

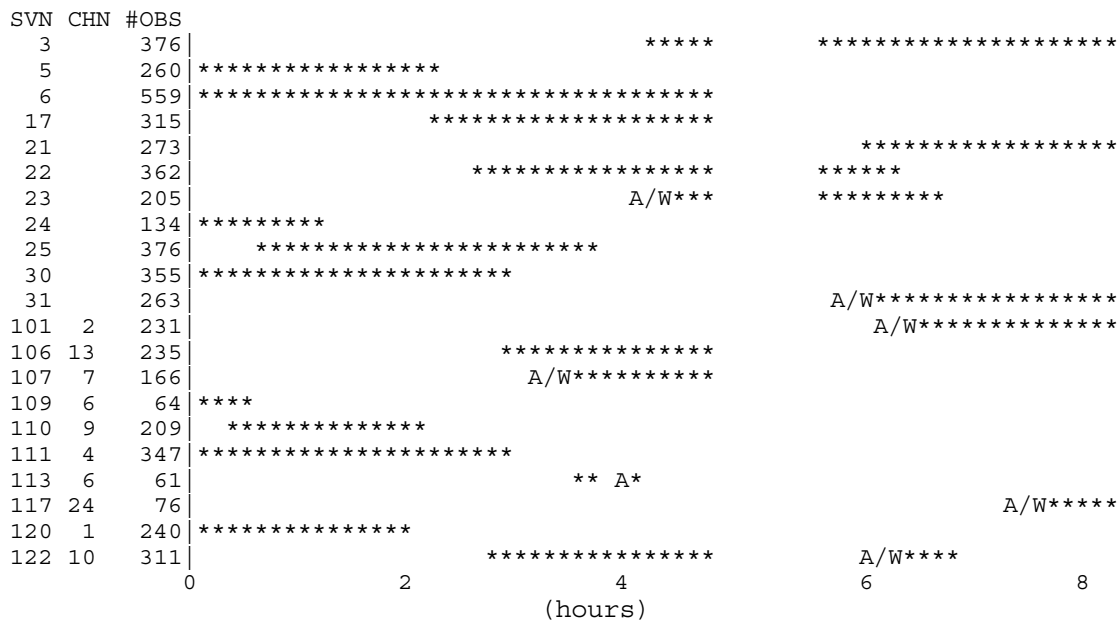


Figure 6.24: Observations of Baseline WTZZ-BODE, Session 167

Baseline WTZZ-BRUC, Session 167

The observations of the baseline WTZZ-BRUC (41.4 km length) of session 167 include a gap affecting all GLONASS satellites as may be seen in Figure 6.25. Due to this gap two “GLONASS observation clusters” are present and we cannot expect to resolve a double difference ambiguity for any two satellites belonging to different observation clusters. One GPS and two GLONASS single difference ambiguities are therefore expected to remain unresolved in this case (see Table 6.11).

In fact, double difference N_5 and N_1 GLONASS ambiguities between the two GLONASS observation clusters were resolved which “connect” the two clusters to one and reduce the number of unresolvable single difference ambiguities. The L5 processing resolved one GLONASS/GPS double difference ambiguity, because the ambiguity resolution criterion was fulfilled by the fractional part of 0.002 cycles and the formal error of 0.012 cycles. The two satellites of this double difference ambiguity are marked with “R” in Figure 6.25. The resolution of a GLONASS/GPS double difference ambiguity is critical due to the receiver-dependent term Δt_w of the system time difference. The connection of the two GLONASS observation clusters and the resolution of a GLONASS/GPS double difference ambiguity led to one unresolved single difference N_5 ambiguity (see Table 6.11).

The resolution of the double difference N_1 ambiguities was successful for several GLONASS satellite pairs in different GLONASS observation clusters and the two GLONASS observation clusters were phase-connected again. Three GLONASS/GPS double difference N_1 ambiguities were resolved, where all satellite pairs include GLONASS satellite 117. No double difference N_1 ambiguity between GLONASS satellite 117 and any other GLONASS satellite was resolved. It has to be mentioned, that 91 observations could be processed. This may result in a weakly determined real valued estimate for the corresponding ambiguity. Double difference GLONASS/GPS ambiguities between satellite 117 and a GPS satellite might be accepted by the ambiguity resolution algorithm, if this weakly determined estimate meets the ambiguity resolution criterion. However, in this case satellite 117 “changes over” to the GPS observation cluster and the system time bias exists now between satellite 117 and the remaining GLONASS satellites, also. This behaviour forbids the resolution of double difference GLONASS ambiguities between satellite 117 and any other GLONASS satellites. For this baseline three N_1 single difference ambiguities remained unresolved, the single difference ambiguity of satellite 117 (as representative of the GPS observation cluster) and two ambiguities of two other GLONASS satellites.

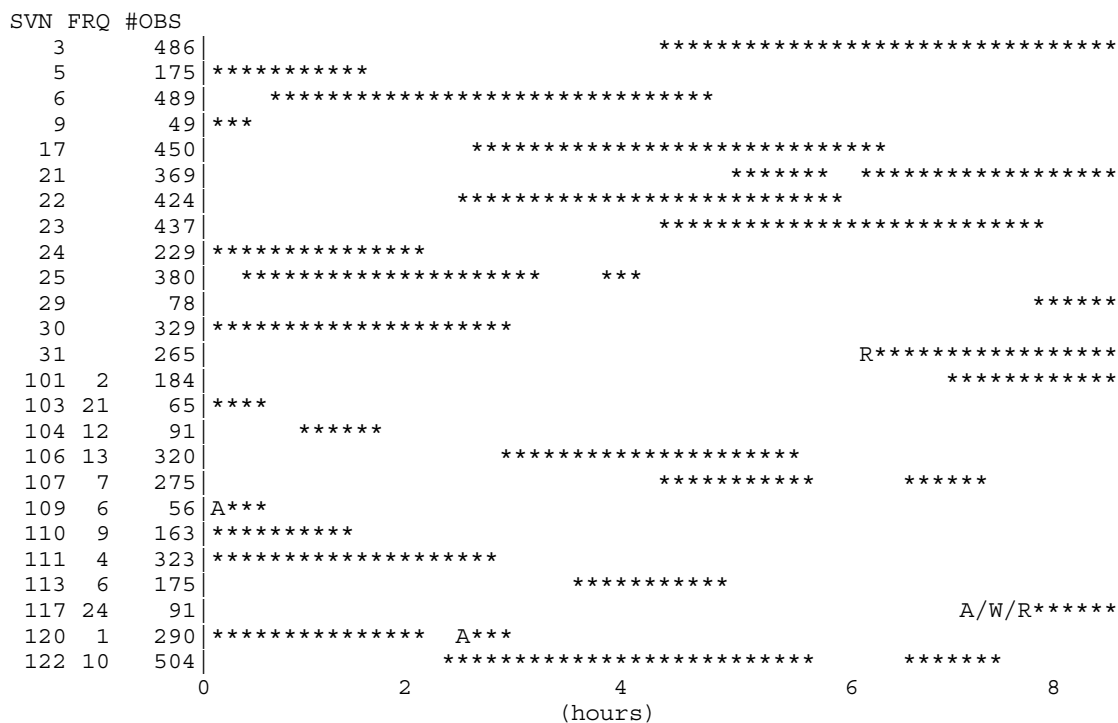


Figure 6.25: Observations of Baseline WTZZ-BRUC, Session 167

Summary of Baseline Processing

From processing the three baselines we conclude, that the ambiguity resolution algorithm of Section 4.2 was successfully used for baselines between 16 and 58 km length. The success of the ambiguity resolution was less sensitive to the length of the baselines, but depend heavily on the number of continuous observations. We found the highest percentage of resolved double difference ambiguities for the shortest session, but no gaps occurred in this session.

If no GLONASS satellite pair with small wavelength difference is present within an observation cluster, it may not be possible at all to resolve a GLONASS double difference ambiguity using our approach, because all possible combinations of the satellites show large single difference bias terms.

The resolution of combined GLONASS/GPS double difference ambiguities is critical if a receiver-dependent term Δt_w of the system time difference exists. Such ambiguities may be accepted by the ambiguity resolution algorithm, if the specified criteria are fulfilled. The ambiguity resolution algorithm might be changed not to accept any combined GLONASS/GPS double difference ambiguity, as long as the receiver-dependent term Δt_w is not known.

7. The International GLONASS Experiment (IGEX-98)

The International GLONASS Experiment (IGEX-98) is the first global GLONASS observation and analysis campaign for geodetic and geodynamics applications. It is organized by

- Commission VIII, International Coordination of Space Techniques for Geodesy and Geodynamics (CSTG) of the International Association for Geodesy (IAG),
- the International GPS Service (IGS), and
- the Institute of Navigation (ION).

It was also supported by the International Earth Rotation Service (IERS).

For duration of the campaign it is the goal to collect the observations, transfer data to global data centers and to analyse the data. Due to the fact, that all GLONASS satellites are equipped with laser reflectors, a close cooperation between IGEX-98 and the ILRS (International Laser Ranging Service) has been established. The main objectives of IGEX-98 are:

- Set up a global GLONASS observation network,
- test GLONASS data processing software,
- determine GLONASS orbits of meter-quality or better in a well defined Earth-fixed reference frame (namely the ITRF),
- gain insight into GLONASS orbit modeling peculiarities (solar radiation pressure, attitude, etc.),
- study common GPS/GLONASS processing strategies,
- collaborate with the SLR community to evaluate the accuracy of the determined GLONASS orbits,
- determine transformation parameters between the GLONASS operational reference frame PZ-90 and ITRF or WGS84,
- connect the GPS and GLONASS time systems,

7. The International GLONASS Experiment (IGEX-98)

- compare receiver equipment performance,
- compare the separate and combined satellite systems on a global basis, and
- foster participation and cooperation with Russian agencies and organizations.

The campaign was originally planned for a period of three months between September 20 and December 20, 1998. Due to the large number of receivers, which were being installed but not yet operational in early September 1998, the campaign was postponed and started on October 19, 1998. During the time period of the campaign an average number of 12 to 14 GLONASS satellites were operational. On December 30, 1998, three new GLONASS satellites were launched. In order to make use of these new satellites and because of the late installation of some IGEX receivers it was decided to extend the campaign till April 19, 1999.

During IGEX-98 the following geodetic receiver types were being used:

- Combined dual-frequency GPS/GLONASS receivers,
- dual-frequency GLONASS receivers,
- combined single-frequency (L1) GPS/GLONASS receivers and
- single-frequency GLONASS receivers.

A map of the operational IGEX stations as of February 1999 is given in Figure 7.1. The network consisted at that time of 52 stations with 39 dual-frequency and 13 single-frequency receivers. For the IGEX campaign an infrastructure comparable to that of the IGS was established. Intensive use was made of the Internet in order to transfer the observation data from the stations to regional and global data centers. IGEX analysis centers are using the data to generate results. The results of several analysis centers will be compared and, furthermore, a comparison with results from independent techniques, e.g., SLR, will be performed.

The Bundesamt für Kartographie and Geodesy (BKG) in Frankfurt, Germany participates in the IGEX-98 campaign with the operation of three GLONASS/GPS receivers, as a regional data center for Europe, and as an IGEX Analysis Center. In addition, SLR observations to GLONASS satellites are performed (and analysed) at BKG's fundamental station in Wettzell, Germany. Results from processing combined GLONASS/GPS observations at BKG are presented in the sequel.

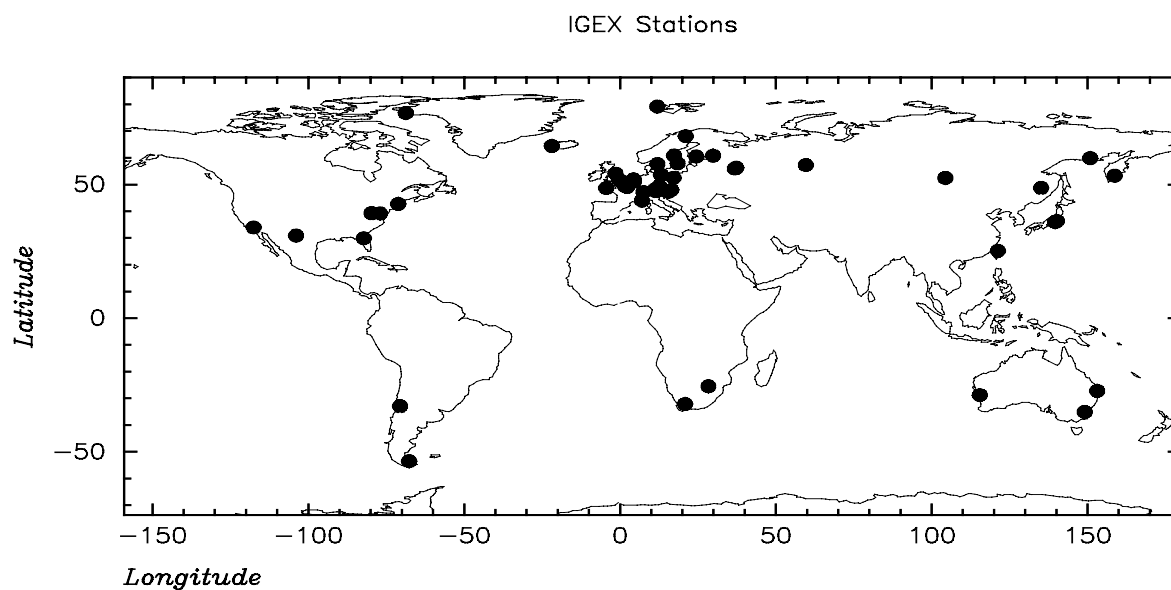


Figure 7.1: Operational IGEX Stations in February, 1999

7.1 Routine Processing Scheme

In this section we describe the regular processing scheme used at BKG for IGEX observations. The main BKG products are:

- Precise Orbits for GLONASS satellites in the ITRF 96,
- station by station estimates for the system time difference between GLONASS and GPS time, and
- transformation parameters between PZ-90 and ITRF 96.

A report with the weekly analysis results is regularly submitted to IGEXMAIL. A summary of the processing steps is given in Figure 7.2.

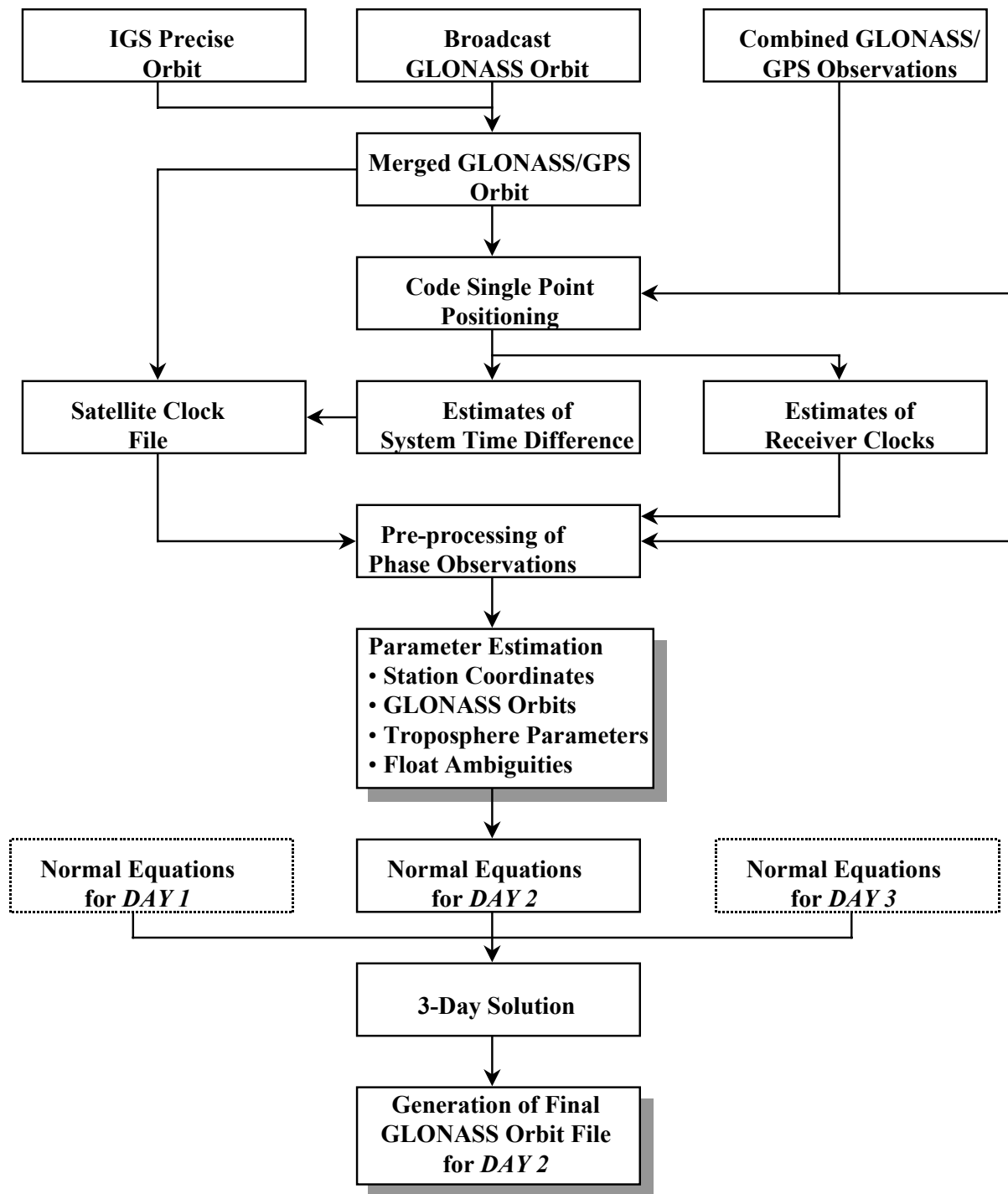


Figure 7.2: Processing Scheme for the Computation of Precise GLONASS Orbits

Orbit Improvement

For the GPS satellites the final precise orbits as provided by the IGS are used. No attempt is made to improve the orbits of the GPS satellites. The GPS orbit files are merged with broadcast GLONASS orbits to a common GLONASS/GPS orbit file in a unique reference system (nominally the ITRF) and referred to the GPS system time scale (see Figure 5.01). A code single point positioning is performed for each station solving for station coordinates and receiver clock corrections. If both, GLONASS and GPS observations, are available for a station the system time difference is estimated as well.

The estimates of the system time difference are introduced into the phase observations by applying one common system time correction (the average from all stations) to all GLONASS satellite clock offsets. As shown in eqns. (5.10) and (5.12), this will contribute to a reduction of the system-dependent part Δt^v but not of the receiver-dependent part Δt_w of the system time difference term in the phase observation equation.

A first orbit improvement for the GLONASS satellites is performed after phase pre-processing step. The results are stored into a normal equations file. Six initial conditions and nine radiation pressure parameters are determined per satellite. Finally, the normal equations of three days are combined in order to generate a 3-day arc for each GLONASS satellite. The middle day of each arc is saved into the resulting orbit file. To monitor the precision of the orbits, a 7-day arc is fitted through the satellite positions of seven individual days (one GPS week) for each GLONASS satellite. The RMS error of the differences between the daily orbits and the 7-day arc is taken as an indicator of the quality of the improved GLONASS orbits. Table 7.1 shows these RMS errors for GPS week 981. An overall precision of 20 to 30 cm for the satellite positions was found. This is much better than the RMS error of the broadcast ephemerides given in Table 1.07.

Day of Year	GLONASS Satellite Numbers												Units: cm	
	103	104	106	109	110	111	112	113	115	116	117	118	120	122
298	13	22	25	14	67	16	17	17	19	25	48	15	11	11
299	22	16	23	11	43	8	37	13	17	52	27	10	7	6
300	28	32	16	23	41	12	34	16	10	35	39	21	6	16
301	26	32	18	17	59	9	49	24	13	36	37	14	11	12
302	14	29	29	14	50	29	12	14	9	28	29	18	12	7
303	7	10	45	9	66	26	60	17	8	17	43	8	20	9
302	11	16	26	8	86	19	46	12	22	48	14	11	11	8
ALL	19	24	27	15	61	19	40	17	15	36	35	14	12	10

Table 7.1: Orbit Repeatability of Improved GLONASS Orbits for GPS Week 0981, Daily Solutions Compared to 7-Day Arc

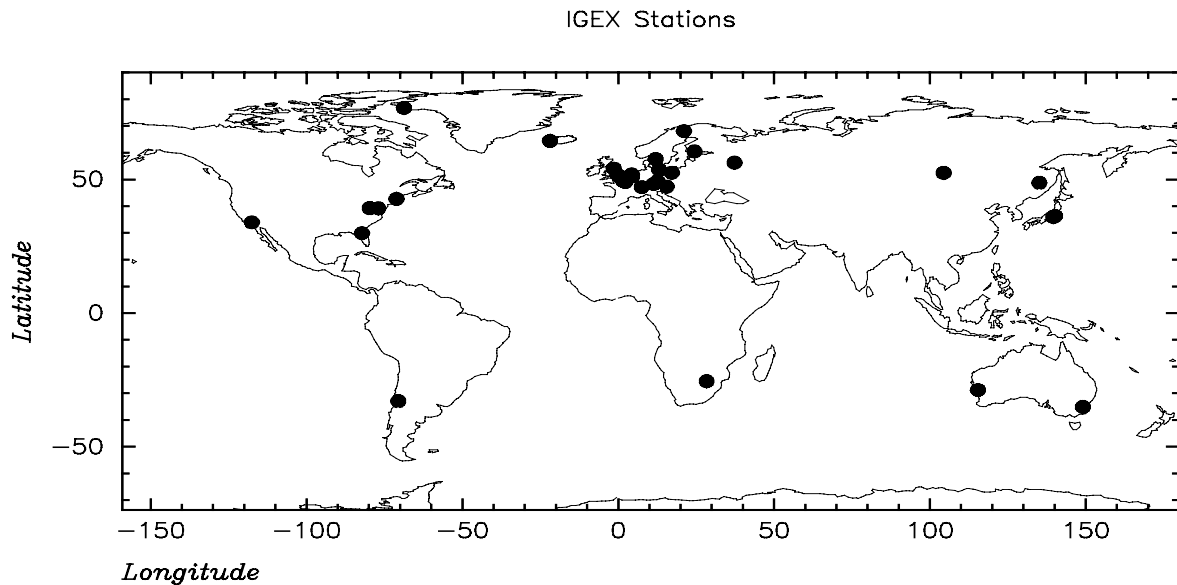


Figure 7.3: IGEX Stations with Dual Frequency Receivers Processed at BKG in December, 1998

Site Coordinate Comparison

The ionosphere-free linear combination L3 was used for this purpose. A total of 32 IGEX stations with dual-frequency receivers were selected for the analysis as shown in Figure 7.3. The coordinates of one station (Zimmerwald in Switzerland) were held fixed to the ITRF 96 values. Figure 7.4 gives the RMS errors of a coordinate comparison of the 7 1-day solutions of GPS week 984. The repeatability of about 5 mm in the horizontal position and 15 mm in the height is comparable to the quality of global solutions from GPS observations. Stations with large RMS values have only few observations or are very isolated.

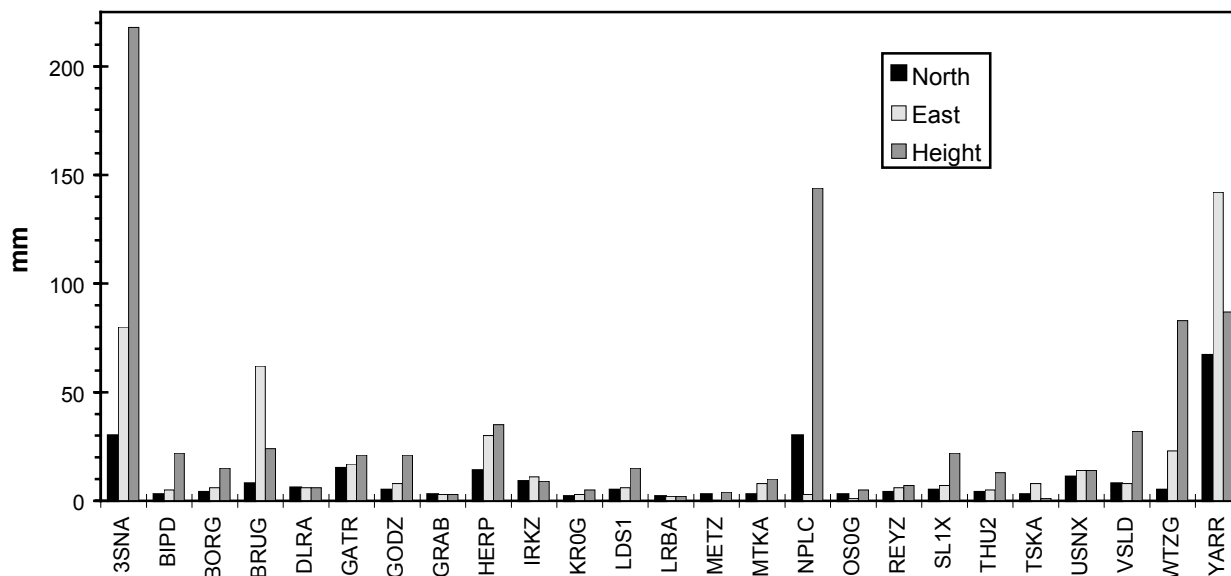


Figure 7.4: Coordinate Repeatability of 1-Day Solutions for GPS week 0984

7.2 Estimates of the System Time Difference

For each IGEX station processed the system time difference between GLONASS and GPS time was estimated in the code single point positioning, provided observations from both systems were available. As introduced in eqn. (5.04) a receiver clock bias τ_r may exist between GLONASS and GPS observations apart from the system dependent terms τ_c , τ_u and τ_g . The results of the IGEX campaign confirm the existence of such biases for all receiver types.

Figure 7.5 shows the estimates of the system time difference for 20 IGEX stations. Nearly identical estimates were found for identical receiver types. However, discrepancies of up to 2 μsec occur between different receiver types. For all Ashtech Z18 receivers the system time difference was determined to be approximately 50 $n\text{sec}$. The 3S-Navigation receivers show values of about 1 μsec with the exception of one receiver of this type, located in Wettzell, Germany. The estimates for Wettzell were determined to about -700 $n\text{sec}$. It has to be mentioned that this receiver was one of the first produced by the manufacturer and may include different hardware components. One JPS Legacy receiver was included in the processing and shows less stable estimates of the system time difference compared to other receivers. Following the information from the JPS company the receiver in Gainesville, Florida, was operated with old firmware for the period shown in the Figure 7.5. The estimates of the ESA/ISN receiver in Leeds, UK, amount to approximately -900 $n\text{sec}$. All estimates,

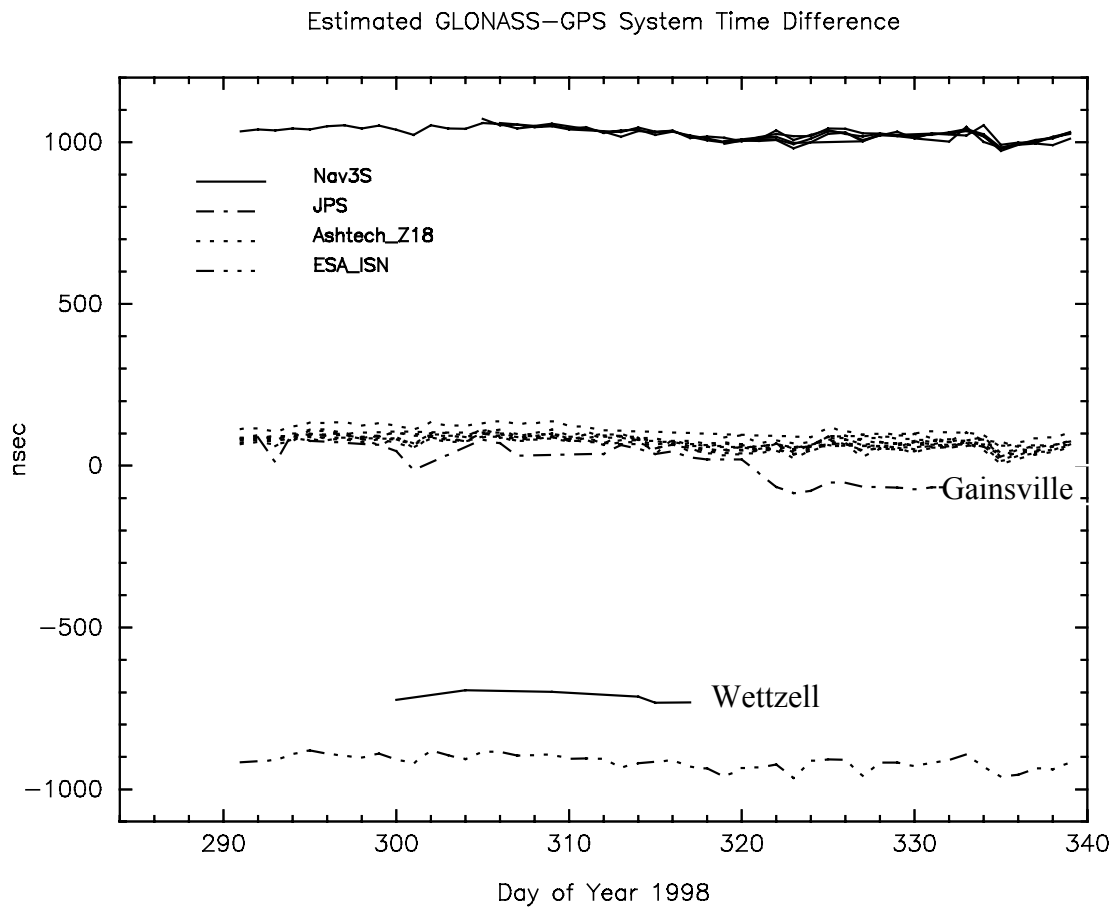


Figure 7.5: Results of Code Single Point Positioning for IGEX Stations

with the exception of the receiver in Wettzell, are in quite close agreement (if we take the „modulo ($1 \mu\text{sec}$)“ function for each estimate).

Daily values of $t_{UTC} - t_{GLONASS}$ are determined at BIPM and published in the Circular T. In Figure 7.6 the daily estimates of BIPM and the corresponding results of the IGEX campaign for the station Zimmerwald (Ashtech Z18 receiver) are given. Both curves are highly correlated but shifted by approximately 200 nsec. The BIPM values are calculated from observations made at the Van Swinden Laboratorium Delft, Netherlands. The daily values are corrected by 1285 nsec in order to ensure continuity with the BIPM estimates of January 1, 1997. For the time before 1997 the BIPM estimates were calculated from GLONASS observations collected at the University of Leeds, UK. The uncertainty of the BIPM values for $t_{UTC} - t_{GLONASS}$ is of the order of several hundred nsec.

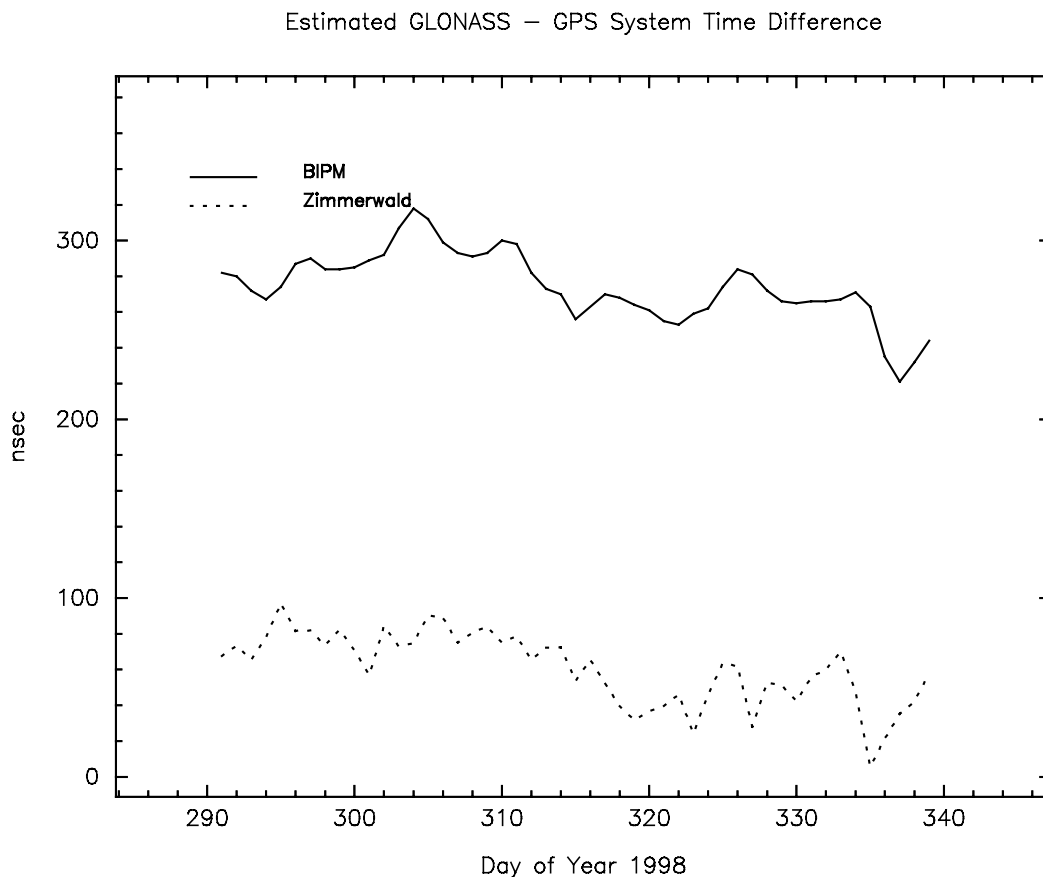


Figure 7.6: Comparison of BIPM and IGEX Estimates of the System Time Difference Between GLONASS and GPS

GLONASS/GPS Receiver Biases for Ashtech Z-18 Receivers

In order to look at the estimates of the GLONASS/GPS system time difference of Ashtech Z-18 receivers in more detail, the estimates of Figure 7.5 are given separately in Figure 7.7. Almost identical day to day variations of all Ashtech Z-18 receivers involved can be seen in Figure 7.7. However, biases of up to 50 *nsec* between the receiver-specific curves show up. We may use the difference between the curves of the two receivers to compute the receiver-dependent term of the system time difference Δt_{wkl} (see eqn. 5.11) for the specified receiver pair (called “differential receiver bias”). A more efficient computation of the differential receiver biases may be obtained by computing mean day to day changes of the GLONASS/GPS system time differences and by correcting the receiver-dependent estimates for these changes. The mean day to day changes could be computed in two steps. In the first step the difference of the receiver-specific system time difference estimates between two successive observations is computed. The mean values of these differences for all receivers involved may be computed in the second step. Mean changes of the system time difference for the Ashtech Z-18 receivers of Figure 7.7 computed in this way are given in Figure 7.9 (bottom curve in each picture).

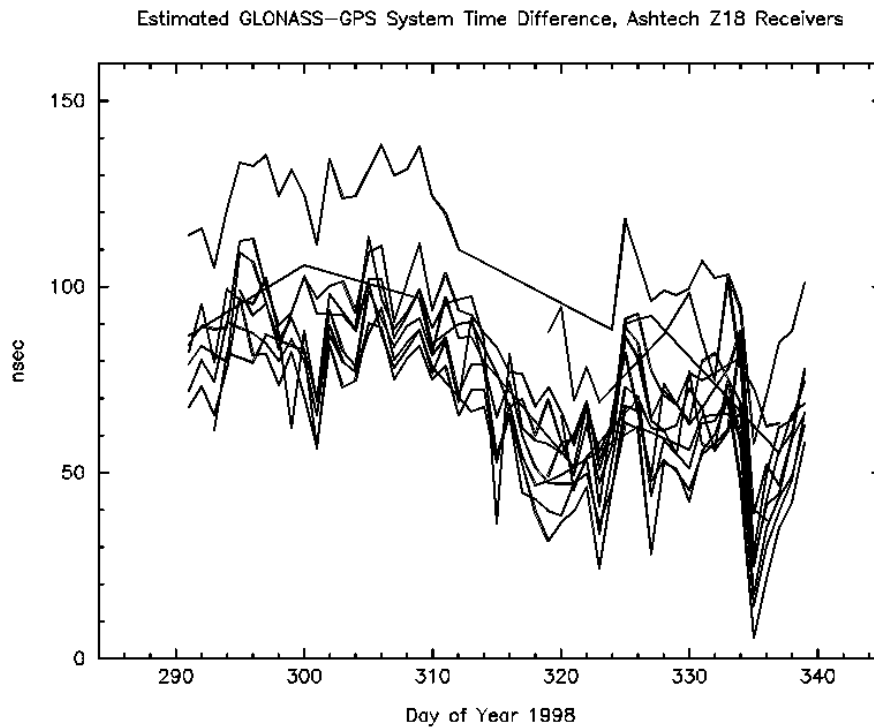


Figure 7.7: Ashtech Z-18 GLONASS/GPS System Time Difference

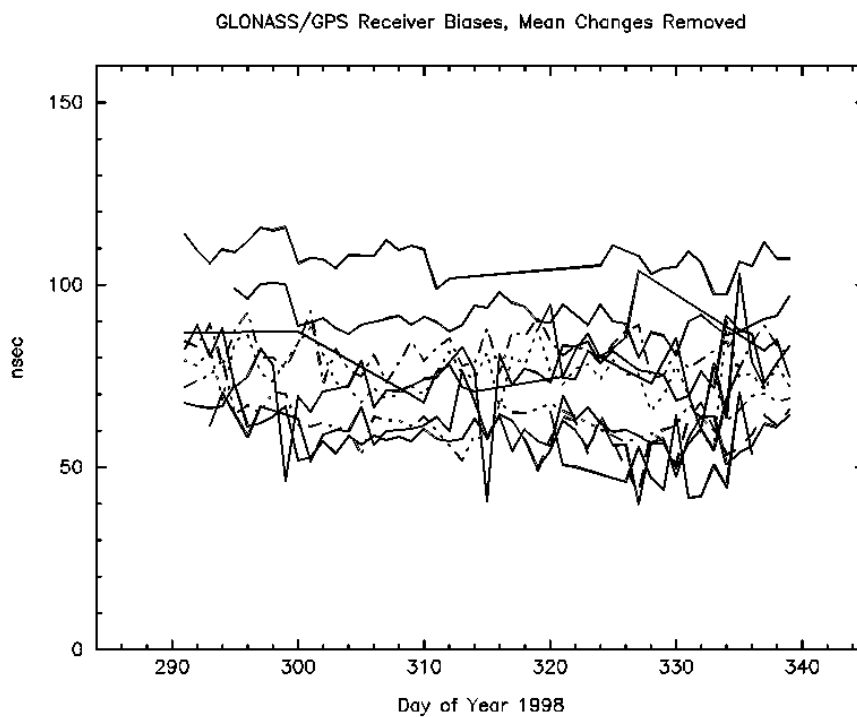


Figure 7.8: Ashtech Z-18 GLONASS/GPS System Time Difference, Mean Changes Removed

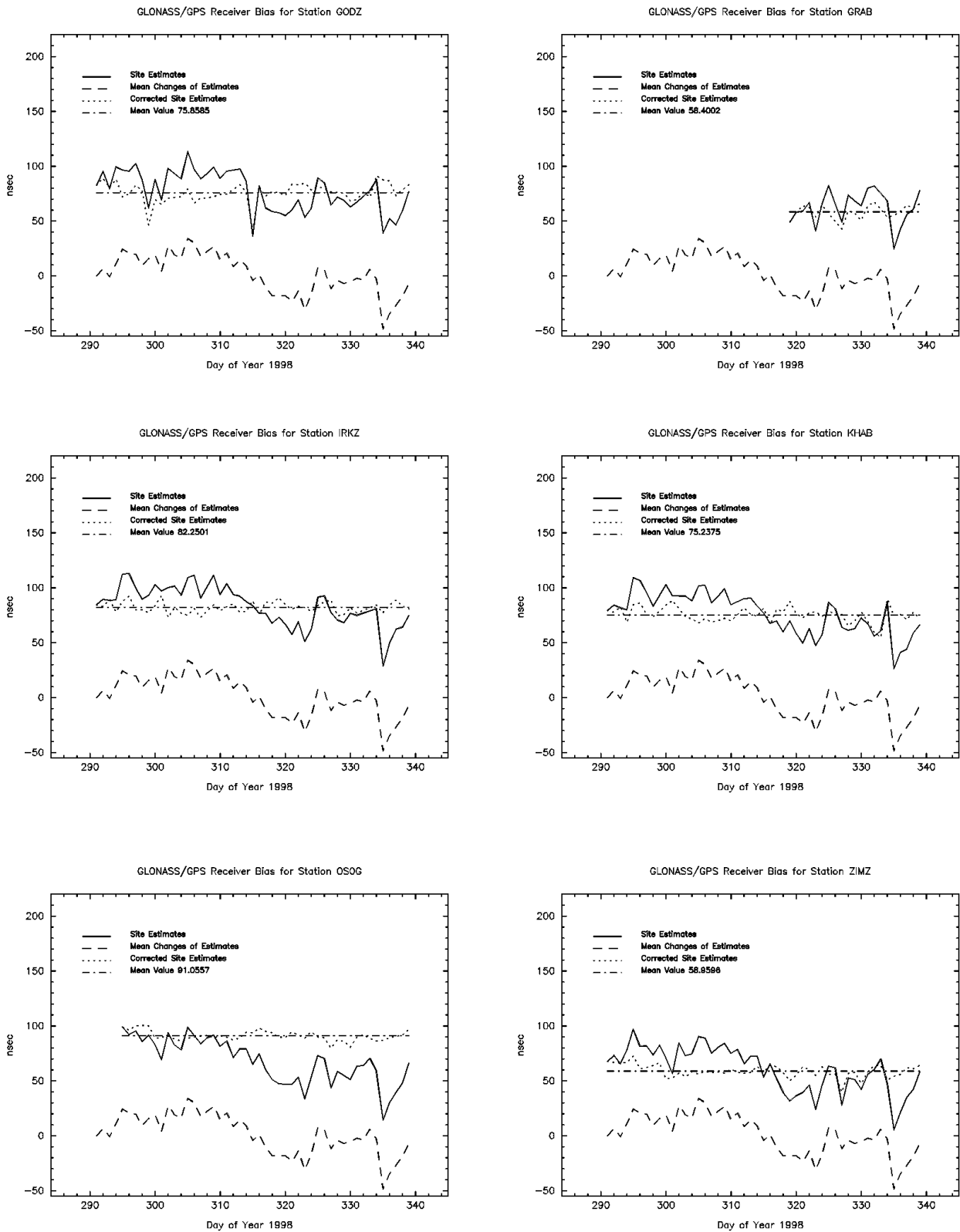


Figure 7.9a: Ashtech Z-18 GLONASS/GPS Receiver Biases

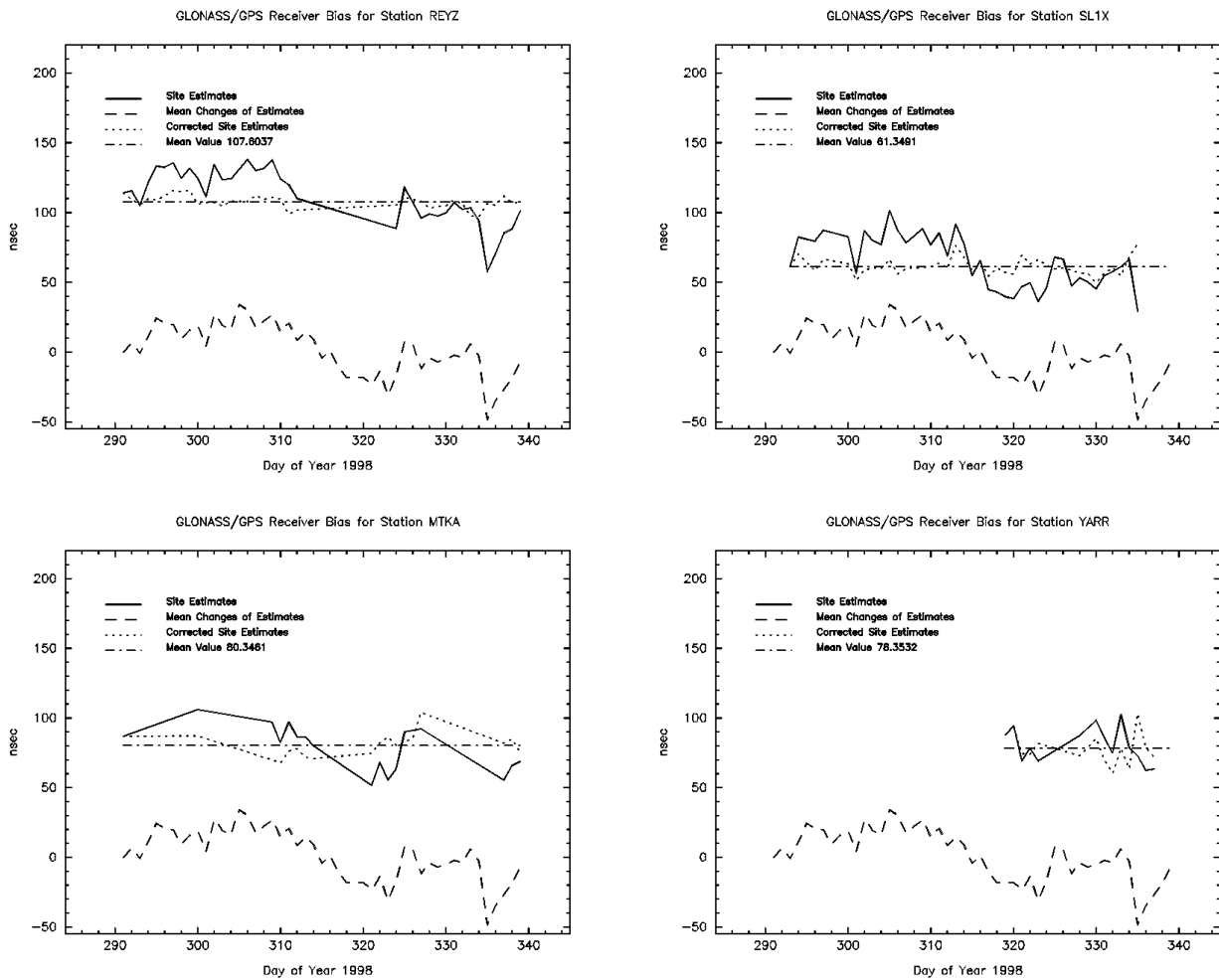


Figure 7.9b: Ashtech Z-18 GLONASS/GPS Receiver Biases

The receiver-specific parts of the system time difference after the correction of their mean changes are given in Figure 7.8. Systematic effects between the curves of different receivers are no longer present in Figure 7.8. Some outliers show up, e.g., in days 299 and 314, but the corresponding estimates of the system time difference were not used in the computation of the mean day to day changes by using a majority voting.

Figure 7.9 shows four curves for each receiver, namely the original estimates of the GLONASS/GPS system time difference, their mean day to day changes, and the estimates of the system time difference corrected for their mean changes. These corrected system time differences were used to compute a mean value for each receiver, which are given in Figure 7.9, too. Mean values of all Ashtech Z-18 receivers processed by us are summarized in Table 7.2 and may be used to compute the differential receiver biases of all possible receiver combinations.

Ashtech Z-18		3S-Navigation	
Station Name	GLONASS/GPS Receiver Bias [nsec]	Station Name	GLONASS/GPS Receiver Bias [nsec]
REYZ	107.60	BORG	1033.64
GODZ	75.86	CSIR	1049.92
GRAB	58.40	3SNA (IRVI)	1064.23
IRKZ	82.25	NPLC	1006.61
KHAB	75.24	SANG	998.78
MTKA	80.34		
OS0G	91.06		
SLIX	61.35		
YARR	78.35		
ZIMZ	58.96		

Table 7.2: Mean Values of Corrected System Time Differences

The receiver-specific estimates of the system time difference of the station OS0G in Figure 7.9 are very similar to the mean changes of the estimates. Therefore, the corrected estimates of the system time difference of station OS0G show very small variations around its mean value. Much larger variations of the corrected system time difference around its mean value were found for station GODZ in Figure 7.9. These are caused by the discrepancy between the receiver-specific estimates and the mean changes of the estimates.

GLONASS/GPS Receiver Biases for 3S-Navigation Receivers

The estimated GLONASS/GPS system time differences from the 3S-Navigation receivers of Figure 7.5 are given in Figure 7.10. Similar day to day variations are observed in Figure 7.10 for all 3S-Navigation receivers involved. Mean changes of the estimated system time differences were computed and used to correct the receiver-dependent estimates. These corrected system time differences are given in Figure 7.12 for each 3S-Navigation receiver and their corresponding mean values. The mean values of the corrected system time estimates are summarized in Table 7.2 and may be used to compute the differential receiver biases for all receiver pairs.

The mean changes of the system time difference as computed from Ashtech Z-18 and 3S-Navigation receivers are given separately in Figure 7.11. Both receiver types lead to nearly identical results for the changes of the system time difference. The discrepancy between the two curves in Figure 7.11 for the period day 291 to 312 may be caused by the small number of 3S-Navigation receivers, that were available during this period.

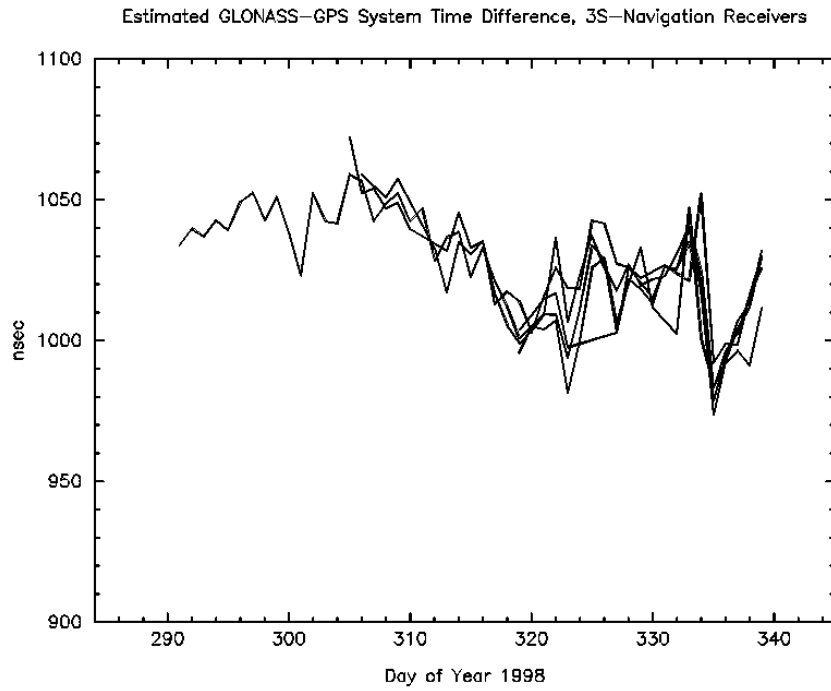


Figure 7.10: 3S-Navigation GLONASS/GPS System Time Difference

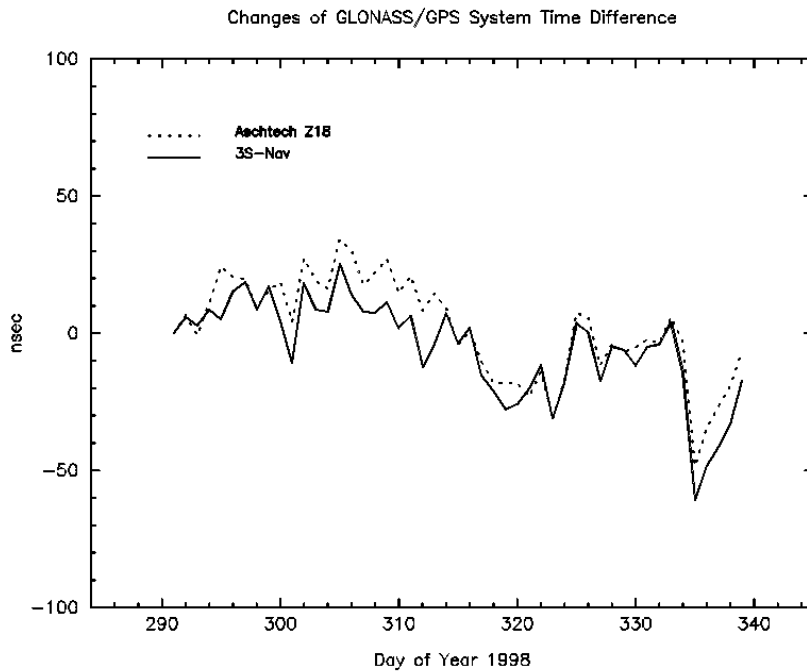


Figure 7.11: Mean Changes of GLONASS/GPS System Time Differences from Different Receiver Types

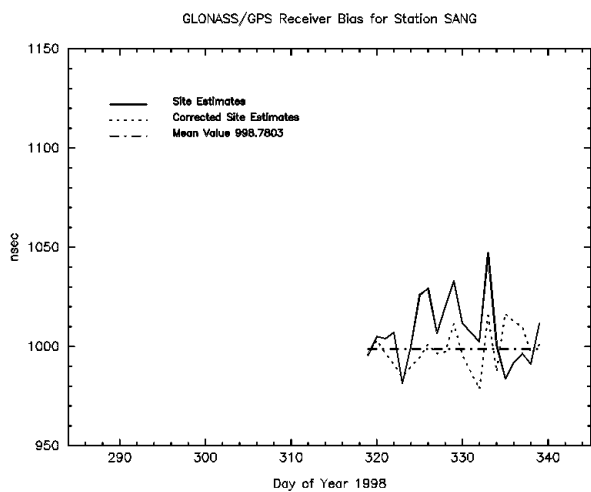
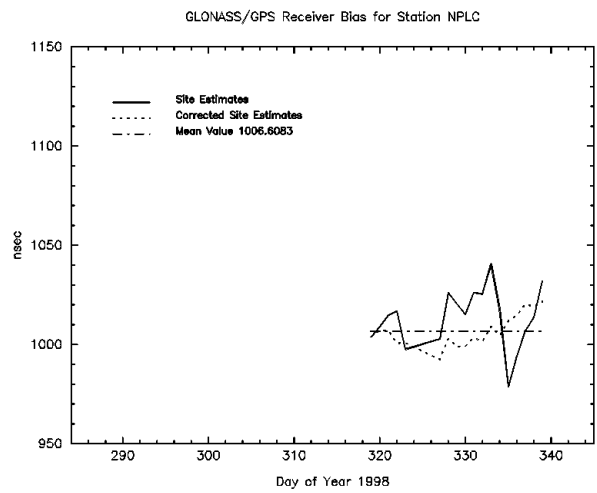
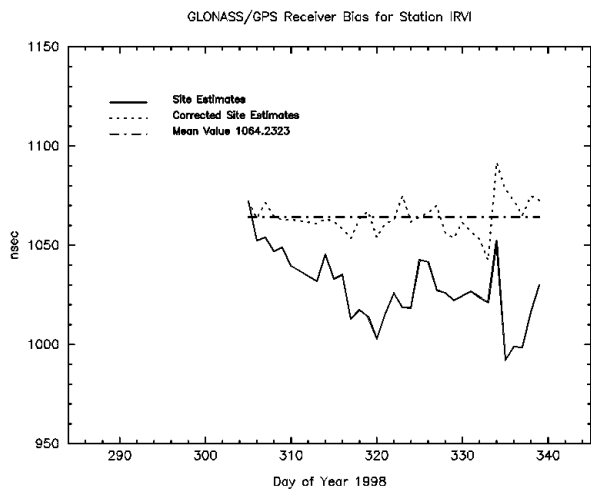
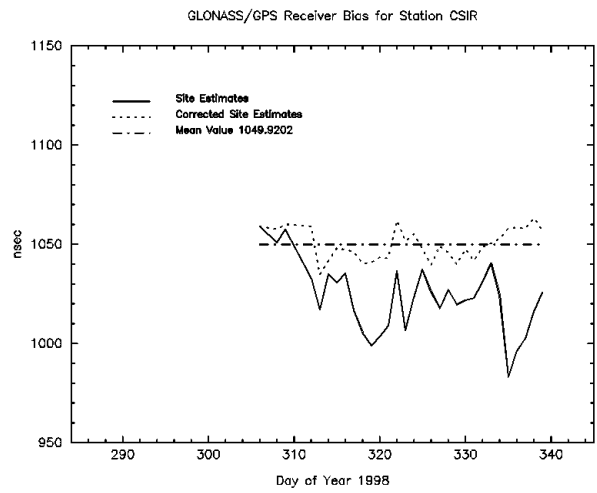
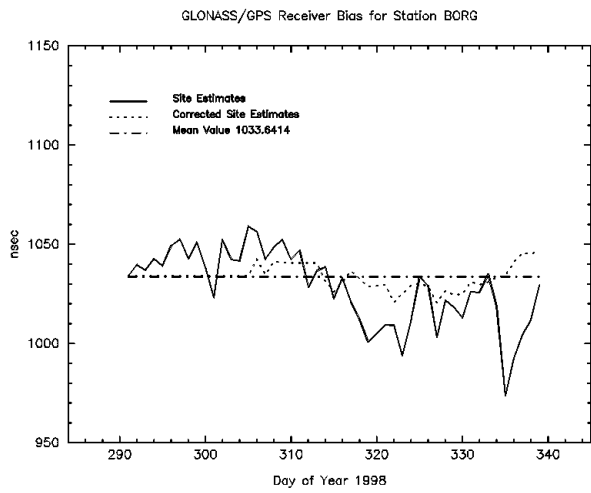


Figure 7.12: 3S-Navigation GLONASS/GPS Receiver Biases

7.3 Transformation Parameters between PZ-90 and ITRF 96

Results from Satellite positions

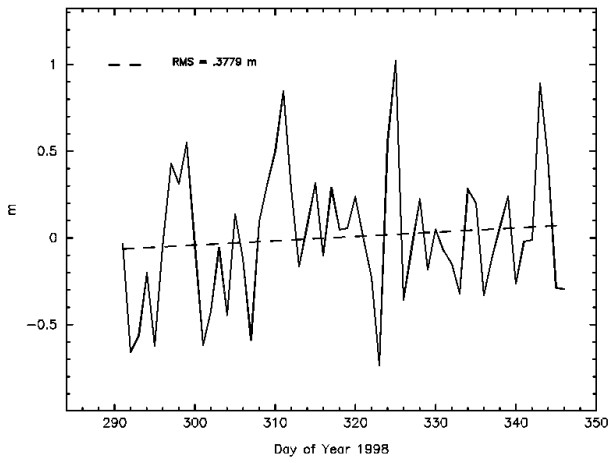
In Table 1.04 we gave the transformation parameters between PZ-90 and ITRF 96 of two experiments in 1996. New transformation parameters between PZ-90 and ITRF 96 were calculated using the results of the IGEX campaign. The GLONASS satellite positions in PZ-90 are provided in the broadcast messages. The orbit improvement for the GLONASS satellites, as shown in Figure 7.2, yields the satellite positions in ITRF 96, because the ITRF 96 coordinates of one station are held fixed and because the orbits of the GPS satellites are given (and kept fixed) in the ITRF 96. Thus, two coordinate sets for the satellite positions are available, one in each system. The two sets may be used to estimate the parameters of a seven parameter Helmert transformation. The accuracy of the resulting transformation parameters mainly depends on the accuracy of the broadcast orbits, assuming that the improved GLONASS orbits have an accuracy level of about a few decimeter.

The transformation parameters were calculated on a daily basis for the period from day of year 291 to 346, 1998. The results are shown in Figure 7.13. For each transformation parameter linear approximations and the corresponding RMS errors were computed and are given in Figure 7.13. The translation parameters show a scatter of about 0.5 m, which is a consequence of the broadcast orbit quality. On the average the translation parameters in direction of the X- and Z-axis are equal to zero, if the corresponding RMS error of the linear approximation of 0.37 m and 0.62 m are taken in account. The translation in direction of the Y-axis shows a significant drift of 0.48 m for the period of 56 days. All rotation parameters show a significant drift for the period given in Figure 7.13. This confirms the change of the transformation parameters in time, as found in [Mitrikas et. al., 1998]. The most significant parameter is the rotation parameter around the Z-axis, which is determined to a mean value of -358 mas. The scatter of the scale factor estimates decreases with day of year 312, because of the increased number of stations that were used in the processing. The scale parameter shows no linear drift, if we exclude the results of the period before day of year 312 and is determined to a mean value of $1 \cdot 10^{-8}$. As mentioned in Section 1.3.1 we would expect a scale factor of $6.35 \cdot 10^{-8}$, due to the satellite antenna offsets. However, this scale factor could not be confirmed in our results and we may assume, that the GLONASS Broadcast Ephemerides refer to the satellites' center of mass.

The mean values of the transformation parameters over the period analysed are given in Table 7.3. The RMS errors of each of the 7 parameters are derived from the residuals of the daily transformation parameter estimates. These RMS errors of the mean values are much larger than the RMS errors in Figure 7.13 because no linear drift is accounted for. The total RMS error of the IGEX-98 results in the last column in Table 7.3 was computed from the residuals of the transformed satellite positions. It is a measure of the overall quality of the broadcast orbits. The RMS of about 5 m indicates, that the broadcast orbits are in general much better than specified in Table 1.7.

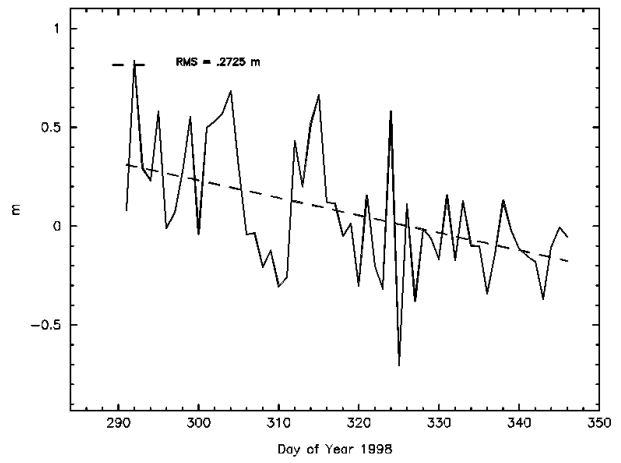
Translation X Axis

Transformation Parameters between PZ-90 and ITRF 96



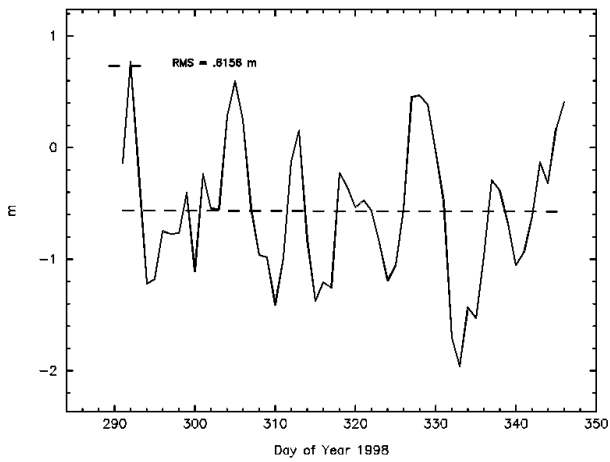
Translation Y Axis

Transformation Parameters between PZ-90 and ITRF 96



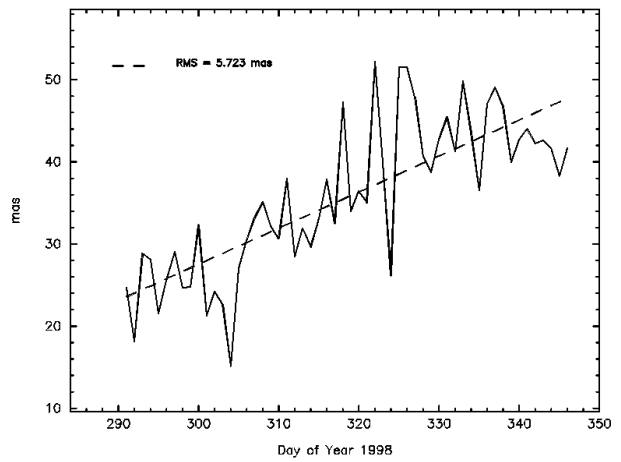
Translation Z Axis

Transformation Parameters between PZ-90 and ITRF 96



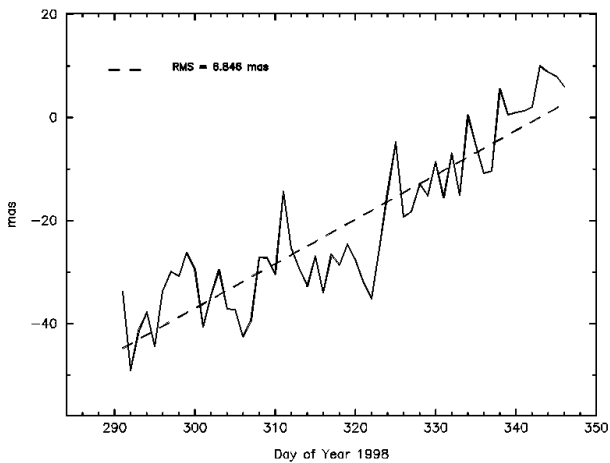
Rotation X Axis

Transformation Parameters between PZ-90 and ITRF 96



Rotation Y Axis

Transformation Parameters between PZ-90 and ITRF 96



Rotation Z Axis

Transformation Parameters between PZ-90 and ITRF 96

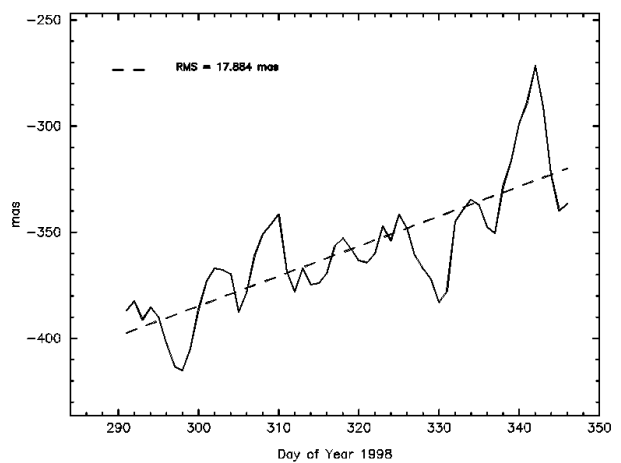


Figure 7.13a: Transformation Parameters from IGEX

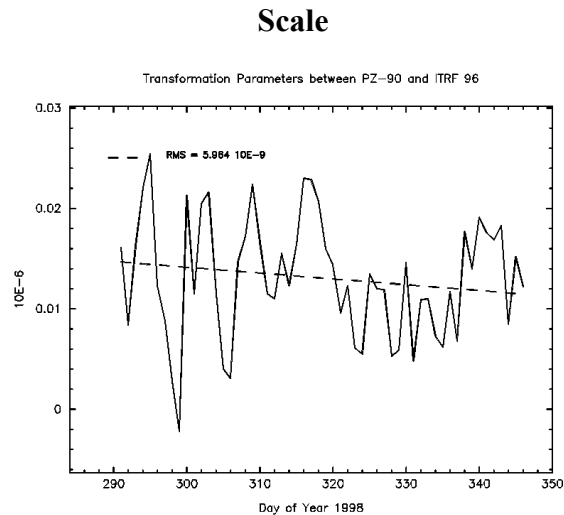


Figure 7.13b: Transformation Parameters from IGEX

Results derived from Station Coordinates

[Bazlov et al., 1999] determined transformation parameters between PZ-90 and WGS-84 using the coordinates of eight reference sites in Russia with known coordinates in both systems. The station coordinates in PZ-90 of the reference sites were derived from observations to „Geodetic inercosmos (Geo-IK)“ satellites. These satellites are equipped with doppler transmitters and laser reflectors. The ITRF and WGS-84 were considered to be coincident at the decimeter level. The reference sites were occupied with dual-frequency GPS receivers in order to determine the station coordinates in the ITRF. A relative accuracy of the order of some decimeters was achieved. After performing a seven parameter Helmert transformation the coordinate residuals show an RMS error of 0.26 m. Because all selected sites are located in Russia, some of the transformation parameters are highly correlated. Therefore, four parameters were selected in the final recommendation for the transformation to be used (see Table 7.2).

If we compare the RMS error of the two approaches in Table 7.2 we must take into account that an RMS error of 5.07 m for the satellite positions corresponds to approximately 1.2 m on the Earth's surface. But even after applying this conversion the RMS error of the transformation by Bazlov et al. is still smaller by a factor of 3 than that of the IGEX results, with the important disadvantage, however, that all participating stations were located on the Russian territory. We have seen in the IGEX-98 results and in [Mitrikas et al., 1998] that the transformation parameters are changing in time. Therefore, the parameters given in Table 7.2 may be used for a specified epoch, only. However, since the beginning of IGEX-98 daily transformation parameters are available and may be used to account for the changes of the parameters. Long periodic changes of the transformation parameters cannot be derived from our results. For this purpose a longer analysis period is required.

$\begin{matrix} \begin{matrix} X \\ Y \\ Z \end{matrix} \\ \text{ITRF-96} \end{matrix} = \begin{matrix} \begin{matrix} X \\ Y \\ Z \end{matrix} \\ \text{PZ-90} \end{matrix} + \begin{matrix} DX \\ DY \\ DZ \end{matrix} + \begin{matrix} Scale & RZ & -RY \\ -RZ & Scale & RX \\ RY & -RX & Scale \end{matrix} \cdot \begin{matrix} X \\ Y \\ Z \end{matrix} \\ \text{PZ-90} \end{matrix}$								
	DX	DY	DZ	RX	RY	RZ	Scale	Total
	RMS	RMS	RMS	RMS	RMS	RMS	RMS	RMS
	[m]	[m]	[m]	[mas]	[mas]	[mas]	[10 ⁻⁶]	[m]
IGEX-98	0.06 ± 0.38	0.07 ± 0.32	-0.57 ± 0.62	35 ± 9.17	-21 ± 15.56	-358 ± 29.12	0.01 ± 0.006	5.07
Bazlov et al. 1999	-1.08 -	-0.27 -	-0.90 -	- -	- -	-160 -	-0.12 -	0.38

Table 7.3: Transformation Parameter between PZ-90 and ITRF 96

7.4 Ambiguity Resolution

For a subset of four IGEX stations, namely Graz, Onsala, Vernon and Zimmerwald, a parameter estimation process including ambiguity resolution was performed for days 341 to 346, 1998. All these stations are equipped with Ashtech Z18 receivers. The ITRF 96 coordinates for Zimmerwald were held fixed and baselines of distances between 508 km and 1,207 km between Zimmerwald and the other stations were processed. Table 7.4 shows the number of ambiguity parameters for all baselines and the number of ambiguities, that could be fixed to integers. The fixed L5 ambiguities were introduced into the narrow lane according to Section 6.3 to resolve the N1 ambiguities. On the average about 90 % of the ambiguities could be resolved.

The RMS errors of the coordinate repeatability for the selected six days in the case of ambiguity-free and ambiguity-fixed solutions are given in Table 7.5. In particular, significantly improvement in longitude component was found, as expected after a successful ambiguity resolution step.

Sess.	Baseline	Number of Single Difference Ambiguities	Number of Resolved Double Difference Ambiguities		Percentage of Resolved Double Difference Ambiguities	
			L5	L1	L5	L1
341	ZIMZ-GRAB	75	67	65	89 %	87 %
	ZIMZ-LRBA	50	29	27	58 %	54 %
	ZIMZ-OS0G	66	62	60	94 %	91 %
342	ZIMZ-GRAB	75	70	68	93 %	91 %
	ZIMZ-LRBA	71	63	61	89 %	86 %
	ZIMZ-OS0G	67	64	62	96 %	93 %
343	ZIMZ-GRAB	87	77	75	88 %	86 %
	ZIMZ-LRBA	81	74	72	91 %	89 %
	ZIMZ-OS0G	69	62	60	89 %	87 %
344	ZIMZ-GRAB	91	83	82	91 %	90 %
	ZIMZ-LRBA	84	75	73	89 %	87 %
	ZIMZ-OS0G	76	66	64	87 %	84 %
345	ZIMZ-GRAB	87	75	72	86 %	83 %
	ZIMZ-LRBA	79	62	58	78 %	73 %
	ZIMZ-OS0G	71	43	39	60 %	55 %
346	ZIMZ-GRAB	106	91	87	86 %	82 %
	ZIMZ-LRBA	79	68	67	86 %	85 %
	ZIMZ-OS0G	75	67	65	89 %	87 %
ZIMZ-GRAB		= Zimmerwald - Graz	:	610 km Distance		
ZIMZ-LRBA		= Zimmerwald - Vernon	:	508 km Distance		
ZIMZ-OS0G		= Zimerwald - Onsala	:	1207 km Distance		

Table 7.4: Ambiguity Resolution for IGEX Stations

		GRAB [mm]	OS0G [mm]	LRBA [mm]
Ambiguity-free Solutions	Latitude:	3.6	4.0	3.4
	Longitude:	4.0	4.1	7.7
	Height:	6.1	4.9	5.9
Ambiguity-fixed Solutions	Latitude:	3.6	3.2	3.1
	Longitude:	2.5	1.4	3.0
	Height:	8.3	5.2	4.4
<hr/>				
Improvement Factor (float/fixed)	Latitude:	1	1.2	1.1
	Longitude:	1.6	2.9	2.6
	Height:	0.7	0.9	1.3

Table 7.5: RMS of Coordinate Repeatability Before and After Ambiguity Resolution

7.5 Coordinates of IGEX Stations

Here we show the coordinate time series of six selected IGEX stations for the time period from day 290 to 354, 1998. The selected stations with the corresponding receiver and observation types are given in Table 7.6. Four of the stations are occupied by Ashtech Z18 receivers, which allows for in a combined GLONASS/GPS processing. The other two stations are equipped with a 3S-Navigation and an ESA/ISN receiver, respectively, collecting no dual-frequency observations for the GPS satellites. Therefore, only GLONASS observations were used to process the two latter time series.

The differences to the mean value of the daily estimates over the specified period are given in Figure 7.14. The ITRF 96 coordinates of the station Zimmerwald were held fixed. A coordinate repeatability within a few centimeters was found for all stations. The results for the stations BORG and LDS1 demonstrate that by processing only GLONASS observations we may reach the centimeter accuracy level in a global network solution as well.

Abbreviation	Station Name	Country	Receiver Type	Observation Type
BIPD	Sevres	France	Ashtech Z18	GLONASS/GPS
BORG	Brussels	Belgium	3S-Navigation	GLONASS
GODZ	Greenbelt, MD	USA	Ashtech Z18	GLONASS/GPS
IRKZ	Irkutsk	Russia	Ashtech Z18	GLONASS/GPS
LDS1	Leeds	UK	ESA/ISN	GLONASS
METZ	Metsahovi	Finland	Ashtech Z18	GLONASS/GPS

Table 7.6: Receiver and Observation Types of Selected IGEX Stations

7. The International GLONASS Experiment (IGEX-98)

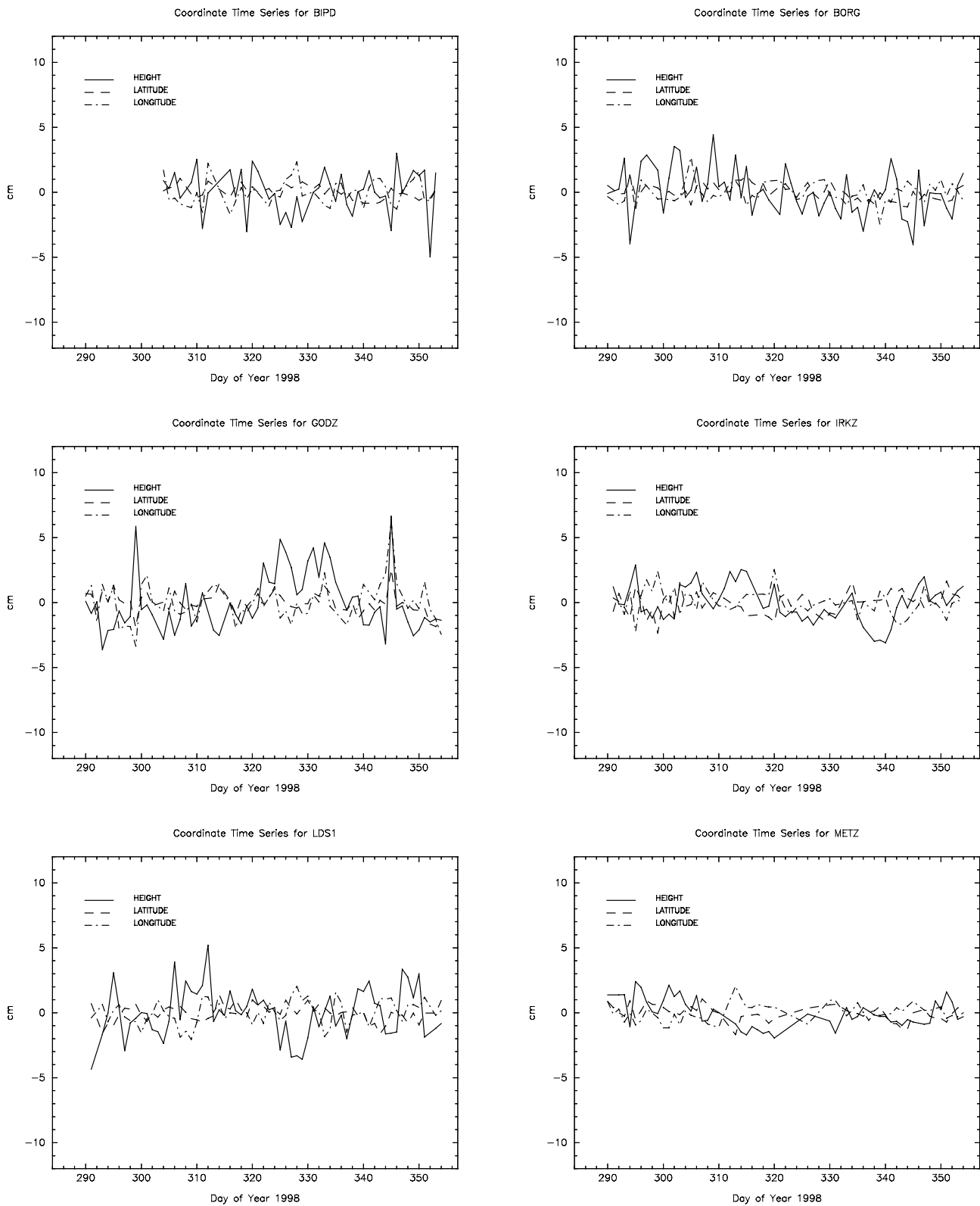


Figure 7.14: Coordinate Time Series of Selected IGEX Stations

8. Conclusion

When introducing and discussing the GLONASS system we have seen, that the satellite constellation and the signal structure is comparable to that of the GPS. In the theoretical part dealing with all essential processing steps of GLONASS observations we showed how the processing had to be performed. Observation equations for combined GLONASS/GPS observations were developed and represent a generalization of the GPS observation equations. The observation equations and the algorithms are validated in the second part of this work.

Differences between GLONASS and GPS (reference system for the satellite positions, system time scale) were taken into account by generating a common satellite ephemerides file for GLONASS and GPS satellites in a unique reference frame (ITRF 96) and by converting all epochs to the GPS system time scale. An additional parameter has to be introduced into the observation equation of combined GLONASS/GPS observations in order to account for the system time difference.

The satellite-specific frequencies used in GLONASS have to be taken into account in all phase observation equations and produce a single difference ambiguity term on the double difference level which is not present in the GPS. This bias term affects cycle slip detection and ambiguity resolution. In case of cycle slip detection a new approach was presented in order to correct the cycle slips on the single difference level. The double difference ambiguity parameters are resolved in an iterative approach. We solve for one double difference ambiguity parameter in each iteration step, starting with the satellite pair associated with the smallest wavelength difference. The bias term is small for such satellite pairs and the correct double difference ambiguity usually may be resolved. The RMS errors of the single difference ambiguities decrease after each successfully performed iteration step and allow it to resolve the double difference ambiguities for satellite pairs with large wavelength differences. If the RMS error of the single difference ambiguities is significantly smaller than one cycle, it might even be possible to resolve the ambiguities on the single difference level. In the case of combined GLONASS/GPS observations even the GPS ambiguities might be resolved on the single difference level, provided a combined GLONASS/GPS double difference ambiguity has been resolved. This option is not available when using GPS observations only. However, we found receiver specific biases preventing the resolution of combined GLONASS/GPS double difference ambiguities.

Once the ambiguities would be resolved on the single difference level, the carrier phase observation could be used for precise time transfer (as opposed to frequency transfer) between two stations. Carrier phase observation could then be used in the same way as code observations.

8. Conclusion

Two quantities are not yet determined with high accuracy. The first one is the system time difference between GLONASS and GPS. We found a receiver dependent bias term which does not allow it to estimate a system time difference common to all receivers. This bias term should be removed by the manufacturers of GLONASS/GPS receivers. If this bias term has been removed it might be possible to resolve combined GLONASS/GPS double difference ambiguities. The second item refers to the transformation parameters between the PZ-90 and ITRF reference frames, which are determined with decimeter accuracy at present. We have seen in Section 7 that the transformation parameters are functions of time. Since the beginning of the IGEX-98 campaign daily transformation parameters are available from BKG and other IGEX analysis centers. These transformation parameters are derived from two sets of satellite positions in the ITRF 96 and the PZ-90. The broadcast satellite positions are used for positions in the PZ-90 and determine the quality of the transformation parameters. In order to determine the transformation parameters with higher accuracy, a global set of station coordinates given in the PZ-90 has to be known with an accuracy of about a few cm. Due to the fact that improved GLONASS orbits in the ITRF 96 are available from IGEX-98 transformation parameters are no longer required for using the GLONASS in precise applications, however.

All phase observations are modeled with satellite-specific frequencies; a good preparation for the planned new third civil GPS signal and the planned European navigation satellite system Galileo. A full combination of GLONASS and GPS in global solutions may contribute to a Global Navigation Satellite System (GNSS).

Appendix A. GLONASS Satellite Launch History

Block No.	GLONASS No. (slot/frequency)	Cosmos No.	Launch Date	Put into Operation	End of Operation (withdrawn)
1	224 (01/--)	1413	12.10.82	15.10.82	12.01.84 (16.04.84)
2	222 (03/--)	1490	10.08.83	03.09.83	05.07.84 (31.10.85)
2	223 (02/--)	1491	10.08.83	31.08.83	27.09.84 (09.06.88)
3	220 (18/--)	1519	29.12.83	07.01.84	27.09.84 (28.01.88)
3	219 (17/--)	1520	29.12.83	15.01.84	30.06.86 (16.09.86)
4	218 (19/--)	1554	19.05.84	13.06.84	16.08.85 (16.09.86)
4	217 (18/--)	1555	19.05.84	18.06.84	25.10.85 (17.09.87)
5	216 (02/10)	1593	04.09.84	22.09.84	28.11.85 (19.05.88)
5	215 (03/--)	1594	04.09.84	28.09.84	04.09.86 (16.09.86)
6	224 (01/--)	1650	18.05.85	28.06.85	08.11.85 (29.11.85)
6	221 (01/07)	1651	18.05.85	14.06.85	09.08.87 (17.09.87)
7	209 (18/04)	1710	25.12.85	24.01.86	28.02.87 (16.03.89)
7	210 (17/19)	1711	25.12.85	24.01.86	16.05.87 (16.09.87)
8	203 (02/11)	1778	16.09.86	19.10.86	20.02.87 (13.07.89)
8	202 (03/20)	1779	16.09.86	19.10.86	15.07.88 (24.10.88)
8	201 (08/22)	1780	16.09.86	19.10.86	15.06.88 (10.10.88)

Appendix A. GLONASS Satellite Launch History

Block No.	GLONASS No. (slot/frequency)	Cosmos No.	Launch Date	Put into Operation	End of Operation (withdrawn)
9	-	1838	24.04.87	Failed launch	
9	-	1839	24.04.87	Failed launch	
9	-	1840	24.04.87	Failed launch	
10	229 (--/--)	1883	16.09.87	12.10.87	06.06.87 (03.07.89)
10	228 (--/--)	1884	16.09.87	12.10.87	30.08.88 (15.12.88)
10	227 (17/--)	1885	16.09.87	07.10.87	01.02.89 (09.03.89)
11	-	1917	17.02.88	Failed launch	
11	-	1918	17.02.88	Failed launch	
11	-	1919	17.02.88	Failed launch	
12	235 (07/--)	1946	21.05.88	15.06.88	10.05.90 (22.10.90)
12	234 (08/--)	1947	21.05.88	15.06.88	19.03.91 (18.09.91)
12	233 (01/--)	1948	21.05.88	15.06.88	11.06.91 (18.09.91)
13	238 (17/--)	1970	16.09.88	11.10.88	21.05.90 (22.10.90)
13	237 (18/--) (1)	1971	16.09.88	11.10.88	31.08.89 (30.11.89)
13	236 (19/--) (2)	1972	16.09.88	11.10.88	01.11.91 (12.08.92)
14	239 (02/09)	1987	10.01.89	01.02.89	14.03.93 (03.02.94)
14	240 (03/06)	1988	10.01.89	01.02.89	16.02.92 (02.06.92)
14	241	1989	10.01.89	Geodetic reference satellite	
15	231 (24/--)	2022	31.05.89	04.07.89	25.01.90 (13.03.90)
15	230 (19/--)	2023	31.05.89	17.06.89	18.11.89 (13.03.90)
15	232	2024	31.05.89	Geodetic reference satellite	

Block No.	GLONASS No. (slot/frequency)	Cosmos No.	Launch Date	Put into Operation	End of Operation (withdrawn)
16	242 (17/21)	2079	19.05.90	20.06.90	23.04.94 (17.08.94)
16	228 (19/03)	2080	19.05.90	17.06.90	27.07.94 (27.08.94)
16	229 (20/15)	2081	19.05.90	11.06.90	18.08.92 (20.01.93)
17	247 (07/13)	2109	08.12.90	01.01.91	17.03.94 (10.06.94)
17	248 (04/14)	2110	08.12.90	29.12.90	29.10.93 (20.01.94)
17	249 (05/19) (4)	2111	08.12.90	28.12.90	09.06.96 (15.08.96)
18	750 (22/11)	2139	04.04.91	28.04.91	29.09.94 (14.11.94)
18	753 (21/20)	2140	04.04.91	28.04.91	06.01.92 (04.06.93)
18	754 (24/14)	2141	04.04.91	04.05.91	26.02.92 (16.06.92)
19	768 (03/22)	2177	30.01.92	24.02.92	09.01.93 (29.06.93)
19	769 (08/02)	2178	30.01.92	22.02.92	23.05.97 (24.06.97)
19	771 (01/17) (3)	2179	30.01.92	18.02.92	25.10.86 (21.12.96)
20	756 (18/24) (6)	2204	30.07.92	19.08.92	27.06.97 (05.08.97)
20	772 (21/08)	2205	30.07.92	29.08.92	29.06.94 (27.08.94)
20	774 (24/01)	2206	30.07.92	25.08.92	18.05.96 (26.08.96)
21	773 (02/05)	2234	17.02.93	14.03.93	09.03.94 (17.08.94)
21	759 (06/23) (5)	2235	17.02.93	25.08.93	30.06.97 (05.08.97)
21	757 (03/12)	2236	17.02.93	14.03.93	27.07.97 (23.08.97)
22	758 (18/10)	2275	11.04.94	04.09.94	Operational
22	760 (17/24)	2276	11.04.94	18.05.94	Operational

Appendix A. GLONASS Satellite Launch History

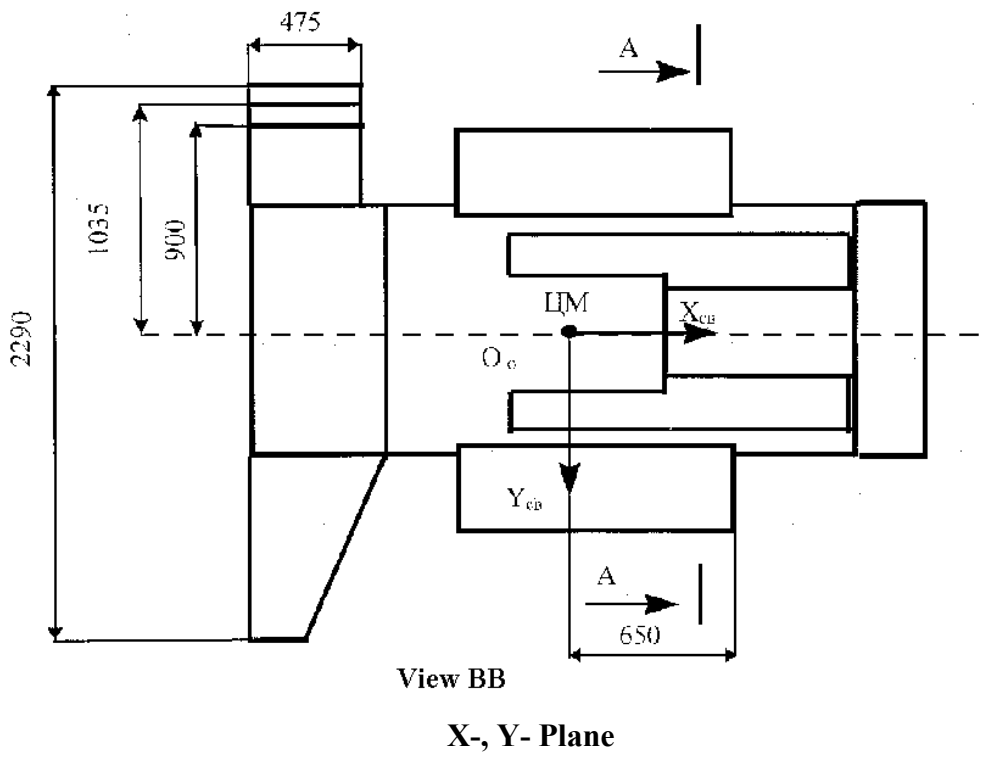
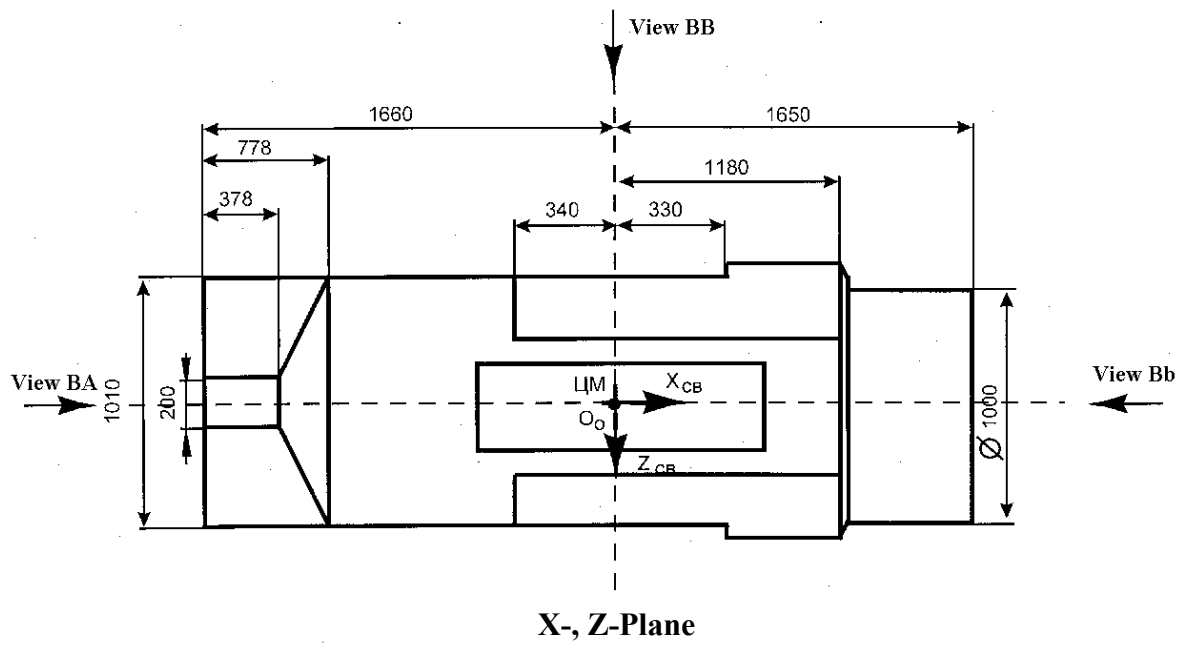
Block No.	GLONASS No. (slot/frequency)	Cosmos No.	Launch Date	Put into Operation	End of Operation (withdrawn)
22	761 (23/03)	2277	11.04.94	16.05.94	24.07.97 (29.08.97)
23	767 (12/22) (7)	2287	11.08.94	07.09.94	05.11.98 (03.02.99)
23	770 (14/09)	2288	11.08.94	04.09.94	20.11.97
23	775 (16/22)	2289	11.08.94	07.09.94	Operational
24	762 (04/12) (7)	2294	20.11.94	11.12.94	Operational
24	763 (03/21)	2295	20.11.94	15.12.94	Operational
24	764 (06/13)	2296	20.11.94	16.12.94	Operational
25	765 (20/01)	2307	07.03..95	30.03.95	Operational
25	766 (22/10)	2308	07.03.95	05.04.95	Operational
25	777 (19/03)	2309	07.03.95	05.04.95	17.07.97 (26.12.97)
26	780 (15/04)	2316	24.07.95	26.08.95	operational
26	781 (10/09)	2317	24.07.95	22.08.95	operational
26	785 (11/04)	2318	24.07.95	22.08.95	operational
27	776 (09/06)	2323	14.12.95	07.01.96	operational
27	778 (09/11)	2324	14.12.95		spare
27	782 (13/06)	2325	14.12.95	18.01.96	operational
28	779 (01/02)	2364	30.12.98	18.02.99	operational
28	784 (08/08)	2363	30.12.98	29.01.99	operational
28	786 (07/07)	2362	30.12.98	29.01.99	operational

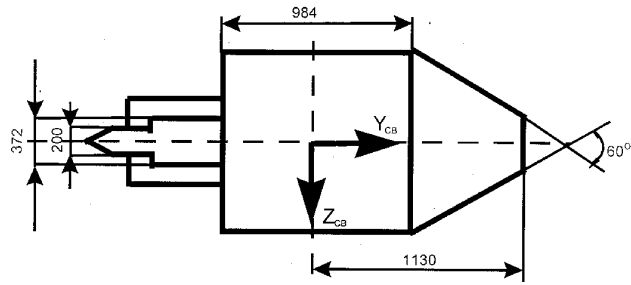
Notes:

- 1) On 6 August 1989 SV 237 had been moved from slot 18 to slot 20
- 2) On 5 August 1989 SV 236 had been moved from slot 19 to slot 18
- 3) On 2 September 1993 frequency channel of SV 771 had been changed from 17 to 23
- 4) On 2 September 1993 frequency channel of SV 249 had been changed from 19 to 23
- 5) On December 1994 SV 759 had been moved from slot 6 to slot 7 and on 2 September 1993 frequency channel of SV 771 had been changed from 23 to 21
- 6) SV 756 had been moved from slot 18 to slot 21
- 7) On 27 September 1994 frequency channels of both SV 767 and SV 775 had been changed from 21 to 22

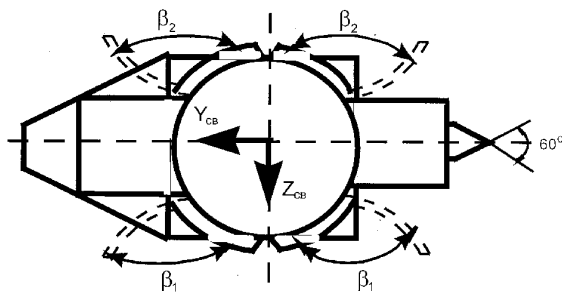
Appendix B. GLONASS Satellite Specifications

Satellite mass	: 1411 - 1415 kg
Area of solar panels	: 23.616 m ²
Specifications in the body-fixed reference frame (X, Y, Z):	
Opening of thermocontrol folds on +Z side	: 0 - 5 deg
Opening of thermocontrol folds on -Z side	: 80 - 85 deg
Phase center position of TT&C receiving antenna	: X = -1626 mm : Y = 730 mm : Z = 145 mm
Phase center position of TT&C transmitting antenna	: X = -1676 mm : Y = 700 mm : Z = 200 mm
Panel of retroreflectors's position	: X = -1510 mm : Y = 0 mm : Z = 0 mm
Integral phase center of navigation antennas	: X = -1620 (+/-) 130 mm : Y = 0 mm : Z = 0 mm
Satellite orientation:	
<ul style="list-style-type: none"> • Negative X-axis is pointed to Earth's center of mass • Positive Z-axis is solar panel axis • Positive Y-axis completes right-hand system (X,Y,Z), points to the "sun-side" 	
<i>Source: NPO PM(Karasnoyarsk), 1999</i>	



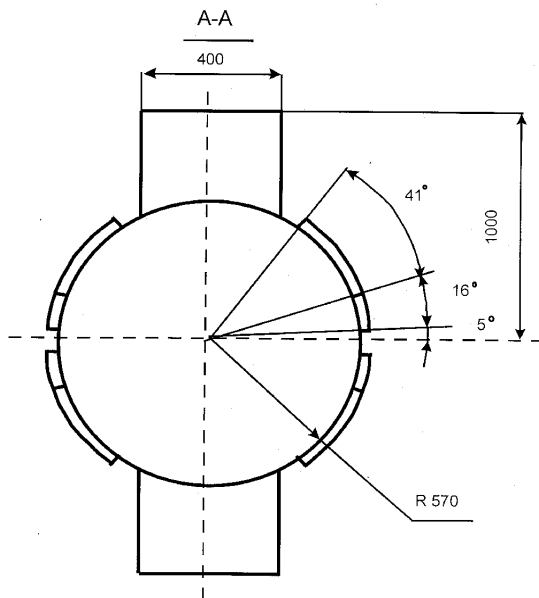


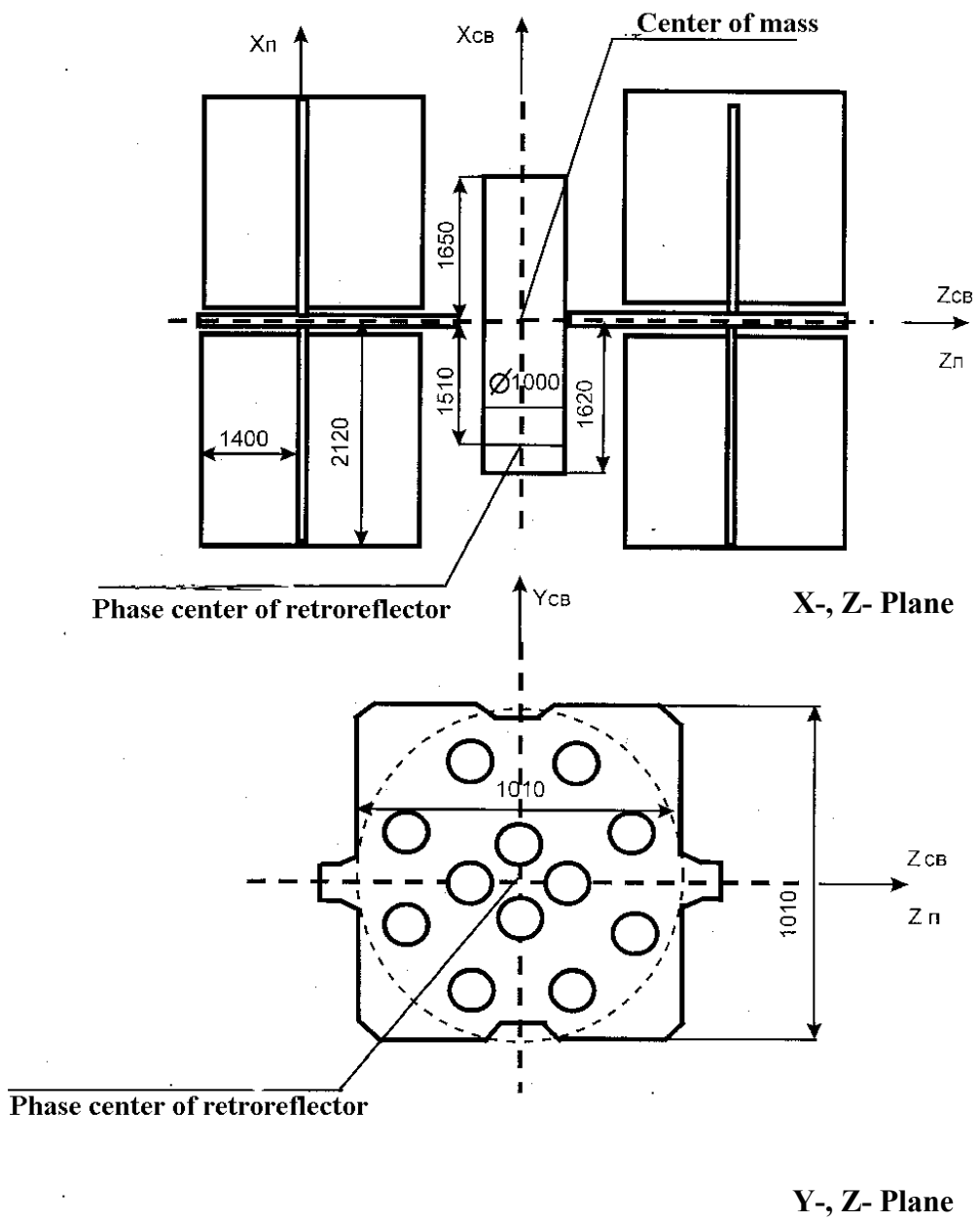
View BA



View Bb

Y-, Z- Plane





References

- Balendra A., Kim S., Beser J. (1994): *Fully Integrated GLONASS Dual Frequency P Code and GPS/GLONASS Single Frequency C/A Code Receiver - Features and Performance*, ION GPS-94, September 20-23, 1994
- Bazlov Y.A., Galazin V.F., Kaplan B.L., Maksimov V.G., Rogozin V.P. (1999): *GLONASS to GPS, A New Coordinate Transformation*, GPS World, Volume 10, No. 1, January 1999
- Beser J. (1994): *A New Line of GPS/GLONASS Receivers and Simulators*, ION GPS-94, September 20-23, 1994
- Beutler G., Brockmann E., Fankhauser S., Gurtner W., Johnson J., Mervart L., Rothacher M., Schaer S., Springer T., Weber R. (1996): *Bernese GPS Software Version 4.0 Documentation*, Astronomical Institute University of Berne
- BIPM (1999): *Circular T*, Bureau International Des Poids Et Mesures, Time Section, Paris, 1999
- CGSIC (1994): *Summary Record 24th Meeting of the Civil GPS Service Interface Committee (CGSIC)*, September 1994
- CSIC (1997): *Coordinational Scientific Information Center of Russian Space Forces*, Moscow, Russia, http://mx.iki.rssi.ru/SFCSIC/SFCSIC_main.html
- Divis D. A. (1996): *GNSS/MSS Spectrum Battle*, GPS World June 1996
- FRP (1996): *Federal Radionavigation Plan*, Department of Transportation and Department of Defense, National Technical Information Service, Springfield, Virginia 22161, 1996
- NIMA (1997): *Department of Defense World Geodetic System 1984 third edition*, technical report, National Imagery and Mapping Agency, Bethesda, Maryland, USA
- Fairheller S. (1994): *The Russian GLONASS System: A US Air Force/Russian Study*, ION Symposium 1994
- Flament D., Pieplu J. M. (1997): *GLONASS Contribution to EGNOS Performance*, First European Symposium on Global Navigation Satellite System, Munich, Germany, 21 - 25 April, 1997

- Gouzhva Y., Korniyenko V., Lutchenko A. (1993): *A promising way to structural design of the GLONASS/GPS radionavigation set*, Journal for Satellite-Based Positioning, Navigation and Communication, 4/93, December 1993
- Gouzhva Y. G., Gevorkyan A. G., Bogdanov P. P., Ovchinnikov V. V. (1994): *Full Automated System for Receiving and Processing GLONASS Data*, ION GPS-94, September 20-23, 1994
- Gurtner W. (1997): *RINEX, The Receiver Independent Exchange Format Version 2 ,updated revision*, Astronomical Institute University of Berne
- Habrigh H. (1998): *Experiences of the BKG in processing GLONASS and combined GLONASS/GPS observations*, Proceedings of the IGS Analysis Center Workshop, Darmstadt, February 9-11, 1998
- Habrigh H., Gurtner W., Rothacher M. (1998): *Processing of GLONASS and Combined GLONASS/GPS Observations*, 32nd COSPAR Scientific Assembly, Nagoya, Japan, 12-19 July, 1998
- Habrigh H. (1999): *Kombinierte Auswerteverfahren für GLONASS and GPS*, GPS Praxis und Trends '97, Deutscher Verein für Vermessungswesen, Schriftenreihe 35, 1999
- Hahn J. Jülig T. (1997): *Satellite Navigation, the influence of Multipath Propagation and the Role of Ultra-Accurate Clock Synchronisation*, DLR-Nachrichten, Volume 86, June 1997
- Hartman R. (1992): *Joint US/USSR Satellite Navigation Studies*, GPS World, February 1992
- Heitz S. (1986): *Grundlagen Kinematischer und Dynamischer Modelle der Geodäsie, 2nd revision*, Mitteilungen aus den Geodätischen Instituten der Rheinischen Friedrich-Wilhelms-Universität Bonn, Nr. 63, Germany
- Heitz S. (1980): *Mechanik Fester Körper*, Dümmlers Verlag, Bonn, Germany
- ICD (1995): *GLONASS Interface Control Document*, Coordinational Scientific Information Center of Russian Space Forces, Moscow, Russia
- ICD-GPS-200 (1991): *Navstar GPS Interface Control Document*
- Ivanov N. E., Salistchev V. (1991): *GLONASS and GPS: Prospects for a Partnership*, GPS World, April 1991
- Ivanov V. L. (1994): *Future Development of the GLONASS Space Navigation System*, Intergovernmental Navigation Information Center (INIC), Bulletin No5, 1994

-
- Johnson M. W. (1994): *Interference to GNSS Receivers in the Civil Aviation Environment*, ION GPS-94, September 20-23, 1994
- Kleusberg A. (1990): *Comparing GPS and GLONASS*, GPS World, November/December 1990
- Koch K. R. (1980): *Parameterschätzung und Hypothesentests in linearen Modellen*, Dümmler Verlag Bonn, 1980
- Landau H., (1988): *Zur Nutzung des Global Positioning Systems in Geodäsie und Geodynamik*, Schriftenreihe Studiengang Vermessungswesen der Universität der Bundeswehr München, Neubiberg
- Landau H., Vollath U. (1996): *Carrier Phase Ambiguity Resolution using GPS and GLONASS Signals*, Proceedings of the 9th International Technical Meeting of the Satellite Division of the Institute of Navigation, ION GPS-96
- Landau H. (1999): *Erfahrungen beim Einsatz von GPS/GLONASS Technologien in der Vermessung*, GPS Praxis und Trends '97, Deutscher Verein für Vermessungswesen, Schriftenreihe 35, 1999
- Lebedev M. G., Gorev V. V., Ganin A. A., Kulnev V. V. (1996): *GLONASS on the way to wide-area international civilian application*, Coordinational Scientific Information Center of the Russian Space Forces and Central Research Institute of the Russian Space Forces, Moscow, Russia, April 1996
- Lechner W. (1992): *NAVSTAR GPS and GLONASS - Competitors or Initial Elements of a Future Global Satellite Navigation System ?*, Journal for Satellite-Based Positioning, Navigation and Communication, 1/92, March, 1992
- Lechner W., Vieweg S. (1994): *Recent Experiences with combined GPS/GLONASS Measurements Utilizing 3S-Navigation R100 Receivers*, Journal for Satellite-Based Positioning, Navigation and Communication, 1/94, March, 1994
- Leick A., (1995): *GPS Satellite Surveying 2nd ed.*, John Wiley & Sons, Inc., USA
- Leick A., Li J., Beser J., Mader G. (1995): *Processing GLONASS Carrier Phase Observations -Theory and First Experience-*, ION GPS-95 Meeting, September 12-15, 1995
- Leisten O. P. (1994): *Compact Circuitry for GLONASS Reception*, ION GPS-94, 1994
- Lewandowski W., Azoubib J. (1998): *GPS+GLONASS: Toward Subnanosecond Time Transfer*, GPS World, November 1998
- Lowe D., Capaccio S., Walsh D., Daly P., Richards G., Wolfe A., Mistry H. (1997): *GPS and GLONASS LAAS and RAAS Flight Trials with RMS Integration*, First European

References

- Symposium on Global Navigation Satellite Systems, Munich, Germany, 21 - 25 April, 1997
- Mai W., Zarraoa N., Jungstand A. (1997): *Stability of GLONASS Satellite Clocks*, First European Symposium on Global Navigation Satellite Systems, Munich, Germany, 21 - 25 April, 1997
- Mathes A. (1998): *GPS und GLONASS als Teil eines hybriden Meßsystems in der Geodäsie am Beispiel des Systems HIGGINS*, Deutsche Geodätische Kommission, Reihe C, Heft Nr. 500, 1998
- Malys S., Slater J. (1994): *Maintenance and Enhancement of the World Geodetic System 1984*, Proceedings of the 7th International Technical Meeting of the Satellite Division of the Institute of Navigation, ION GPS-94, Salt Lake City, Utah
- McCarthy D. D. (1996): *IERS Conventions*, International Earth Rotation Service (IERS), Technical Note 21
- Mervart L. (1995): *Ambiguity Resolution Techniques in Geodetic and Geodynamic Applications of the Global Positioning System*, Dissertation, University of Berne, Switzerland, 1995
- Misra P.N., Abbot R. I., Gaposchkin E.M. (1996): *Transformation Between WGS-84 and PZ-90*, Proceedings of the 9th International Technical Meeting of the Satellite Division of the Institute of Navigation, ION GPS-96, Kansas City, Missouri
- Mitrikas V.V., Revniviykh S. G., Bykhanov E. V. (1998): *WGS 84/PR 90 Transformation Parameters Determination Based On Laser And Ephemerides Long-Term GLONASS Orbital Data Processing*, ION-GPS89, September 15-19, 1998, Nashville, USA
- Remondi B.W. (1989): *Extending the National Geodetic Survey Standard Orbit Formats*, Technical Report NOS 133 NGS 46, NOAA, Rockville, Maryland
- Rosbach U., Habrich H., Zarraoa N. (1996): *Transformation Parameters Between PZ-90 and WGS-84*, Proceedings of the 9th International Technical Meeting of the Satellite Division of the Institute of Navigation, ION GPS-96, Kansas City, Missouri
- Rosbach U., Hein G. (1996): *Treatment of Integer Ambiguities in DGPS/DGLONASS Double Difference Carrier Phase Solutions*, Proceedings of the 9th International Technical Meeting of the Satellite Division of the Institute of Navigation, ION GPS-96
- Rothacher M. (1992): *Orbits of Satellite Systems in Space Geodesy*, Schweizerische Geodätische Kommission, Volume 46
- Schaer S. (1999): *Mapping and Predicting the Earth's Ionosphere Using the Global Positioning System*, Dissertation, University of Berne, Switzerland, 1999

Van Dierendonck A., Birnbaum M., Kopitzke E., Russell S. (1978): *The GPS Navigation Message*, Navigation, Journal of the Institute of Navigation, Volume 25, No.2 , pp. 147-165, Washington

Walsh P., Daly P. (1996): *GPS and GLONASS Carrier Phase Ambiguity Resolution*, Proceedings of the 9th International Technical Meeting of the Satellite Division of the Institute of Navigation, ION GPS-96, Kansas City, Missouri

Willis P., Beutler G., Gurtner W., Hein G., Neilan R., Slater J. (1998): *The International GLONASS Experiment IGEX-98*, Final Version (March 6, 1998), Pascal Willis, IGN Paris, France

Zarraoa N., Mai W., Jungstand A. (1997): *Das russische satellitengestützte Navigationssystem GLONASS - ein Überblick*, Zeitschrift für Vermessungswesen, Heft 9, September 1997

Zarraoa N., Mai W., Sardon E., Jungstand A. (1998): *Preliminary evaluation of the Russian GLONASS system as a potential geodetic tool*, Journal of Geodesy, 72: 356-363, 1998

Curriculum vitae

Name: Heinz Habrich
Geburtsdatum: 27. Januar 1964
Geburtsort: Euskirchen
Heimatort: Karben, Deutschland

1970 – 1972 Grundschule Mechernich-Kommern

1972 – 1974 Grundschule Zülpich-Schwerfen

1974 – 1983 Gymnasium Zülpich, Abschluß mit dem Zeugnis der Allgemeinen Hochschulreife

1983 – 1984 Grundwehrdienst bei der Bundeswehr

1984 – 1990 Studiengang Geodäsie an der Universität Bonn, Diplomarbeit zum Thema *Untersuchungen zur Leistungsfähigkeit des Aero Service Mini-Mac 2816 GPS Meß- und des Aims Auswertesystem*, Abschluß mit dem Diplom für den Studiengang Vermessungswesen

1990 – 1995 Wissenschaftlicher Angestellter am Institut für Angewandte Geodäsie (jetzt Bundesamt für Kartographie und Geodäsie) in Frankfurt am Main in der Abteilung Geodätische Forschung

1995 Übernahme in das Beamtenverhältnis zum Wissenschaftlichen Rat am Bundesamt für Kartographie und Geodäsie in Frankfurt am Main in der Abteilung Geodäsie